AD-A046 242 HUGHES AIRCRAFT CO CULVER CITY CALIF F/G 17/9
THE NULL FILTER MOBILE RADAR FEASIBILITY STUDY.(U)
JUL 77 R A BIRGENHEIER, C H LARSON F19628-76-C-0175
UNCLASSIFIED HAC-P77-161 RADC-TR-77-233 NL

1 OF 2
AD
A046 242



AD A046242

RADC-TR-77-233
FINAL TECHNICAL REPORT
JULY 1977

THE NULL FILTER MOBILE RADAR FEASIBILITY STUDY

Hughes Aircraft Company

Approved for public release; distribution unlimited

AD No.
DDC FILE COPY

ROME AIR DEVELOPMENT CENTER
AIR FORCE SYSTEMS COMMAND
GRIFFISS AIR FORCE BASE, NEW YORK 13441

DDC
RECEIVED
NOV 2 1977
B

This report has been reviewed by the RADC Information Office (OI) and is releasable to the National Technical Information Service (NTIS). At NTIS it will be releasable to the general public, including foreign nations.

This technical report has been reviewed and approved for publication.

APPROVED:

J. Leon Poirier

J. LEON POIRIER
Project Engineer

Allan C. Schell

APPROVED: ALLAN C. SCHELL
Acting Chief,
Electromagnetic Sciences Division

FOR THE COMMANDER: John P. Huss

Plans Office

UNCLASSIFIED

SECURITY CLASSIFICATION OF THIS PAGE (When Data Entered)

REPORT DOCUMENTATION PAGE	READ INSTRUCTIONS BEFORE COMPLETING FORM
1. REPORT NUMBER: RADC-TR-77-233	2. GOVT ACCESSION NO. / 3. RECIPIENT'S CATALOG NUMBER
4. TITLE (and Subtitle): THE NULL FILTER MOBILE RADAR FEASIBILITY STUDY.	5. TYPE OF REPORT & PERIOD COVERED: Final Report, Apr 76 - Mar 77
	6. PERFORMING ORG. REPORT NUMBER: HAC - P77-161, HAC-Ref D6618
7. AUTHOR(s): R. A. Birgenheier, C. H. Larson, J. I. Glaser	8. CONTRACT OR GRANT NUMBER(s): F19628-76-C-0175
9. PERFORMING ORGANIZATION NAME AND ADDRESS: Hughes Aircraft Company, Centinela and Teale Sts, Culver City, California 90230	10. PROGRAM ELEMENT, PROJECT, TASK AREA & WORK UNIT NUMBERS: 61102F, 563505-OA, 45
11. CONTROLLING OFFICE NAME AND ADDRESS: Deputy for Electronic Technology (RADC) ETER, Hansom Air Force Base, MA 01731, Dr. J. Leon Poirer, Contract Monitor	12. REPORT DATE: Jul 77
	13. NUMBER OF PAGES: 120
14. MONITORING AGENCY NAME & ADDRESS (if different from Controlling Office): 131p.	15. SECURITY CLASS. (of this report): Unclassified
	15a. DECLASSIFICATION/DOWNGRADING SCHEDULE

16. DISTRIBUTION STATEMENT (of this Report)

Approved for public release; distribution unlimited

DDC RECEIVED NOV 2 1977 B

17. DISTRIBUTION STATEMENT (of the abstract entered in Block 20, if different from Report)

18. SUPPLEMENTARY NOTES

19. KEY WORDS (Continue on reverse side if necessary and identify by block number)

Null Filtering, moving target indication, parallel processing, clutter suppression, LSI, microprocessing, jammer nulling, adaptive antenna

20. ABSTRACT (Continue on reverse side if necessary and identify by block number)

see other side

DD FORM 1 JAN 73 1473 EDITION OF 1 NOV 65 IS OBSOLETE

172 300

UNCLASSIFIED

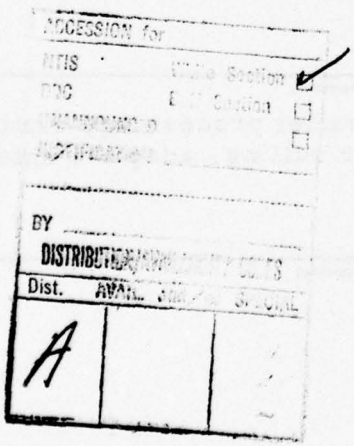
SECURITY CLASSIFICATION OF THIS PAGE (When Data Entered)

Block 20. (Continued)

NULL FILTER MOBILE RADAR

ABSTRACT

The investigation of the NFMRAD by state-of-the-art LSI microelectronic hardware was performed. The hardware required for a representative implementation of NFMRAD was investigated and critical hardware items were identified. It was found that the high-precision, high-rate complex multipliers required at each channel of NFMRAD had the major impact on system cost. For the parameters considered in this study, these multipliers add an incremental cost of approximately 300 thousand dollars compared with a more conventional radar design approach. It was found that for the parameters of NFMRAD considered in this study, peak antenna sidelobes of -25 to -30 dB can provide adequate sidelobe clutter suppression for all but severe radar scenarios. An jammer nulling algorithm that takes advantage of the parallel receiving channels of NFMRAD was analyzed and found to work well against a single jammer. An alternate approach to NFMRAD was suggested that could provide MTI and an ECCM capability with a substantial reduction in price below the price of the full NFMRAD implementation.



EVALUATION

1. This is the Final Report on Contract F19628-76-C-0175. It covers analysis of the Null Filter Mobile Radar (NFMRAD) carried out between April 1976 and March 1977. The analysis includes the detail system design of a typical airborne radar system, an estimate of the hardware required to do the extensive signal processing, and an analysis of the vulnerability of the NFMRAD system to jamming. This work was done under TPO 28.

2. The work is of importance because it clearly identifies and puts into perspective many of the problems encountered in implementing an airborne surveillance radar required to detect slow moving ground targets from stand off distances. The report shows that the NFMRAD concept may be a viable alternative for a stand off surveillance radar.

J. Leon Poirier

J. LEON POIRIER
Project Engineer

Preceding Page BLANK - NOT FILMED

CONTENTS

1.0 SUMMARY 1

2.0 THE NFMRAD CONCEPT 3

The Receiving Array Weighting. 5

3.0 SYSTEM DESIGN CONSIDERATIONS 13

Baseline Parameters 13
Transmitter Waveform 14
Beamforming and Doppler Filtering. 16
Clutter Considerations 26

The Clutter Model 29
Clutter Power Profiles 35
Signal-to-Clutter Ratio 35

Jammer Considerations. 41
Dynamic Range 42
NFMRAD Detection Sensitivity Calculation 45

4.0 SYSTEM IMPLEMENTATION. 51

NFMRAD Functional Description 51

Major System Segments. 52
Pulse Compression 54

Hardware Considerations 55

Antenna, Receiver, Transmitter, and Exciter 56
Digital Signal Processing 58
Beamforming Function 62
Doppler Filter Function 65
Track Processor 66
Post Processing Function 68
Master Timing and Mode Control 75

5.0 ELECTRONIC COUNTER-COUNTERMEASURES 77

Functional Implementation 81
Evaluation of Performance of ECCM 84
Conclusions and Recommendations 94

CONTENTS (Concluded)

6.0 AN ALTERNATIVE NFMRAD APPROACH 95

General Description 95
Adaptive Subarrays. 97
Ground Moving Target Indication 98
Summary 101

7.0 CONCLUSIONS 102

APPENDIX A. EFFECTIVE POST-DETECTION INTEGRATION OF OVERLAPPED DATA 105

APPENDIX B. THREE-CHANNEL PROCESSOR FOR MAXIMIZATION OF TARGET-TO-INTERFERENCE RATIO 118

LIST OF ILLUSTRATIONS

Figure		Page
1	The AMTI Problem	4
2	NFMRAD Clutter Rejection Concept	6
3	Complementary Doppler-Filtering and Beamforming	8
4	Typical Infinite Impulse Response Filter	20
5	Proposed Doppler Filter Frequency Response	21
6	Doppler Filter Frequency Characteristics	23
7	Combined Antenna Null and Doppler Filter Characteristics	25
8	Geometry for Clutter Calculations	28
9	Land Clutter Data	30
10	Sea Clutter Data	31
11	Ambiguous Clutter Returns	33
12	Clutter Return Power Profiles	36
13	Geometry for Signal-To-Clutter Calculation	38
14	Effective Clutter Cross Section of Range Bin Doppler Filter Output	40
15	NFMRAD Functional Block Diagram	51
16	Transmit/Receive Module Functional Configuration	56
17	IQ Representation of Signal Phasor	64
18	Doppler Filter Functional Block Diagram	66
19	Target Track Functional Diagram	67
20	NFMRAD Post Processing Function	69
21	Sliding Window Accumulator Detail	73
22	Timing Diagram of NFMRAD Incorporating ECCM Algorithm	82
23	Implementation of ECCM Adaptive Algorithm	83

LIST OF ILLUSTRATIONS (Continued)

Figure		Page
24	Geometry of NFMRAD and Interfering Jammer	86
25	Jammer-To-Noise Ratio Versus Time	92
26	NFMRAD Antenna Pattern Versus Angle	93
27	Three-Channel MTI Radar With Adaptive Jammer Nulling	96
28	Amplitude Weighting of Overlapped Subarrays	98
29	GMTI Doppler Processor	100
30	Three-Channel Null-Pattern Gain	101

LIST OF TABLES

Table		Page
1	Transmit/Receive Module Functional Requirements	55
2	System Cost Comparison	61
3	PDI Range Rates and Range Bin Shift Periods	71
4	Number of Operations and Number of Storage Registers Used by ECCM Algorithm	85
5	Parameters Chosen for Simulation	91

1.0 SUMMARY

Detection and tracking of moving targets are a primary concern of the United States Air Force. Surveillance radars that employ moving target indication (MTI) provide important information that is utilized for the alert of an oncoming threat. MTI is also utilized as a means of gathering intelligence data regarding movement of enemy forces. The high precision offered by moving target tracking (MTT) radars provides the accuracy required for guidance of weapons.

A problem that has plagued MTI/MTT radars is poor signal-to-clutter performance. The Rome Air Development Center (RADC/ETER) has been involved in developing methods for the improvement of signal-to-clutter performance of air-to-air surveillance radars. One technique, termed the Null Filter Mobile Radar (NFMRAD), described in References 1 and 2, is based on the placement of antenna nulls over angular regions that correspond to the bandpasses of doppler filters. The NFMRAD concept involves utilization of a separate receiving beam for each doppler filter which is accomplished by performing all beam forming and doppler filtering by digital processing. The resolution and coverage rate required of NFMRAD are reflected in a large amount of computation per unit time. Therefore, any practical implementation of the NFMRAD that offers high reliability and cost effectiveness must be realized with LSI microelectronic technology.

The objective of the study reported herein was the investigation of the feasibility of implementation of the NFMRAD by state-of-the-art LSI microelectronic technology. The major task was to determine the processing hardware required for a representative implementation of the NFMRAD.

---

1. W. B. Goggins, G. J. Sletten, and F. S. Holt, "New Concepts in AMTI Radar," Proc. Adaptive Antenna Systems Workshop, Volume I, Report No. NRL 7803, Naval Research Laboratory, Washington, D. C., September 30, 1974, pp. 93-110.

2. W. B. Goggins, G. J. Sletten, and F. S. Holt, "New Concepts in AMTI Radar," Microwave Journal, January 1974, pp. 29-35.

Another task was to determine the performance that could be expected of the NFMRAD implementation.

The basic NFMRAD concept is presented in Section 2. A discussion of the system design considerations, including transmitter waveform parameters, receiver power profiles, A/D converter dynamic ranges, doppler filtering and beamforming, and detection sensitivity, is provided in Section 3. A functional description of a NFMRAD implementation is given in Section 4; a description of each of the major system segments and the implications of these segments with regard to their hardware implementation are included. A detailed description of the functional implementation of a jammer nulling technique and a preliminary evaluation of its performance are provided in Section 5. A three-channel MTI approach is introduced in Section 6 as potentially more cost effective than the full NFMRAD approach. The three-channel approach provides ECCM and detection of targets that reside in either mainlobe or sidelobe clutter. Conclusions and recommendations for the follow-on study are provided in Section 7.

2.0 THE NFMRAD CONCEPT

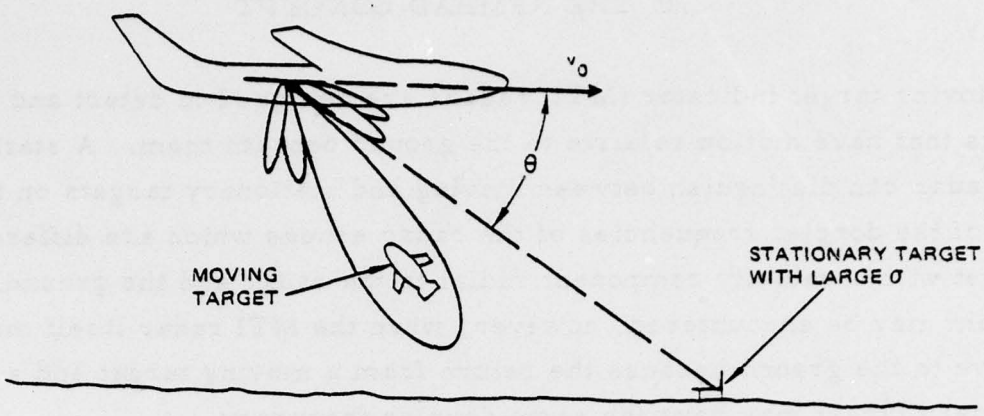
Moving target indicator (MTI) radars are designed to detect and track targets that have motion relative to the ground beneath them. A stationary MTI radar can distinguish between moving and stationary targets on the basis of the doppler frequencies of the radar echoes which are different for a target with a velocity component radial to the radar and the ground. A problem may be encountered, however, when the MTI radar itself moves relative to the ground because the return from a moving target and a stationary target may have the same doppler frequency.

The AMTI problem is illustrated by Figure 1, in which an aircraft is shown moving at a velocity v_0 and angle θ from a stationary target. The doppler frequency of the echo from the stationary target is given as

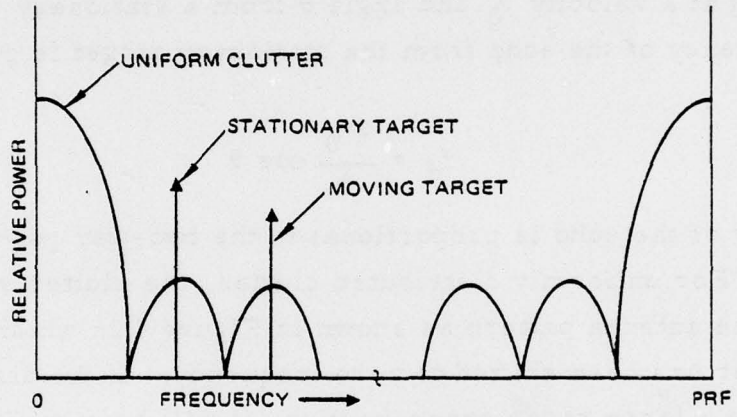
$$f_d = \frac{2v_0}{\lambda} \cos \theta \qquad (1)$$

and the power of the echo is proportional to the two-way power pattern of the antenna. For uniformly distributed clutter, the clutter spectrum has the form of the antenna pattern as shown in Figure 1 in which the mainlobe clutter doppler has been shifted to zero frequency. If the discrete stationary target has a large radar cross-section, it will be significantly larger in amplitude than the average clutter return and will have a large spectral component at a frequency given by Equation (1). A moving target in the mainlobe of the antenna with a radial velocity v_1 with respect to the radar platform will also produce a large spectral component at frequency $f_d = 2v_1/\lambda$.

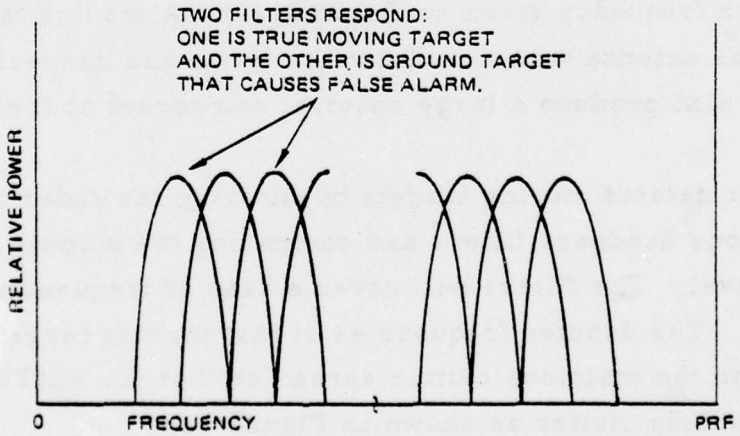
The radar detects moving targets by filtering the radar return with a set of contiguous bandpass filters and comparing the outputs of the filters to a threshold level. The filters will cover a band of frequencies that span the PRF interval. The doppler frequencies of fast moving targets generally will be greater than the mainlobe clutter spread so that for AMTI the doppler filters may exclude clutter as shown in Figure 1c.



a. Scenario



b. Target plus clutter spectra



c. Doppler filter responses

Figure 1. The AMTI problem.

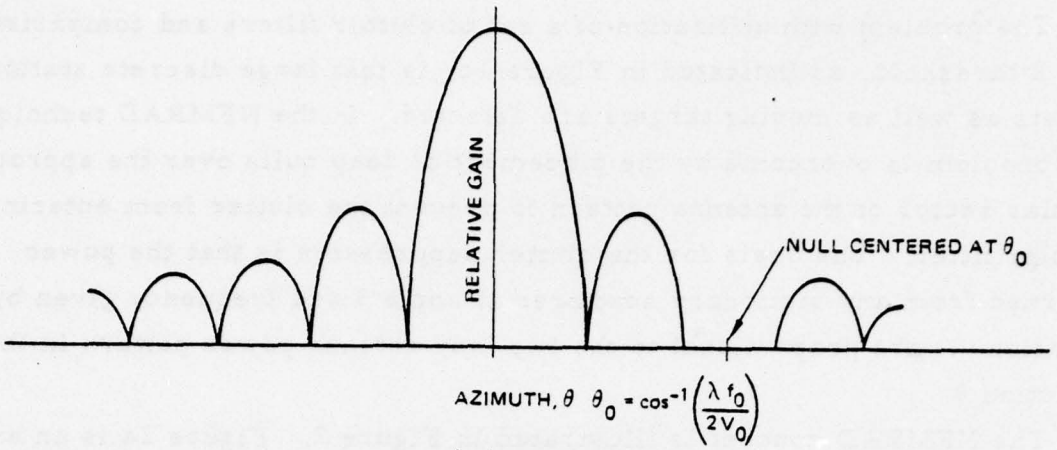
The problem with utilization of a set of clutter filters and comparison with a threshold, as indicated in Figure 1c, is that large discrete stationary targets as well as moving targets are detected. In the NFMRAD technique, this problem is overcome by the placement of deep nulls over the appropriate angular sector of the antenna pattern to prevent the clutter from entering the doppler filter. The basis for the clutter suppression is that the power returned from any stationary scatterer at angle θ and frequency given by Equation (1) are proportional to the two-way antenna power pattern in the direction θ.

The NFMRAD concept is illustrated in Figure 2. Figure 2a is an antenna pattern in which a null has been placed in a sector about θ_0 that corresponds to a band of frequencies centered at f_0. As indicated by Figure 2b, the antenna pattern produces a clutter spectrum in which the clutter including discrete stationary targets at angle θ_0 and doppler frequency f_0 are suppressed. Consequently, stationary targets at azimuth θ_0 will not pass through the doppler filter centered at f_0. On the other hand, moving targets with radial velocity $v_t = \lambda f_0/2$ that are illuminated by the mainbeam of the antenna will not be suppressed and will pass through the doppler filter. Therefore, since clutter in a passband of the doppler filter centered at f_o is rejected, any signal detected at the output of this filter can be identified as a moving target.

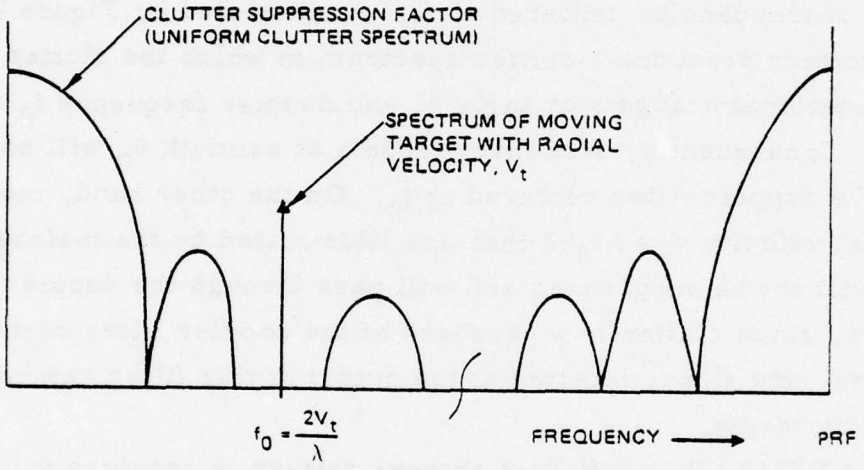
In the NFMRAD, a different antenna pattern is required for each of a bank of doppler filters that are formed simultaneously as indicated in Figure 1c. Since a large number of different antenna patterns must be formed simultaneously, nulls are placed only in the receiving pattern and the receiving beam formation and nulling is performed by digital processing.

THE RECEIVING ARRAY WEIGHTING

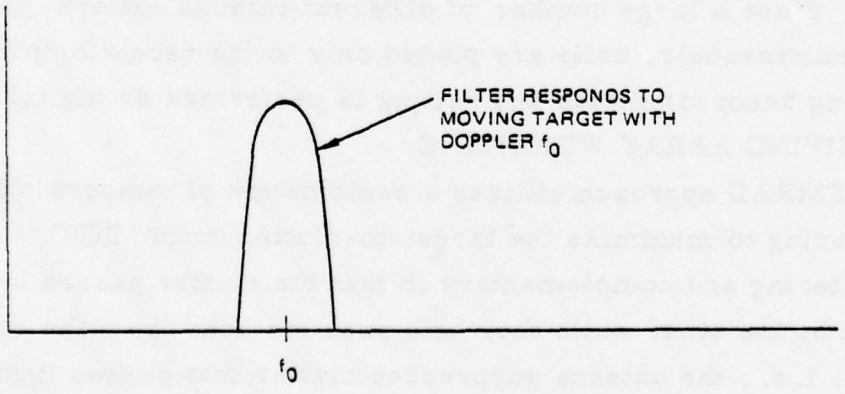
The NFMRAD approach utilizes a combination of temporal (doppler) and spatial filtering to maximize the target-to-clutter ratio (TCR). The two types of filtering are complementary in that the clutter passed by one filter is rejected by the other while they both pass the echo from the moving target of interest, i. e., the antenna suppresses clutter that passes through the bandpass of the doppler filter and the doppler filter suppresses mainlobe



a. Antenna pattern



b. Target plus clutter spectra



c. Doppler filter response

Figure 2. NFMRAD clutter rejection concept.

clutter. The filters are designed by selecting the response characteristics for one filter and determining the weighting coefficients of the other filter from the selected characteristics to maximize TCR. From such a design, the sidelobes of one filter are supressed by the nulls of the other filter.

For the NFMRAD doppler filter and beamforming design, doppler filters have been selected with certain passband characteristics and low sidelobes for mainlobe clutter suppression. Then, based on the selected doppler filter characteristics, the receiving array weights that maximize TCR are determined. An expression for the receiving array weighting has been derived by Goggins and Schindler (Reference 3). Although the array weighting derived in Reference 3 was not used explicitly for any of the results presented in this report, it would be employed in a system implelementation. Since application of the appropriate receiving array weighting is the basis for the whole NFMRAD approach, the discussion presented here would not be complete without giving the relationship of these weights with the system parameters. Therefore, a summary of the derivation of the receiving array weighting will be given that parallels the derivation given by Goggins and Schindler.

A block diagram of an array of M antenna elements is shown in Figure 3a. It feeds signals to a beamformer to produce the output z(t) that is fed to a doppler filter. The relationship between the input and output of the beamformer is given as

$$z(t) = \sum_{k=1}^{M} w_k^* \, y_k(t) = \underline{w}^* \, \underline{y}(t) \qquad (2)$$

where

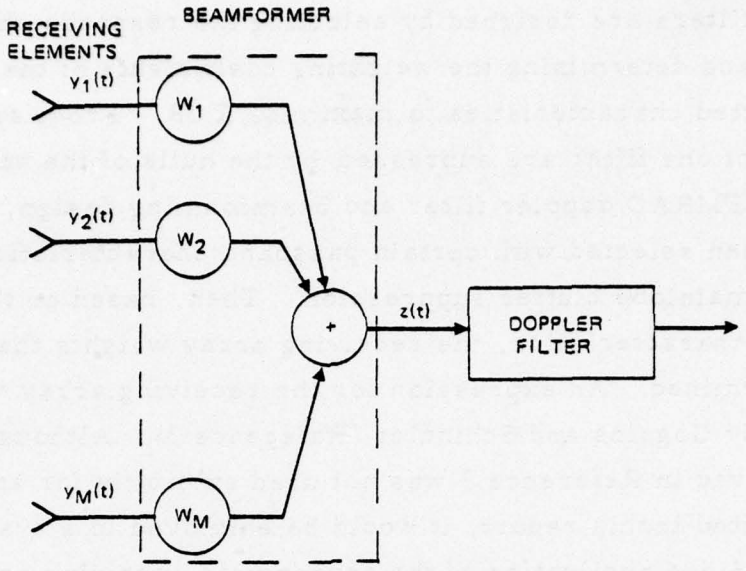
$$\underline{w}^T = (w_1, w_2, \ldots, w_M)^T$$

$$y(t)^T = \left(y_1(t), y_2(t), \ldots, y_M(t)\right)^T$$

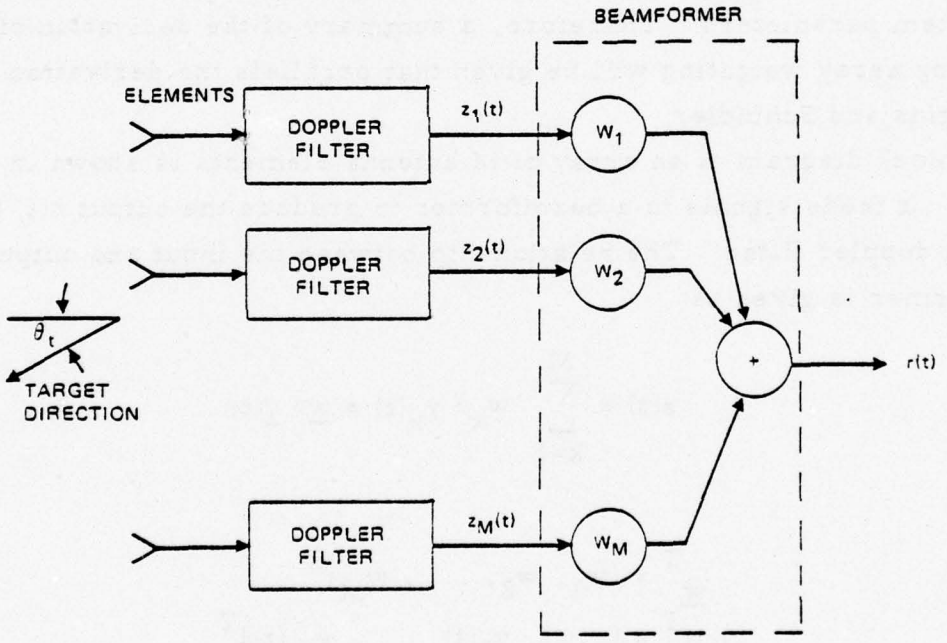
$$\underline{w}^T = \text{transpose of } \underline{w}$$

---

3. W. B. Goggins and J. K. Schindler, Processing for Maximum Signal-to-Clutter in AMTI Radars, AFCRL-TR-74-0577, November 19, 1974.



a. Complementary filters



b. Equivalence of (a)

Figure 3. Complementary doppler-filtering and beamforming.

and

$$\underline{w}^* = \text{complex conjugate transpose of } \underline{w}.$$

The criterion for selection of the weighting $\underline{w}$ is the maximization of the TCR at the doppler filter output. Since the beamformer and doppler filter are linear operations on the input vector $\underline{y}(t)$, the order of these operations may be interchanged as shown in Figure 3b to facilitate the derivation of the optimum weights.

If a moving target is at angle θ_t, as shown in Figure 3b, that produces an echo with a doppler frequency in the passband of the doppler filter, then the desired signal at the set of doppler filter outputs can be expressed as the column vector

$$\underline{s}(t) = \overline{k_1 S \underline{e}} \tag{3}$$

where S is the scattering matrix of the array of antenna elements,

$$\underline{e} = \begin{bmatrix} \exp(jkd \sin\theta_t) \\ \exp(j2kd \sin\theta_t) \\ \vdots \\ \exp(jMkd \sin\theta_t) \end{bmatrix}$$

$k = 2\pi/\lambda$, and k_1 is a constant that depends on parameters of the radar range equation. The target power at the beamformer output is given as

$$TP \propto E\left\{ \left| \underline{w}^* \, \underline{s}(t) \right|^2 \right\}$$

or

$$TP \propto \left| \underline{w}^* \, \underline{a} \right|^2 \tag{4}$$

where

$$\underline{a} = S\underline{e}$$

$E\{\}$ denotes an ensemble average

and

$|\ |$ denotes absolute value

If the output of the array of doppler filters of Figure 3b is written as

$$\underline{z}(t) = \underline{s}(t) + \underline{c}(t)$$

where $\underline{c}^T(t) = (c_1(t),\ c_2(t),\ \ldots\ ,\ c_M(t))^T$ and $c_i(t)$ is the clutter passed by the ith doppler filter, then the clutter power at the beamformer output is

$$CP = E\left\{\left|\underline{w}^*\ \underline{c}(t)\right|^2\right\}$$
$$= \underline{w}^*\ E\left\{\underline{c}(t)\ \underline{c}^*(t)\right\}\underline{w}$$

where $E\{\underline{c}(t)\ \underline{c}^*(t)\}$ is the clutter covariance matrix of the array of doppler filter outputs. The expression derived by Goggins and Schindler is:

$$CP \propto \underline{w}^*\ B\underline{w} \tag{5}$$

where the components of the matrix B are

$$B_{np} = \sum_{m=1}^{N}\sum_{q=1}^{N} S_{mn}\, S_{qp} \sum_{i=1}^{M} \omega_i \exp\left[j(m-q)\ kd\ y_i\right]$$
$$\cdot \left|F\left(\frac{y_i}{\alpha}\right)\right|^2 \left|P_t(\sin^{-1} y_i)\right| \left|f(\sin^{-1} y_i)\right|^2 \tag{6}$$

S_{mn} = the components of the scattering matrix S

ω_i = π/M

M = Number of array elements

y_i = $\cos\left[\frac{(2i-1)\pi}{2M}\right]$ } Not the same y_i used for the signal at an element

d = element spacing

k = $2\pi/\lambda$

λ = radar wavelength

$F(\omega)$ = doppler filter transfer function

α = $(\lambda/2)v_r$

v_r = aircraft velocity

$P_t(\theta)$ = transmitted power pattern

$f(\theta)$ = far-field pattern of the individual elements which is assumed equal for all elements

From Equations (4) and (5), the TCR is given as

$$TCR \propto \frac{\underline{w}^* \underline{a}\, \underline{a}^* \underline{w}}{\underline{w}^* B \underline{w}} \tag{7}$$

Equation (7) is the Rayleigh quotient which is maximized when

$$\underline{w} = B^{-1} \underline{a} \tag{8}$$

As would be expected, the derivation given above shows that the optimum receiving array weighting is a function of the physics of the array as well as the velocity and frequency of the radar platform. In particular, $\underline{w}$ depends on the dimensions of the array and the patterns and self and mutual impedences of the elements of the array. The patterns and impedences of the elements can be predicted theoretically to some degree of accuracy. Because the element parameters are influenced by the airframe which is generally quite complex, in most cases actual measurements are needed to obtain accurate values for $f(\theta)$ and S. The individual elements would have different patterns rather than the identical patterns assumed in the derivation. Moreover, flexures in the airframe will cause a variation of $f(\theta)$ and S as a function of time that may be a significant source of errors. In addition to the phase and amplitude errors introduced by the uncertainties in the antenna array characteristics, other sources of errors such as velocity measurement errors will contribute to the overall errors introduced to the weighting function.

The objective of the study reported here was not the analysis of the sources or the effects of errors; however, this issue is important and will

be addressed during the followon study period. Mc Ilvenna et al. (Reference 4) have performed an analysis for the prediction of pattern performance for given phase and amplitude errors. In the followon to this study, Hughes will analyze the various contributors of errors to establish their nature and magnitude so that Mc Ilvenna's results can be utilized to determine the expected pattern performance of NFMRAD.

In the remainder of this report, the feasibility of implementing the NFMRAD concept will be discussed without considering the adverse effects of uncertainties in the parameters from which the receiving array weights are computed. In particular doppler filtering and beamforming are detailed in Section 3.3 in which it is implicitly assumed that the appropriate array weighting coefficients can be made available.

---

4. J. F. Mc Ilvenna et al., Phase and Amplitude Error Sensitivity in Null Steering Antennas, AFCRL report in progress.

3.0 SYSTEM DESIGN CONSIDERATIONS

This section addresses the principal issues regarding the system design of NFMRAD. The baseline NFMRAD parameters and transmitter waveform parameters utilized for this study are presented. Beamforming and doppler filtering are considered, and special features unique to the NFMRAD approach are related. Clutter is discussed in regard to its relationship to the selection of the transmitter waveform parameters, dynamic range of receivers, and A/D converters and the requirements on the null filtering. A jammer was postulated and found to be the determining factor in dynamic range requirements. This section concludes with an evaluation of the detection performance of NFMRAD under the assumption that clutter is adequately suppressed.

BASELINE PARAMETERS

To evaluate the feasibility of the NFMRAD concept, an operational framework must be defined. It is highly desirable to limit the number of variable parameters, and insofar as possible, parameters will be assigned either worst case values or reasonably typical values, depending on the criticality of the parameter.

The assumed general mission for the NFMRAD system is fence or area airspace surveillance, similar to AWACS. Moving airborne targets are to be detected, then at the discretion of the operator, may be tracked continuously or intermittently with a track/search interleaved mode. The inclusion of the capability of detecting ground moving targets should greatly enhance the effectiveness of the radar; this feature, however, is not included in the baseline NFMRAD system which is treated in this report. It is recommended that ground moving target detection be seriously considered as a growth feature.

The radar platform is assumed to be a KC 135 flying at an altitude of 30,000 feet with a velocity of 270 meters per second. A second platform at 60,000 feet and 160 meters per second does not present any problems that differ significantly from those of the faster and lower platform. This report will concentrate on the 30,000 feet altitude and 270 m/s velocity parameters.

The minimum target cross section is 1 square meter. This value is considered to be a "worst case", since most airborne targets are in the 2-10 m^2 (or higher) bracket. The maximum target velocity is assumed to be 600 m/s. The NFMRAD system parameters which are assigned fixed values are

1. The transmit frequency - 300 MHz (λ = 1 meter)
2. A 32-element physical array with 0.4 to 0.5 λ spacing, mounted along the aircraft fuselage
3. An azimuth search scan ±60 degrees from aircraft broadside
4. A "step scan" of 40 mainbeam positions over the 120 degrees azimuth surveillance sector
5. A 120 degree sweep that is to be covered in 30 seconds, providing a 750 ms dwell time at each azimuth position
6. Range coverage from 20 to 150 n. mi. (In track, the coverage window is ±0.5 n. mi. about target range.)
7. 60 meter range resolution in search, which provides approximately 4000 range bins at a 2.5 MHz rate
8. 15 meter range resolution in track, which provides about 60 range bins at a 10 MHz rate
9. Updating of designated targets at a rate of 2/second/target.

Finally, the capability to adaptively control the antenna pattern for anti-jam purposes will be included in the baseline NFMRAD system.

TRANSMITTER WAVEFORM

There is a fundamental dilemma in the selection of the PRF. To enable the sidelobe clutter spectra to be preserved unambiguously with no overlapping or folding, the PRF must be 1080 Hz or higher for a 270 m/s platform velocity, since the forward lobes will extend to +540 Hz and the back lobes go to -540 Hz. For unambiguous range coverage to 150 n. mi, however, the PRF must be restricted to a maximum of 540 Hz. Clearly a 2:1 discrepancy exists in the requirements for having both velocity (sidelobe clutter) and range unambiguity. Several possible solutions are considered:

1. Lower the transmit frequency to 150 MHz. Now a PRF of 540 Hz provides full clutter frequency unambiguous coverage and 150 mile unambiguous range coverage.

2. Keep the 300 MHz transmit frequency and set the PRF at 1080 Hz and use some range resolving method to distinguish targets below 75 miles from those between 75 and 150 miles.
3. Maintain the 300 MHz carrier frequency, use a 540 Hz PRF, and form two nulls per receive beam to attenuate the sidelobe clutter in a given doppler filter.
4. Retain the 300 MHz transmit frequency, establish a range unambiguous PRF of 540 Hz but abandon the distinctive NFMRAD approach of complementary beams and filters altogether and rely on low antenna sidelobes to provide the required signal-to-clutter ratio.

If the transmit frequency were halved to 150 MHz, the number of elements in the array would be reduced from 32 to 16, retaining the same physical size of the array. Then the degrees of freedom available for null formation are reduced, and the width of the antenna main lobe is doubled. In turn, the aximuth resolution is reduced to 20 positions in the ±60 degree sector, and the minimum velocity of flying targets (before falling into the mainlobe clutter frequency domain) is raised from about 17 to 34 meters per second. It should also be noted that the beam will broaden by a factor of two in the elevation dimension, resulting in a directivity loss of 3 dB.

If the PRF were set at 1080 Hz, causing a 2:1 folding in the range coverage, time-shared transmission at two PRFs would be necessary to resolve the range ambiguity. The signal processing task would be complicated somewhat. But of more importance is that a 1080 Hz PRF causes the very strong "altitude return" to appear in range coincidence with 80 mile targets, and the "main bang" blanking of the radar at zero range will also appear at 75 miles.

For a 300 MHz transmit frequency and a range unambiguous PRF of 540 Hz, the requirement of forming two nulls with 32 variable elements is quite tractable. In fact, the formation of two nulls using 32 elements is less of a problem than one null with 16 elements, especially since additional nulls to adaptively counter jammers are a further requirement.

The abandonment of the basic NFMRAD concept in favor of a low sidelobe single channel conventional radar configuration, of course, is always

a possibility. But the purpose of this feasibility study would be defeated if the effort were diverted from the distinctive NFMRAD features to a more conventional approach. In the NFMRAD evaluation process, however, a projected NFMRAD system must be compared with its more conventional counterpart, both in regard to comparative performance and relative costs. One basic question is whether or not the complementary receive beam and doppler filter approach is really necessary for the achievement of acceptable signal to clutter ratios.

In view of all the foregoing considerations, Hughes believes the 300 MHz transmit frequency and 540 PRF are the best choices.

The following parameters are assigned to complete the NFMRAD waveform specification:

1. Average power - 1000 watts
2. Peak power - 25,000 watts
3. Duty cycle - 0.04
4. Pulsewidth - 60 μs
5. Pulse compression ratio - 150 (search), 600 (track).

BEAMFORMING AND DOPPLER FILTERING

The beamforming aspect of a NFMRAD system is straightforward. The output from each of the 32 receive channels is converted to in-phase and quadrature components by an IQ detector, further converted to digital form with an A/D converter, and complex weighted in a digital complex multiplier. The 32 weighted digital words from the 32 channels are simply summed together to form the desired beam. This process is the digital analogy of a phased array antenna in which the signals from the individual antenna elements are coherently combined together in a waveguide or other analog summing network. The feature which most distinguishes the NFMRAD system from similar radars is the simultaneous formation of 32 receive beams out of common input data from the 32 antenna elements. Thus there is not simply one sum of 32 terms, but 32 sums of 32 different sets of terms, each set having 32 members.

Each of the 32 receive beams has an associated dedicated discrete filter. The function required of a filter is to pass the doppler frequencies

corresponding to the portion of sidelobe clutter nulled by the particular receive pattern and to reject all other frequencies, especially those of the strong mainlobe clutter.

The characteristics of a doppler filter which should be considered for the NFMRAD signal processing application are

1. Center frequency
2. Bandwidth
3. Skirt steepness
4. Sidelobe response
5. Passband flatness
6. Impulse response.

The baseline NFMRAD specification for the number of receive beams, and thus for the number of doppler filters, is 32. Ordinarily the filters would be equally spaced over the 540 Hz PRF (16.9 Hz spacing). Of course, since the filters are formed individually and not collectively as in a fast Fourier transform mechanization, there is the freedom to place the center frequencies of the filters in a non-uniform manner. In this way the clutter powers in the filters could be equalized, filter widths that correspond to varying antenna pattern null widths could be varied as a function of the azimuth angles of the nulls. But it is believed that the use of consistent filter widths and thus uniform filter spacing offers the advantages of having common filter integration times and overall system simplicity, and it is assumed that no pressing requirement exists for any other filter arrangement.

The center frequency of a filter generally is determined by the rate of phase rotation implicit in the complex multiplication applied to the filter input data. This complex multiplication may be considered to operate on the data to frequency shift the spectrum so that the desired filter center frequency is translated to zero doppler (DC). The remaining filter circuitry, then becomes a low-pass filter. Minimum system complexity probably would result if the frequency shifting complex coefficients were combined with the beamforming coefficients, and one complex multiplying operation could serve both the beamforming and doppler filtering requirements.

The simplest doppler filter is a digital accumulator which has the familiar "sine x/x" frequency response; however, the relatively high sidelobe response of this filter makes it unacceptable. Amplitude weighting of the data entering the accumulator could be used to provide any desired level of sidelobe response – with a penalty of increased filter bandwidth and thus a lessening of the filter's signal-to-noise gain (amplitude weighting loss).

If finite impulse response (FIR) filters are implemented and the filter formations do not overlap, (i. e. , a given set of data is uniquely weighted and accumulated in a single functional operation), then the amplitude weighting may also be combined with the phase shifting function at the complex multiplier. In this case, a doppler filter would consist of a simple digital accumulator (an adder and storage register). If it were desired to have overlapped filter formation, then multiple accumulators are required, each with a preceding amplitude weighter. The phase shifting (or frequency shifting) function incorporated in the complex multipliers would serve all the overlapped accumulators, and no duplication would be required.

If infinite impulse response (IIR) filters are selected, the complex multipliers may be used to shift the desired frequency to DC, allowing the filters themselves to operate at zero doppler. Since an IIR filter is by nature "self-overlapping", an output is available with each input data point, as opposed to an FIR filter which does not have a valid output value until all data within the impulse response interval has been entered.

The basic purpose of the doppler filter is to enhance the signal-to-clutter ratio of the target return. The various filter characteristics listed previously i. e. , center frequency, bandwidth, skirt steepness, sidelobe response, passband flatness, and impulse response, are parameters which determine the signal-to-clutter improvement of the filters. From frequency domain considerations alone, the most ideal filter would be a rectangle positioned in frequency to correspond to the null established by the beam forming coefficients, having a flat response across the passband, and virtually complete rejection everywhere else. Such a filter, of course, requires an infinite impulse response and is not realizable. Since (in search at least) the antenna beam is pointed at a given direction for a finite interval of time

and during this time a finite number of pulses are transmitted, any filter that may be used, especially in the time domain, has obvious constraints. Additionally it should be recognized, that the hardware implementation of any proposed filter should be examined carefully. Often an "optimum" filter, on the basis of mathematical analysis alone, may require appreciably more hardware (by a factor of 10 or more) then a compromise or approximate filter whose performance differs only by a few tenths of a dB.

With the above discussion as background, the candidates for the NFMRAD doppler filter are narrowed to

1. An adaptive filter
2. A fixed characteristic infinite impulse response (IIR) filter
3. A fixed characteristic finite impulse response (FIR) filter.

Adaptive clutter rejection filters theoretically offer the greatest signal-to-clutter enhancement of any implementation. They have been proposed and discussed in various technical articles. But, as should be anticipated, they are by far the most intricate and complex in actual digital hardware. Although clutter exhibits certain statistical fluctuations, no valid reasons exist to justify the complex and expensive adaptive filter approach for the NFMRAD system. While the a priori jammer locations are completely unknown, thus justifying adaptive anti-jam null placement algorithms, the general characteristics of mainlobe and sidelobe clutter, in power and frequency are deterministic enough to indicate the use of fixed characteristic filters.

Infinite impulse responsive filters establish poles and zeros through feed-forward and feed-back paths that include weighting coefficients, as shown in Figure 4.

This particular filter has three poles and three zeros. Although a given IIR filter can assume many different forms, in general such a filter will require considerable hardware in its implementation for anything more extensive than a simple one or two pole filter. Special care must be given to the number of bits carried in the interior of the filter, since high gains can occur easily at certain internal points and require a large number of bits in the digital realization of the filter. As previously mentioned, the

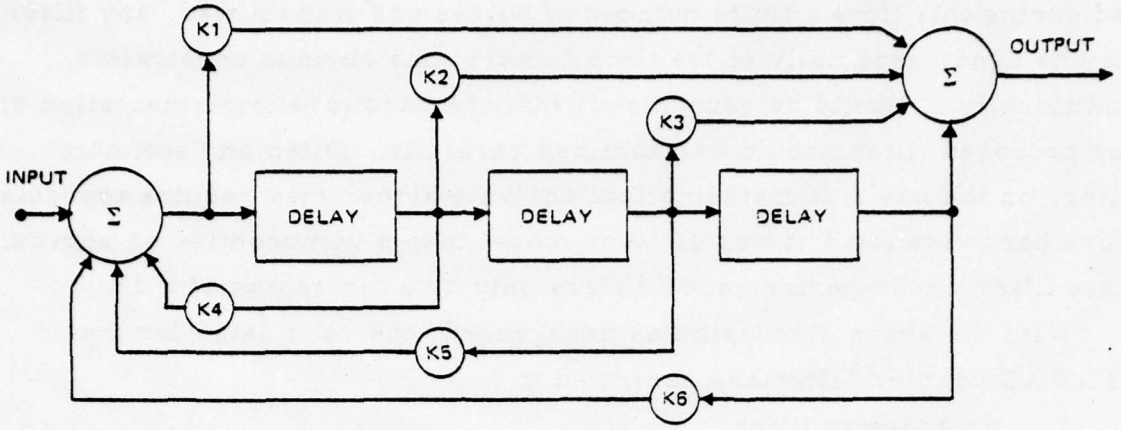


Figure 4. Typical infinite impulse response filter.

advantage of an IIR filter is that it is "self-overlapping", and after an initial filter settling period, an output is available with each new input sample. The output may be sampled as often as desired, usually as dictated by the filter bandwidth, which in turn determines the correlation characteristics of successive filter outputs.

Since the NFMRAD mainbeam is pointed in a given direction for a finite duration and since a moving target will remain in any range bin a limited amount of time, actually no "infinite" impulse response can occur, only a truncated segment of the impulse response. The impulse response of any filter must be in actuality finite; thus, it seems obvious that the better approach is to directly determine the filter's impulse response through weighting the data as they appear at the filter input and accumulating the resultants. This, of course, is the standard FIR approach.

Assuming that the NFMRAD doppler filters are to be FIR in form, then the time duration and the actual values of the impulse response need to be determined. From the baseline parameters given earlier in this report, the formation of 32 contiguous doppler filters requires at least 32 data samples for the filter formation. With 60 m range bins, a maximum expected target velocity of 400 m/sec and a PRF of 540 Hz; a maximum of $60 \times 540/400 = 81$ valid samples exists for a doppler filter under worst case target conditions, so that the impulse response should range between 32 and 81 points.

The weights or values of the impulse response determine the filter's frequency response. One suggested response is as shown in Figure 5.

The sidelobes of the filter are down a certain amount to properly reject the sidelobe clutter not nulled by the receive antenna pattern. Additional attenuation is provided for the mainlobe clutter frequency, as shown. This filter characteristic can be achieved by two cascaded filter sections or alternatively by a single section whose impulse response is the convolution of the responses of the individual sections.

The "safest" doppler filter characteristic would be when all sidelobes are down the amount dictated by mainlobe clutter. Any strong signal or interference at a doppler frequency different from that of mainlobe clutter would be filtered out also. The price paid for a filter with uniformly low sidelobes is minimal. For example, the "loss" associated with 70 dB Chebyshev weighting is 2.2 dB, and this loss can be more than recovered

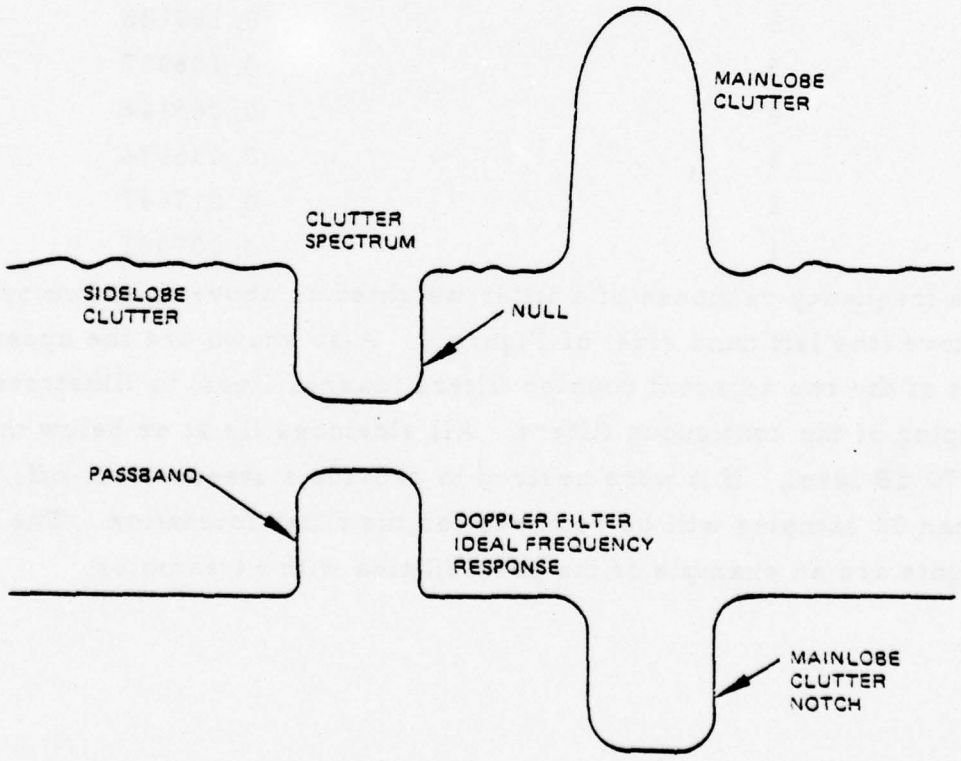


Figure 5. Proposed doppler filter frequency response.

with overlapped filter formation and nearly twice the post detection integration (PDI) ratio compared with non-overlapped filter formation. The real weights of a 70 dB Chebyshev filter (32 sample points) are given below. The weights are symmetrical about the center weight: 17 is equal to 16, 18 is equal to 15, 19 to 14, etc.

Number	Chebyshev
16	1.000000
15	0.970771
14	0.914579
13	0.835700
12	0.739929
11	0.633947
10	0.524611
9	0.418289
8	0.320288
7	0.234481
6	0.163126
5	0.106907
4	0.065144
3	0.036134
2	0.017547
1	0.007482

The frequency response of a filter weighted as above is shown by the solid curve (the left hand side) of Figure 6. Also shown are the uppermost portions of the two adjacent doppler filters (dashed lines) to illustrate the overlapping of the contiguous filters. All sidelobes lie at or below the dashed 70 dB level. If it were desired to provide a steeper roll-off, then more than 32 samples will be required for the filter formation. The following weights are an example of the possibilities with 64 samples.

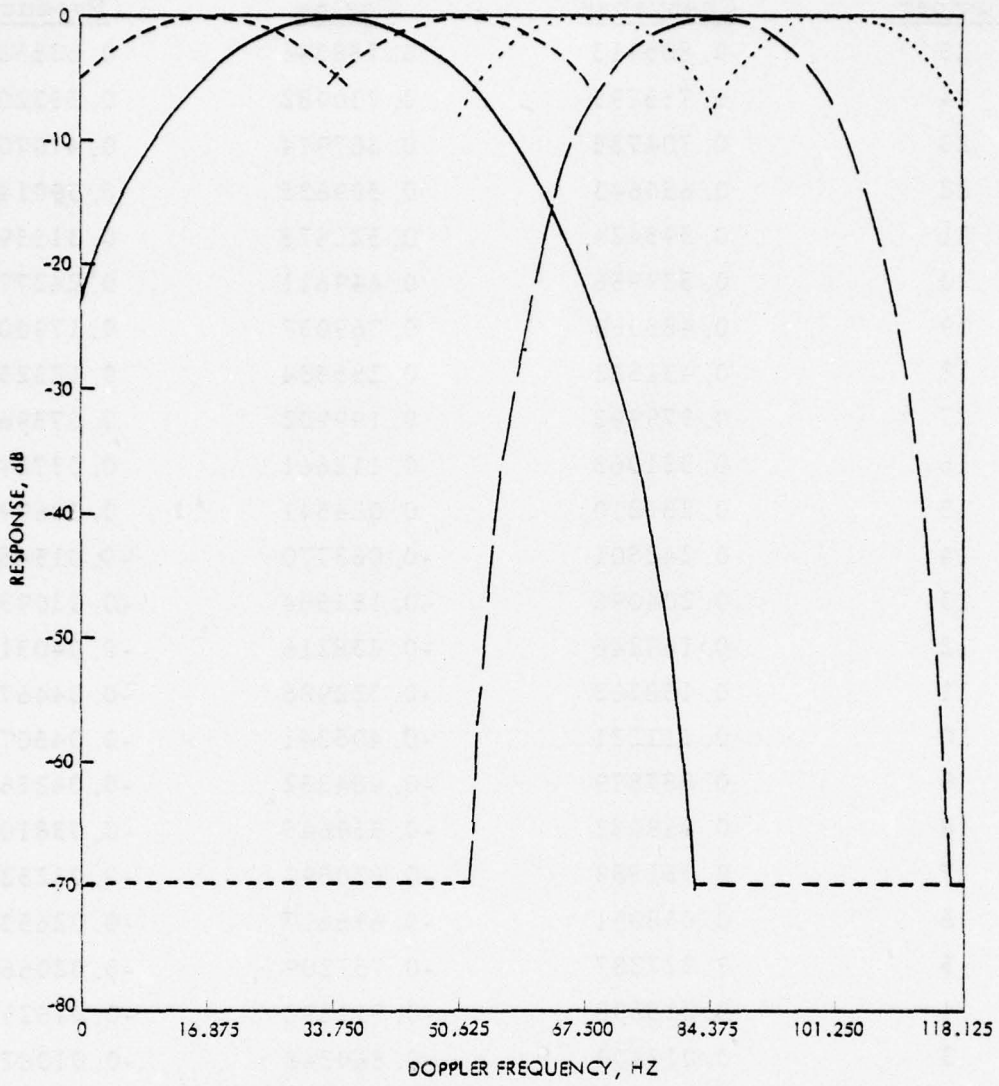


Figure 6. Doppler filter frequency characteristics.

Number	Chebyshev	Cosine	Product
32	1.000977	0.999024	1.000000
31	0.993344	0.991230	0.984632
30	0.978234	0.975702	0.954465
29	0.955954	0.952562	0.910605
28	0.926951	0.921990	0.854640
27	0.891804	0.884225	0.788535
26	0.851198	0.839561	0.714632

Number	Chebyshev	Cosine	Product
25	0.805913	0.788346	0.635339
24	0.756795	0.730982	0.553204
23	0.704735	0.667914	0.470702
22	0.650643	0.599635	0.390148
21	0.595424	0.526678	0.313597
20	0.539956	0.449611	0.242771
19	0.485069	0.369037	0.179008
18	0.431522	0.285584	0.123236
17	0.379993	0.199902	0.075962
16	0.331063	0.112661	0.037298
15	0.285210	0.024541	0.006999
14	0.242801	-0.063770	-0.015484
13	0.204096	-0.151584	-0.030938
12	0.169246	-0.238216	-0.040317
11	0.138302	-0.322988	-0.044670
10	0.111221	-0.405241	-0.045071
9	0.087879	-0.484332	-0.042562
8	0.068082	-0.559645	-0.038102
7	0.051583	-0.630591	-0.032528
6	0.038091	-0.696617	-0.026535
5	0.027287	-0.757209	-0.020662
4	0.018838	-0.811892	-0.015294
3	0.012409	-0.860242	-0.010675
2	0.007674	-0.901880	-0.006921
1	0.005923	-0.936481	-0.005547

Again the weights are symmetrical about the center of the array so only half the values are shown. These weights were generated by multiplying the weights of a 64 point 73 dB Chebyshev filter by the cosine of 0.45 x 540 Hz phased so that the peak lies at the center of the array. The frequency characteristics of this filter are shown on Figure 6 (on the right half) by the dashed curve. Portions of adjacent filters are shown by the dotted curve. This filter has a flatter top and narrower base than the 32-point filter. The

penalty for employing this filter is increased hardware required for a fourfold filter formation overlap. This additional hardware requirement, however, is not major.

Figure 7 shows how each filter might "fit in" with a typical antenna null. The antenna pattern shown was formed with 32 elements and is a result of another program at Hughes. It is believed to be fairly representative of the type of nulls the NFMRAD antenna might form. The 32 point filter might be slightly too wide, although the 37 dB combined antenna-filter attenuation peaks might be acceptable (dashed lines). As would be expected, the narrower 64 point filter does better (dotted lines).

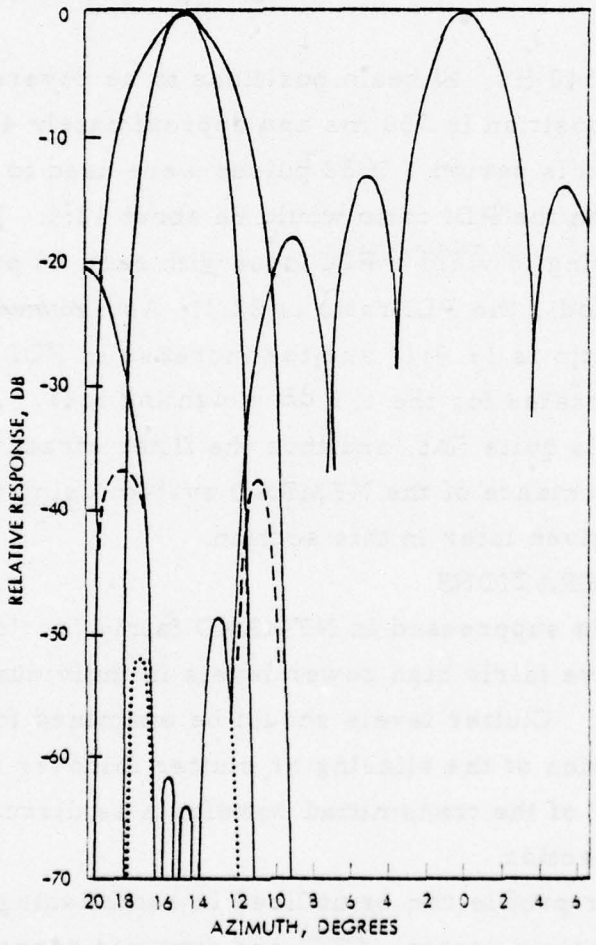


Figure 7. Combined antenna null and doppler filter characteristics.

It should be generally conceded that the 64 point filter presents better overall performance in the frequency domain than that shown in Figure 7, for example. But there should be assurances that no penalty has been paid in overall detection performance, etc. This topic covered in the following paragraphs.

The signal-to-noise gain of the filter is determined by the amplitude weights. The DC amplitude gain is the sum of the weights, and so the DC power gain is the sum squared. The AC power gain is the sum of the square of the weights. The signal-to-noise gain is the square of the sum of the weights divided by the sum of the square of the weights. For the weights given for the 64 sample filter, the signal-to-noise gain is 1.5 dB below 32:1 coherent integration. Thus, the amplitude weighting loss may be set at 1.5 dB.

With a PRF of 540 Hz, 40 beam positions to be covered in 30 seconds, the dwell time per position is 750 ms and approximately 400 pulses are transmitted during this period. If 32 pulses were used to form the filters without overlap, then the PDI ratio would be about 12:1. With 64 pulse filters and overlapping to yield a PDI input with each 16 pulses (after an initial 64 pulse period), the PDI ratio is 22:1. As shown in Appendix A, the effective PDI ratio is 19.9:1, and the increase in PDI from 12:1 to nearly 20:1 clearly compensates for the 1.5 dB weighting loss. Additionally, the mainlobe response is quite flat, and thus the filter straddle loss is minimal. The detection performance of the NFMRAD system using the recommended 64 pulse filters is given later in this section.

CLUTTER CONSIDERATIONS

Clutter power is suppressed in NFMRAD fairly far "down stream" and may, in fact, achieve fairly high power levels in individual channels before suppression occurs. Clutter levels should be examined for several reasons:

1. Consideration of the aliasing or clutter foldover aided in selection of the PRF of the transmitted waveform as discussed in the previous section.
2. The clutter profile can be utilized in establishing the receiver sensitivity time control (STC) and dynamic range. In a jamming environment, however, the dynamic range of individual receiver

channels may be dictated by the jammer power levels rather than clutter levels.

3. For a given clutter model, the signal-to-clutter ratios (SCRs) can be determined and utilized in the establishment of the requirements for the null depths of NFMRAD.

An expression for the clutter power in the individual receiver channels is utilized for the calculation of single channel clutter profiles in this subsection. RADC/ETER provided the clutter models for lands and moderately rough sea that were used for calculations. The model was also utilized in computation of ambiguous to nonambiguous clutter power levels which provided the insight required for PRF selection. This subsection concludes with a calculation of the SCR at the doppler filter output as a function of antenna gain; the SCR calculation shows the clutter suppression that must be provided by the antenna for detection of a given sized target.

Expression for Clutter Power

An expression can be derived for the clutter in a receiver channel by consideration of the geometry shown in Figure 8. If the transmitting antenna with gain G_T illuminates an area on the ground as shown in the figure, then the power density of the illumination is

$$P_I = \frac{\hat{P}_T G_T}{4\pi R^2}$$

where

$\hat{P}_T$ = peak transmitter power

The power reflected from the area is

$$P_{refl.} = P_I [\sigma_0 A_c]$$

where A_c is the effective clutter area as shown in Figure 8 and $\sigma_0 A_c$ is the radar cross-section of the patch. The clutter power at the radar receiver is

$$P_c = \frac{\hat{P}_T G_T A_e (\sigma_0 A_c)}{(4\pi)^2 R^4}$$

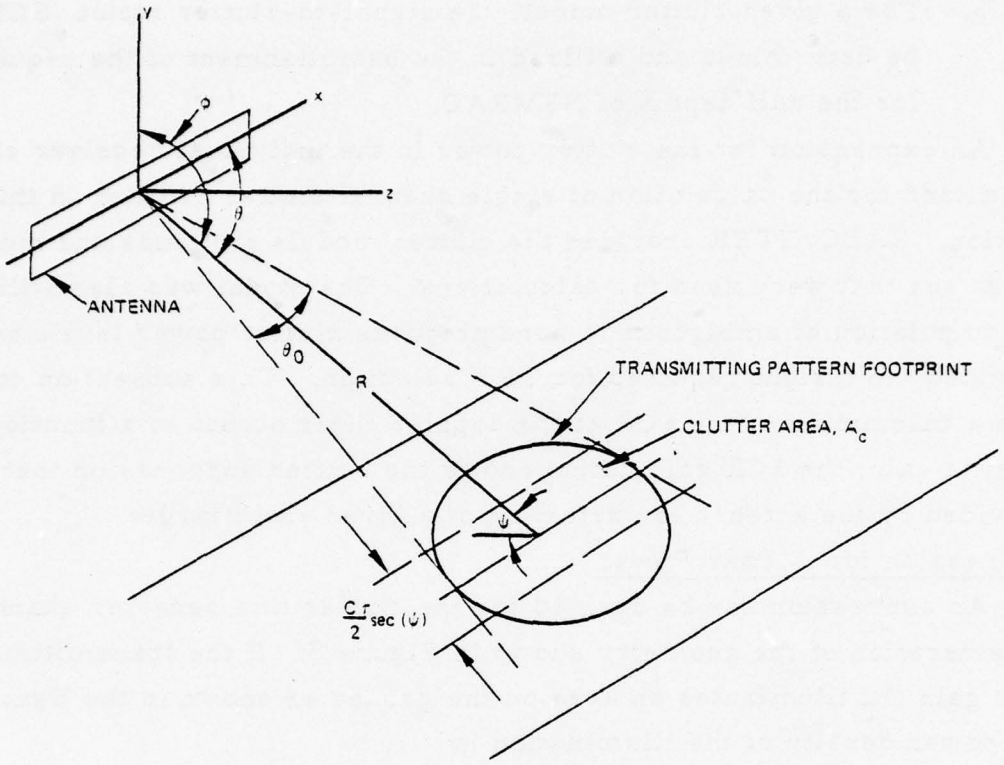


Figure 8. Geometry for clutter calculations.

where A_e is the effective area of the receiving aperture. If the radar transmitting antenna is uniformly weighted, then the effective width of the clutter patch is given by the 4 dB beamwidth of the antenna. The length of the patch is simply the range resolution length projected onto the ground which is $c\tau\sec(\psi)/2$ as shown in the figure. The clutter area, therefore, is given as

$$A_c = \frac{c\tau}{2} \sec(\psi)\, R\, 2 \tan\frac{\theta_0}{2}$$

so that the received clutter power is given as

$$P_c = \frac{\hat{P}_T\, G_T\, A_e\, \sigma_0\, c\tau\, \sec(\psi)\, \sin(\theta_0)}{2(4\pi)^2\, R^3} \qquad (9)$$

where θ_0 is the 4 dB beamwidth.

The grazing angle ψ can be given as

$$\psi = \tan^{-1}\left(\frac{h}{X} + \frac{X}{2a}\right) - \frac{X}{a}$$

where

$$X = R\sqrt{1 - \left(\frac{h}{R} + \frac{R}{2a}\right)^2}$$

h is the altitude of the aircraft, and a is 4/3 radius of earth where the 4/3 factor is utilized to account for the tendency of the transmitted wave to follow the curvature of the earth.

The Clutter Model

The clutter data collected for this study by Dr. Poirier of RADC/ETER is presented in Figures 9 and 10. The two sets of curves in these figures show the log-normal variation appropriate for farm land and sea clutter. In these curves, the cross-section σ is given for values of the grazing angle ψ ranging from 0 to 90 degrees. σ(in dB) is assumed to obey a log-normal distribution with a mean value of σ_0. The center curve in each case represents $\bar{\sigma}_0$; the upper and lower curves represent the 94th and 16th percentile values, respectively. The broken curves in each figure are an estimate of the values expected for small grazing angles; these values were computed from the expression $\sigma = K \sin^n \psi$ where n = 1 for land clutter and n = 1.5 for sea clutter.

A number of additional data points are shown that represent the mean value of the cross-section reported for cities or mountains or that have been used in the performance specifications in several new radars. In general, these points are representative of σ_0 for the UHF and L-band frequencies. From the figures it is seen that the majority of the additional data points are within one standard deviation of the mean value curve; therefore, for this study the central solid curves were used for σ_0 in evaluation of system

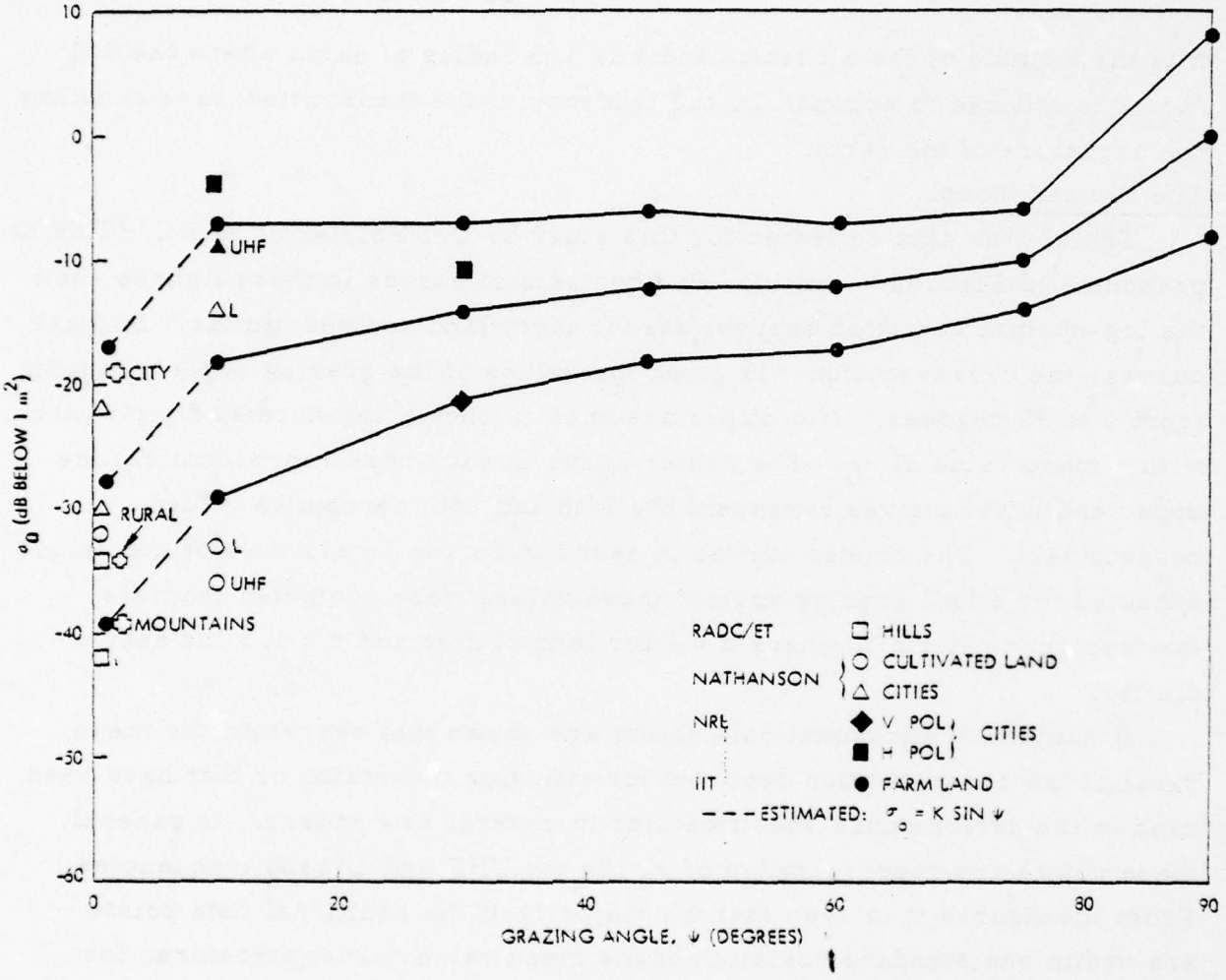


Figure 9. Land clutter data.

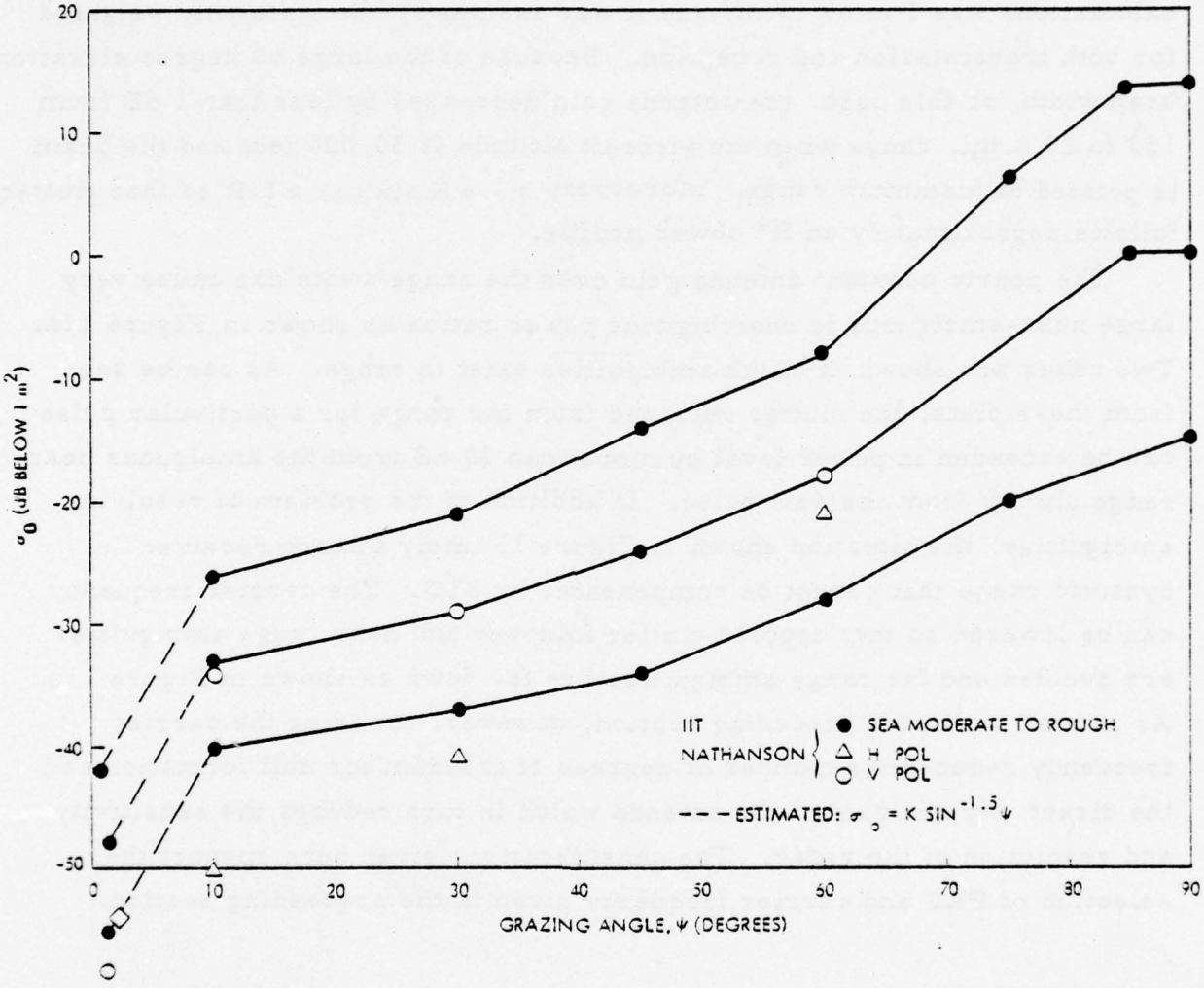


Figure 10. Sea clutter data.

performance. The references cited by Dr. Poirier in presentation of the clutter data are given as References 5 through 8 in this report.

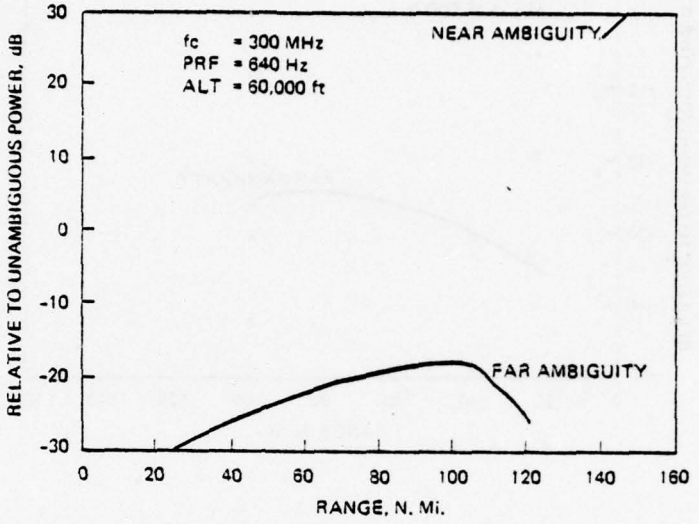
Clutter Ambiguities

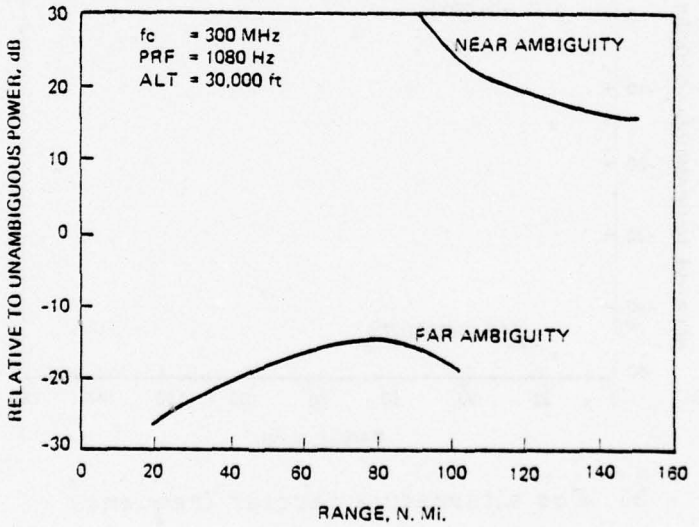
The NFMRAD clutter model and Equation (9) were utilized in calculating the ambiguous to nonambiguous clutter ratios for various PRFs, radar altitudes, and radar carrier frequencies. The antenna size utilized for these calculations was 1 m by 16 m, and it was assumed to be uniformly weighted for both transmission and reception. Because of the large 60 degree elevation beamwidth for this case, the antenna gain decreases by less than 1 dB from 150 to 20 n. mi. range when the aircraft altitude is 30,000 feet and the beam is pointed at maximum range. Moreover, $\sigma_0 \approx K \sin(\psi) \propto 1/R$ so that clutter follows approximately an R^4 power profile.

The nearly constant antenna gain over the range swath can cause very large near-ambiguous to unambiguous power ratios as shown in Figure 11a. Two cases are shown in which ambiguities exist in range. As can be seen from these plots, the clutter returned from far range for a particular pulse can be exceeded in power level by more than 30 dB from the ambiguous near-range clutter from the next pulse. In addition to the problem of resolving ambiguities, the situation shown in Figure 11 imply a large receiver dynamic range that cannot be compensated by STC. The carrier frequency can be lowered so that doppler clutter foldover and near range ambiguities are avoided and far range ambiguities are far down as shown in Figure 11b. As pointed out in the preceding section, however, lowering the carrier frequency reduces the number of degrees of freedom for null formation and the directivity and gain of the antenna which in turn reduces the sensitivity and resolution of the radar. The considerations given here support the selection of PRF and carrier frequency given in the preceeding section.

---

5. F.E. Nathanson, Radar Design Principles, McGraw-Hill, 1969.
6. R. Carlson and L. Greenstein, A Distributed and Discrete Clutter Model for AWACS, IIT Research Inst., Tech. Rpt., No. 2, 1969.
7. W.W. Guinard, NRL Terrain Clutter Study, Phase 1, 1967.
8. Private communications concerned with performance/design goals for a number of new radar systems, 1975.

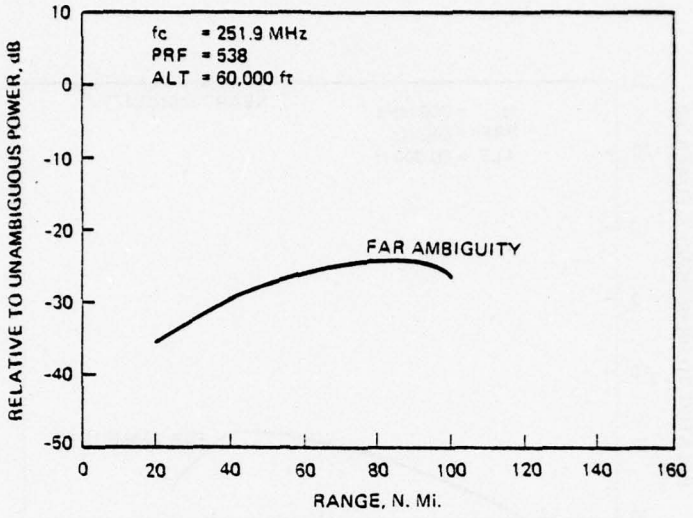


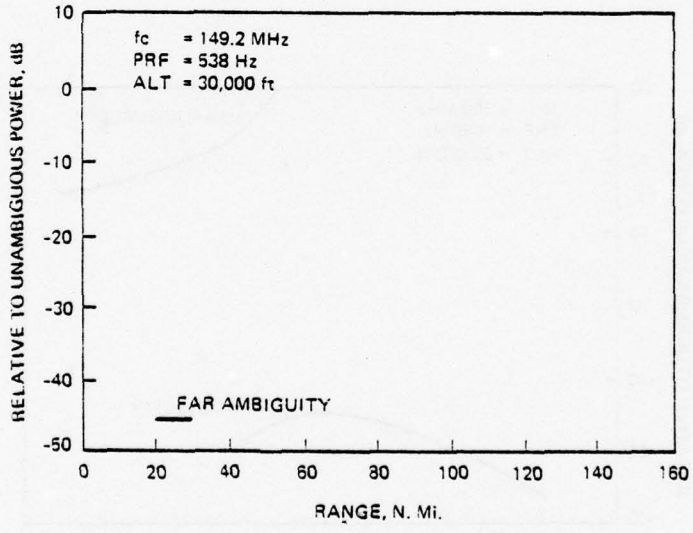


a. For baseline carrier frequency (continued)

Figure 11. Ambiguous clutter returns.

Figure 11. (concluded)





b. For alternative carrier frequency

Figure 11. Ambiguous clutter returns.

Clutter Power Profiles

For the radar parameters given earlier and the clutter data given in Figures 10 and 11, Equation (9) was utilized to calculate the clutter power in a single receiver channel as a function of the time delay after a transmitted pulse. These calculations were made for a transmitting antenna size of 2 x 16 meters and a receiving element size of 2 by 0.5 meters.

Plots of the land and sea clutter return power profiles are given in Figure 12. A unit of time delay on these plots corresponds to 1/50 of a PRI so that 50 units correspond to a range of 150 n. mi. For these plots, the transmitting beam was pointed at 0 degrees azimuth and 150 n. mi. range. The null seen at 1/9 ms time delay is caused by the first null of the antenna.

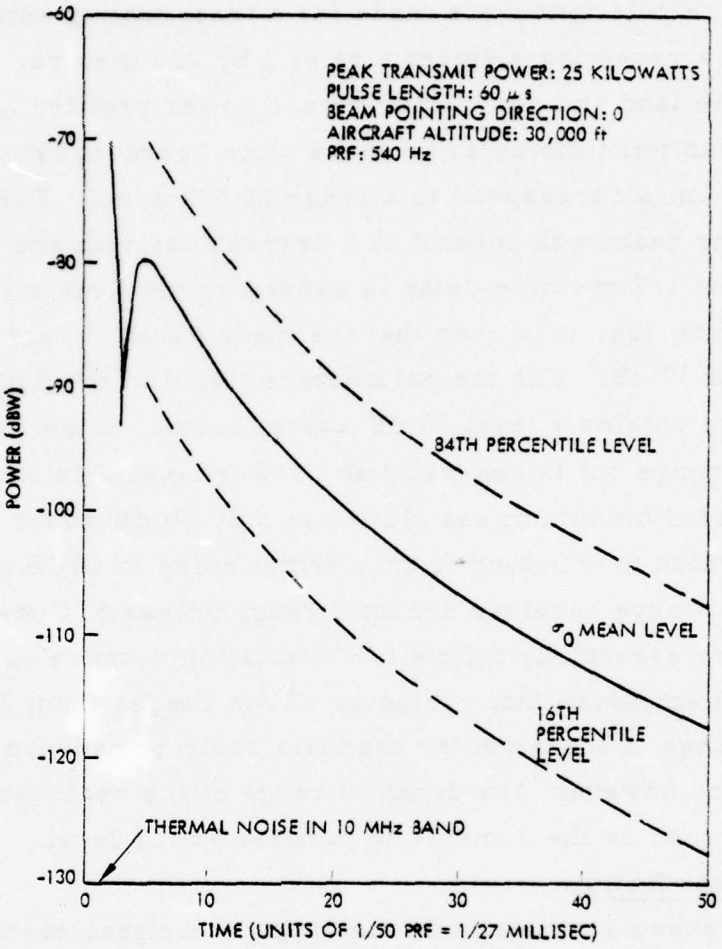
From Figure 12a, it is seen that the mean value of land clutter varies over a range of 37 dB. For the parameters listed in the figure, clutter from minimum range obtains a level 50 dB above thermal noise. Sea clutter varies over a larger range but is generally at a lower level than land clutter; for the parameters listed maximum sea clutter is only 30 dB above thermal noise. Land clutter which may extend from thermal noise to 60 dB above thermal noise would employ a large receiver dynamic range unless STC were employed. The clutter contours essentially follow $1/\tau^4$ variation because $\sigma_0 \approx K/R$; therefore, if an STC were employed that varied as τ^4 for ranges from 20 to 150 n. mi., the dynamic range of the receiver channels could be reduced by 35 dB. As described later, however, the dynamic range of the receiver channels could well be determined by the dominating jammer power level.

Signal-to-Clutter Ratio

The most expedient method of computing the signal-to-clutter ratio of a doppler filter output of a range bin is to consider the area of a clutter patch competing with a target; the dimensions of the clutter patch are determined by the range resolution and the doppler filter bandwidth.

Under the assumption of nonambiguous range coverage, the ground clutter competing with a target at range R will be that from an annulus with a height a and a circumference $2\pi\tau$ as defined in Figure 13a. It is seen that a is the component of the length on the ground covered by the pulse length τ normal to the line of sight from which

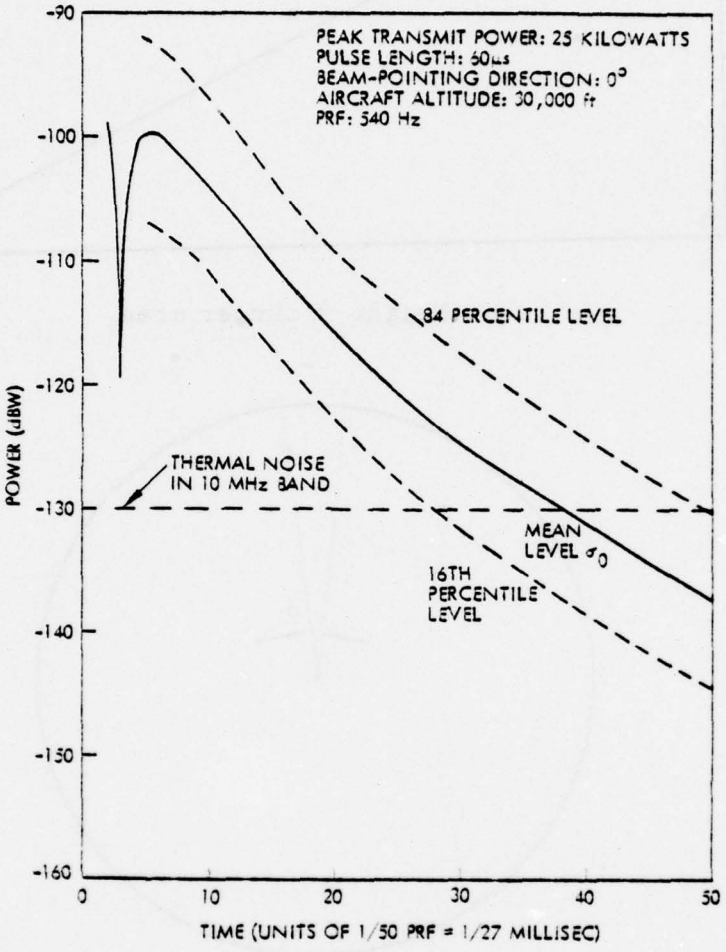
$$a = \tau \tan \psi$$



a. For land clutter
(continued)

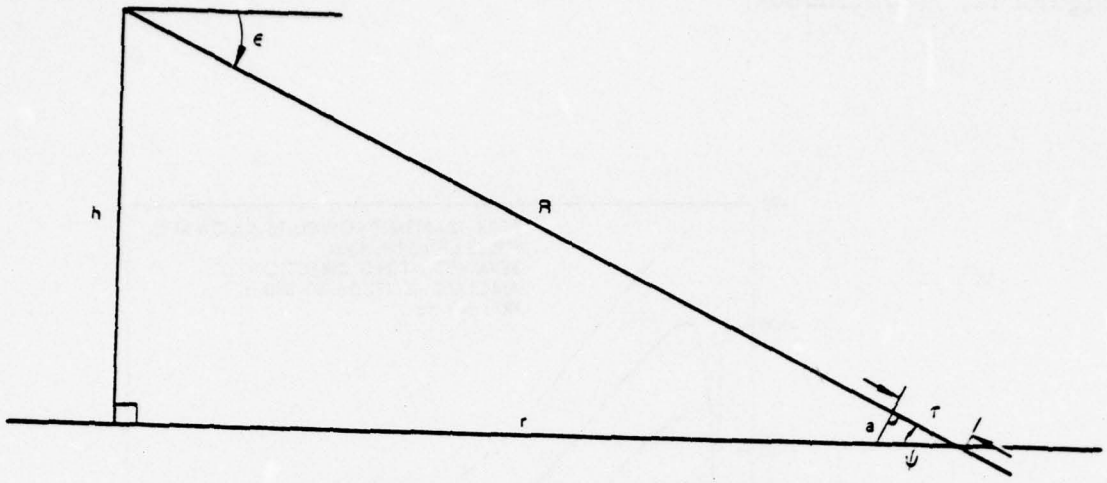
Figure 12. Clutter return power profiles.

Figure 12. (concluded)

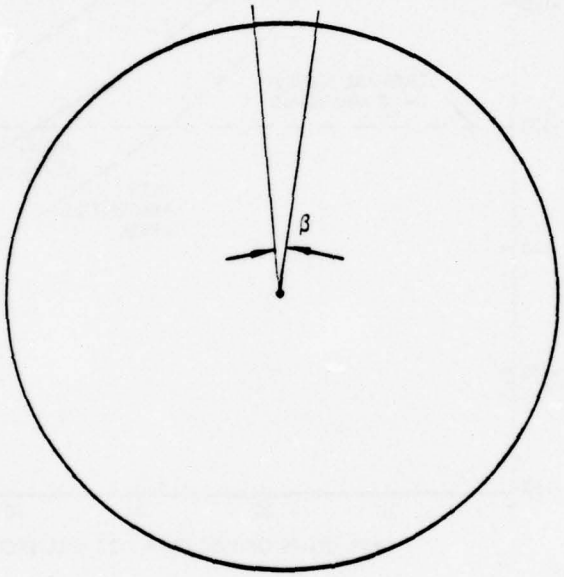


b. For sea clutter

Figure 12. Clutter return power profiles.



a. Height of clutter area



b. Width of clutter area

Figure 13. Geometry for signal-to-clutter calculation.

where ψ is the grazing angle of the transmitted wave with the ground. From the figure it is seen that $\tan \psi = h/r$ so that the area of the annulus having a height a and circumference $2\pi r$ is

$$a\,(2\pi r) = \tau \tan(\epsilon)(2\pi r) = \tau(h/r)(2\pi r) = 2\pi h \tau$$

The area of a segment of the annulus covered by the angle β as shown in Figure 13b is $2\pi h\,\tau(\beta/2\pi) = h\tau\beta$. The equivalent clutter radar cross-section is

$$\sigma_c = h\tau\beta\eta\,(CFOF) \tag{10}$$

where $\eta = \sigma_0/\sin\psi$ and CFOF is the clutter fold-over factor. Notice that the clutter cross-section given by Equation (10) is somewhat pessimistic because of the flat earth approximation.

For a 2.5 MHz NFMRAD range-bin rate, the range bin width is 400 ns that corresponds to 200 feet or 60 meters. An altitude of 30,000 feet is equivalent to 9000 meters. A typical value for β (the azimuth angular width corresponding to a doppler filter) is 2 degrees or 0.035 radian. If CFOF = 2 then the equivalent clutter cross-section in a range bin of a doppler filter is

$$\sigma_c = (9000)(60)(0.35)(2)\,\frac{\sigma_0}{\sin\psi}$$

$$= 18{,}900\,\frac{\sigma_0}{\sin\psi} \tag{11}$$

Equation (11) was computed and plotted in Figure 14 for the mean value $\overline{\sigma_0}$ of the clutter data given in Figures 9 and 10. As can be seen from Figure 14, the average value of σ_c never exceeds 1800 m^2 or 32.6 dBm^2 for the parameters used here. If a SCR of 15 dB is required for a 1 square meter target in the main beam, then a two way antenna mainlobe-to-sidelobe ratio of 47.6 dB is required which should be fairly easily achieved without adaptive null filtering.

Factors that will lead to more stringent antenna sidelobe requirements, however, are (1) an increase to 60,000 feet altitude that will require approximately 6 dB lower two-way sidelobe gain, (2) a reduction in target

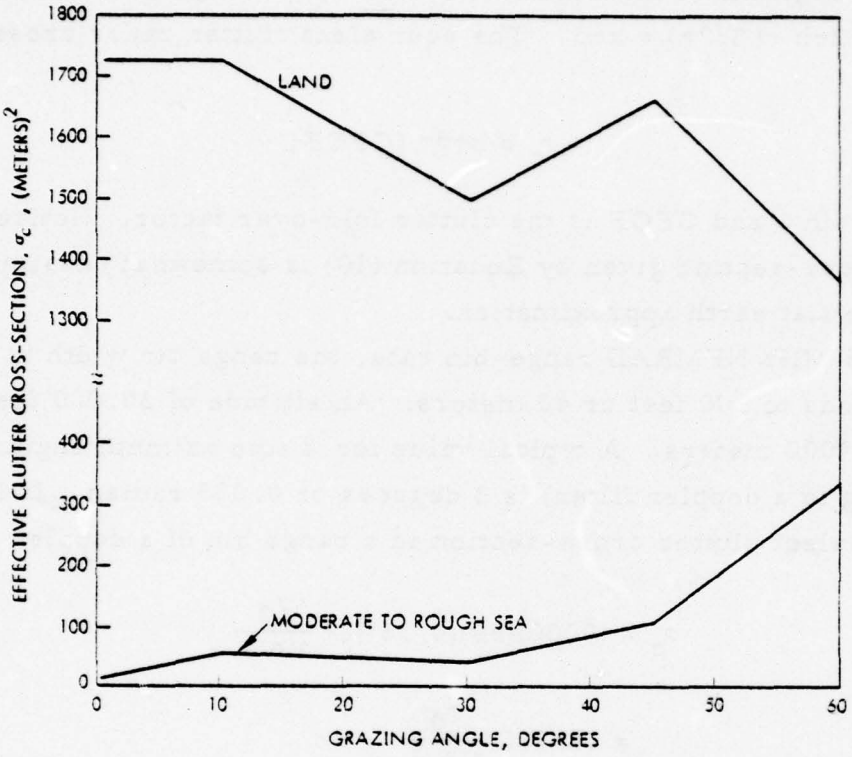


Figure 14. Effective clutter cross section of range bin doppler filter output (no antenna sidelobe suppression).

cross-section by perhaps as much as 10 dB to allow detection of missiles, and (3) an increase in clutter level by 10 dB or more (e.g., the 84 percentile level plotted in Figure 9 is 11 dB greater than the average value used here at 10 degrees grazing angle). Based on these factors, a two-way mainlobe-to-sidelobe ratio of 80 dB or more could be required for a very difficult scenario. It is thus implied that if a -30 dB sidelobe ratio is achieved for the transmitting pattern, for example, then null depths of -50 dB may be required for the receiving pattern. As mentioned earlier, the NFMRAD concept studied under this contract is an open-loop approach that is susceptable to errors so that achieving -50 dB nulls may be difficult. During the follow-on study, achievable null depths will be predicted with the consideration of errors. The conclusion made here, however, is that for the parameters considered in this study, the NFMRAD can provide excellent target detection performance with rather modest antenna sidelobe requirements. Detection performance is considered further later in this section.

JAMMER CONSIDERATIONS

A jamming threat model was not defined for the feasibility study reported herein. Since the consideration of jammer nulling is part of this study, however, a threat model was postulated. The threat postulated for this phase of the study is a single, continuous noise jammer that emits an effective radiated power (ERP) of 50 dB above 1 watt. ERP = $P_J G_J$ where P_J is the average power and G_J is the antenna gain of the jammer. Although the NFMRAD frequency is between the VHF and UHF television bands, 50 dBW is a fairly typical ERP for a high powered television station and should represent a reasonable threat model for the analysis presented here.

The power received from a jammer is given by the familiar path loss equation

$$P_{JR} = \frac{P_J G_J A_e}{4\pi R_J^2} \tag{12}$$

where A_e is the effective area of the receiving antenna and R_J is the range to the jammer. The power that may be received by a single channel from a

50 dBW jammer at a range of 20 n. mi. can be determined by considering the terms of Equation (12):

$P_J G_J$	50 dB(W)
(4π)	-11 dB
R_J^2 (20 n. mi.)	-91.4 dB
A_e (70 percent efficiency)	-1.5 dB (M^2)
P_{JR} =	-53.9 dB(W)

If the receiver noise figure is 4 dB, then the thermal noise power in a 10 MHz band is -130 dB(W); therefore, the jammer-to-noise ratio (JNR) in a single receiver channel is

$$JNR = 76.1 \text{ dB}$$

For the evaluation of ECCM performance in Section 5, a JNR of 75 dB was employed to correspond closely to the jammer levels used here. In the further definition and evaluation of ECCM techniques to be performed during the follow-on study, a threat survey will be conducted to establish a jamming threat that probably will be different than that used here.

DYNAMIC RANGE

If STC were employed that compensated for the $1/R^4$ two-way loss, then the clutter contour of Figure 12a would be essentially constant over the 20 to 150 n. mi. range. Therefore, the dynamic range required for uniform clutter is determined by the CNR at maximum range. The σ_0 mean level is 12.5 dB above thermal noise, and the 84 percentile level is 22.5 dB above thermal noise for the parameters given in Figure 12a. The curves given in Figure 12 apply to uniformly distributed clutter; however, there will also be large discrete clutter points which in an extreme case may have a radar cross-section of $\sigma = 10^6 m^2$. The peak power received by a single channel from a discrete target is given as

$$P_R = \frac{\hat{P} G_T \sigma A_e}{(4\pi R_t^2)^2}$$

where the terms are

$\hat{P}$(peak power)	44 dBW
G_T	21.5 dB
$\sigma(10^6 m^2)$	60 dB(m^2)
A_e (70 percent efficiency)	-1.5 dB (m^2)
$(4\pi)^2$	-22 dB
R_t^4 (150 n. mi.)	-217.8 dB(m^2)
P_R (peak)	-115.8 dBW

Since the thermal noise level of the receiver is -130 dBW, the peak target-to-thermal noise level is

$$\text{CNR (discrete, 150 n. mi.)} = 14.2 \text{ dB}$$

From the consideration of clutter, it can be seen that by employing STC an A/D converter dynamic range of between 20 and 30 dB would be adequate. On the other hand, from the jammer considerations, a jammer at a range of 20 n. mi. that emits 50 dBW of power produces a JNR of 76.1 dB in a single receiver channel; this jammer level is approximately 26 dB above the maximum mean clutter level given in Figure 12a. If a large discrete with $\sigma = 10^6 m^2$ were located at 20 n. mi. range, then the single channel CNR for that discrete is 49.2 dB which is approximately equal to the maximum mean clutter level of Figure 12a.

From the above discussion, it is seen that a 50 dBW jammer at 20 n. mi. range exceeds mean level clutter by at least 26 dB and 84th percentile level clutter by at least 10 dB. Even a 30 dBW jammer at 20 n. mi. range or the 50 dBW jammer at the 150 n. mi. range would produce power levels in a single receiver channel that exceed or are at least comparable to the single channel clutter level. Consequently, the dynamic range required of the receivers and the A/D converters following the receivers will be dictated by the jamming threat.

The distortion added by A/D conversion should be sufficiently low to allow cancellation of jammers by applying adaptive weights after the A/D conversion. If the JNR = 76 dB and distortion is required to be less than the receiver noise level, then the distortion added should be less than -76 dB below the A/D converter input level. The gain of the radar receivers preceding the A/D converters and the number of bits of A/D conversion determine the distortion level. The distortion level generated by a saturating A/D converter when the input signal is assumed Gaussian was analyzed by Gray and Zeoli (Reference 9). They show that the distortion power can be divided into two parts, one due to quantization (Q_N) and another due to saturation (S_N) so that the total distortion power added by the A/D conversion process over the input power, σ^2, can be written as

$$\frac{P_N}{\sigma^2} = \frac{Q_N}{\sigma^2} + \frac{S_N}{\sigma^2}$$

For a given number of bits of quantization, Q_N/σ^2 increases and S_N/σ^2 decreases as the A/D converter input gain increases, and there is an optimum value of input gain that minimizes P_N/σ^2. Gray and Zeoli considered 3 to 10 bit A/D converters; the optimal values of P_N/σ^2 is well approximated by

$$\frac{P_N}{\sigma^2} \simeq 7 - 6M \text{ (dB)}$$

where M is the number of bits of quantization. If M = 14, then

$$\frac{P_N}{\sigma^2} \simeq -77 \text{ dB}$$

which is an acceptable level of distortion for the JNR considered here. If 14 bit A/D converters are employed, then the receiver gain should be set so that

$$\text{A/D saturation} \simeq 5\sigma$$

---

9. G. A. Gray and G. W. Zeoli, "Quantization and Saturation Noise due to Analog-to-Digital Conversion," IEEE Trans. on Aerospace and Electronic Systems, AES-7, 222-223, January 1971.

Since the receiver should not saturate before the A/D converter, the saturation level of the receiver should be at least 14 dB above the average jammer power level. In conclusion, to handle the 50 dBW jammer at 20 n. mi. range, a 14-bit A/D converter is required and the receivers must be able to operate linearly with output power levels 90 dB above the thermal noise level of the receivers.

NFMRAD DETECTION SENSITIVITY CALCULATION

The assumed pertinent NFMRAD system parameters which determine detection sensitivity are given below:

Average transmitter power	1 kW
Transmit frequency	300 MHz (λ = 1 meter)
Antenna array	$2\lambda \times 16\lambda$
Pulse repetition frequency (PRF)	540 Hz
Receiver noise figure	4 dB
Maximum target range	150 n. mi.
Minimum target area	1 square meter

System losses are discussed in later paragraphs.

In the search mode, a 120 degree azimuth scan sector is to be covered by 40 discrete azimuth positions (3 degrees spacing). This compares favorably with the nominal 1/16 radian (3.6 degrees) beamwidth. The azimuth sector is to be scanned once every 30 seconds, which results in a 750 ms dwell time at each azimuth position. With a PRF of 540 Hz, 405 pulses are transmitted at each 750 ms dwell time. It is assumed that this figure is rounded down to 400 pulses.

Each doppler filter is formed from 64 pulses, but because of overlapping, a doppler filter output is available with each 16 pulses (after the initial 64 pulses at each beam position). Since $64 + 21 \times 16 = 400$, post detection integration (PDI) of 22 doppler filter outputs occurs during each dwell time.

The radar range equation will be used to determine the signal-to-noise ratio at the doppler filter output, and then an approach which follows that of Marcum and Swerling* will be used to determine the probability of detection.

The form of the radar range equation to be used here is derived from the basic single pulse signal-to-noise equation:

$$S/N = \frac{PG^2\lambda^2 \sigma L}{(4\pi)^3 R^4 kT_0 \overline{NF} B}$$

where

S/N = signal-to-noise ratio
P = peak transmit power
G = antenna gain
λ = transmit wavelength
σ = effective target radar cross-section (RCS)
L = total system losses
R = range to target
k = Boltzmann's constant (1.38×10^{-23} joules/$^\circ$K)
T_0 = standard reference temperature (290°K)
$\overline{NF}$ = receiver noise figure
B = effective receiver noise bandwidth in Hz

If the bandwidth B is matched to the inverse of the pulsewidth (or compressed pulsewidth) τ, then the terms P/B in the above range equation may be replaced by $P\tau$. Since the average power P_{av} is equal to the peak power times the duty factor, or times $\tau/PRI = \tau PRF$, where PRI is the pulse repetition interval and PRF is the pulse repetition frequency, the terms P/B in the above equation may be replaced by P_{av}/PRF:

$$S/N = \frac{P_{av} G^2 \lambda^2 \sigma L}{(4\pi)^3 R^4 k T_0 \overline{NF} PRF}$$

The parameters of the radar range equation must have consistent units of measure, of course. G, L, and $\overline{NF}$ are dimensionless ratios. P_{av} is in watts, T_0 in degrees Kelvin, PRF in Hz (cycles per second), and k is in joules (watt seconds) per degree Kelvin, and so these terms balance dimensionally. 4π is, of course, a constant. The remaining requirement is that λ^2, σ, and R^2 be in the same units, e.g., meters squared. If R were given

in nautical miles, then the equation must be divided by $(1852)^4$, since there are 1852 meters in a nautical mile.

If the factor $(1852)^4$ is combined with $(4\pi)^3$, k, and T_0, then the equation becomes:

$$S/N = \frac{P_{av} G^2 \lambda^2 \sigma L}{R^4 \overline{NF}\ PRF} \times 10700$$

where

P_{av} = average transmitter power in watts
G = antenna gain as ratio
λ = transmitted wavelength in meters
σ = target RCS in square meters
L = system losses as ratio (less than unity)
R = target range in nautical miles
$\overline{NF}$ = receiver noise figure as ratio
PRF = pulse repetition frequency in Hz

Since $\lambda = c/f$, where c = speed of light (3×10^8 meters/second and f = transmit frequency, choosing the units of f and PRF listed below, and since the coherent integration of n pulses increases the signal-to-noise ratio by a factor of n, the final form of the radar range equation is

$$S/N = \frac{P_{av} G^2 \sigma n L}{R^4 \overline{NF} f^2 PRF} \times 0.963$$

where

P_{av} = average transmitter power in watts
G = antenna gain as ratio
σ = target area in square meters
n = number of pulses integrated
L = total system losses as ratio <1
R = target range in nautical miles
$\overline{NF}$ = receiver noise figure as ratio
f = transmit frequency in GHz
PRF = pulse repetition frequency in kHz

The numerical values for most of the above parameters were listed at the beginning of this section. The antenna gain, assuming an overall efficiency of 70 percent is given by

$$G = \frac{4\pi A}{\lambda^2} \times 0.7 = 128\pi \times 0.7 = 281.5$$

which is equivalent to 24.5 dB.

The term n is set at 32, the number of doppler filters, although 64 pulses are integrated to form the filters. The amplitude weighting loss of 1.5 dB is based on 32:1 coherent integration. If n were to be called out at 64, then the amplitude weighting loss would have to be 4.5 dB, yielding the same overall result. This is a matter of "bookkeeping methods."

The individual losses which comprise the total system loss are estimated below

RF total	0.5 dB
Atmospheric attenuation	0.7
Azimuth beamshape	0.5
Range gate straddle and IF mismatch	1.5
Amplitude weighting	1.5
Doppler filter straddle	0.0
Magnitude detector approx	0.1
Noisy threshold mean	0.1
Digital quantization	0.1
Total losses	5.0 dB

The atmospheric attenuation of 0.7 dB for 150-mile two-way transmission at 300 MHz was derived from Blake (Reference 10).

10. L. F. Blake, A Guide to Basic Pulse Radar Maximum-Range Calculation, Naval Res. Lab. Rept. 5868, December 1962 (reprinted with revisions, December, 1963); second edition, pt. 1, Naval Res. Lab. Rept. 6930, 1969; pt. 2, 1970.

The radar range equation may be calculated using the familiar positive and negative dB equivalents of the component parameters.

		+dB			-dB
P_{av}	1000 W	30.0	0.963		0.2
G^2		49.0	L		5.0
σ	1 m^2	0.0	R^4	150 n. mi.	87.0
n	32	15.1	$\overline{NF}$		4.0
f^2	0.3 GHz	10.5			
PRF	0.540 kHz	2.7			
		107.3			96.2

Therefore, S/N = 107.3 - 96.2 = 11.1 dB.

To convert the 11.1 dB to a probability of detection, the false alarm probability must be determined first.

If it is assumed that a stringent false alarm rate of one per hour will be in effect, and it is further assumed that an STC-like function will confine false alarms to the 100 to 150 mile region, then the number of range bins in the 50 mile region is 50 miles x 1852 meters per mile ÷ 60 meters per range bin = 1500 range bins. The number of doppler filters examined for hits is assumed to be 30 (two filters contain mainlobe clutter), making 45,000 total cells examined for hits. There are 4/3 cell array outputs per second, and 3600 seconds in an hour, making 45,000 x 4/3 x 3600 = 2.16×10^8 cell examinations per hour. The false alarm probability per cell must be the inverse or 4.6×10^{-9}.

The actual determination of the probability of detection P_D will follow that of Marcum and Swerling (References 11 and 12), specifically Equation (45) on page 166 and Equation (II.2), page 277.

---

11. J.I. Marcum, A Statistical Theory of Target Detection by Pulsed Radar (mathematical appendix), RAND Corp. Res. Memo RM-753, 1948; reprinted in IRE Trans. IT-6, No. 2, pp. 145-268, April 1960.
12. P. Swerling, Probability of Detection for Fluctuating Targets, RAND Corp. Res. Memo. RM-1217 (reprinted in IRE Trans. IT-6, No. 2, pp. 269-308, April 1960.

As has been previously determined, the PDI ratio of 22:1 is actually equivalent to 19.9:1.

Equation (45) from Marcum and Swerling is

$$P_{FA} = \sqrt{\frac{N}{2\pi}} \frac{\exp\left[-Y_b + N\left(1 + \ell n \frac{Y_b}{N}\right)\right]}{(Y_b - N + 1)}$$

where

P_{FA} = probability of false alarm (4.6×10^{-9}). This parameter is designated Γ_N in Marcum and Swerling.

N = effective PDI ratio (19.9)

Y_b = normalized threshold setting

$Y_b = 57$ satisfies the above. Assuming a Swerling type I target scintillation, the probability of detection can be derived from Equation (II.2) of Marcum and Swerling, which is

$$P_D = \left(1 + \frac{1}{N\bar{x}}\right)^{N-1} \exp\left(\frac{-Y_b}{1 + N\bar{x}}\right)$$

where

N = PDI ratio (19.9)

$\bar{x}$ = signal-to-noise ratio (11.1 dB or 12.9)

Y_b = normalized threshold (57)

Solving this equation yields a P_D of 0.86.

Then it appears that the NFMRAD system, with operating parameters as stated herein, should provide excellent detection sensitivity out to the maximum range of coverage of 150 n.mi.

4.0 SYSTEM IMPLEMENTATION

This section presents the functional description of the overall NFMRAD system and each major system segment. The discussion is divided into analog and digital processing with emphasis given to the latter. The hardware requirements of individual segments are considered, with emphasis placed on those hardware components that have the most impact on the complexity of an NFMRAD realization.

NFMRAD FUNCTIONAL DESCRIPTION

Figure 15 is a functional block diagram of the overall NFMRAD system. The functions performed by the blocks shown are described briefly in this subsection. Further details of the functions are given in later subsections devoted to individual blocks.

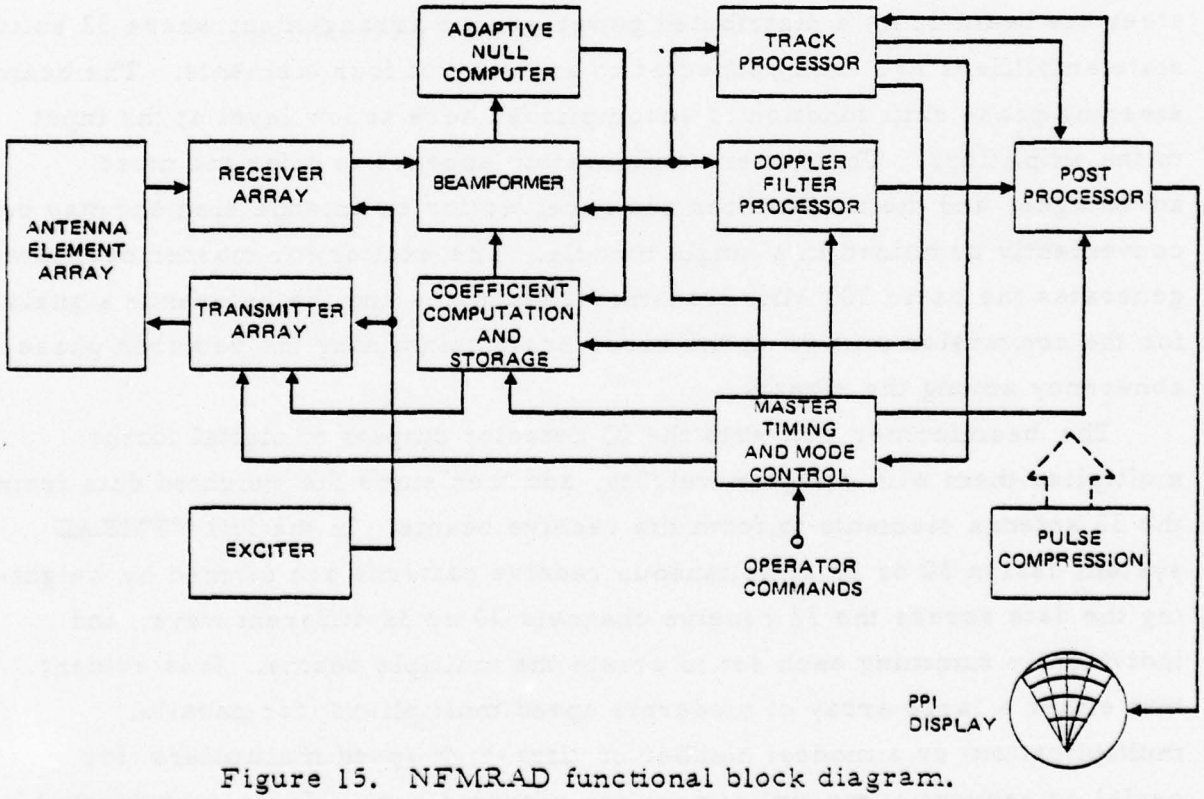


Figure 15. NFMRAD functional block diagram.

Major System Segments

The antenna array consists of 128 elements in a four high (elevation) by 32 wide (azimuth) configuration. There is a $\lambda/2$ (0.5 meter) element spacing. The four elements in the elevation direction at a given point are connected by a power divider network; thus the beam has no elevation control. The 32 arrays of 4 elements are controlled individually to steer the beam in azimuth. Duplexing circuits that route the receive and transmit RF energies from the antenna to the receiver, and from the transmitter to the antenna, respectively, are shown in the antenna array block of Figure 15.

The receiver array consists of 32 separate receivers, one for each of the 32 antenna array elements. A representative receiver design would have a moderate amount of gain at 300 MHz, conversion to a lower intermediate frequency, amplification, and finally conversion to baseband at an IQ coherent detector.

The transmitter could be configured either as a single power source and power splitter with phase shifting elements in the distribution network to steer the beam or as a distributed power source arrangement where 32 solid state amplifiers are each connected to an array of four elements. The beam steering phase shift function is accomplished here at low level at the input to the amplifiers. This latter configuration appears to offer the most advantages, and the transmitter and receiver for an antenna element may be conveniently combined in a single module. The exciter (or master oscillator) generates the basic 300 MHz transmit frequencies and the reference signals for the conversion mixers in the receivers, maintaining the required phase coherency among the signals.

The beamformer converts the IQ detector outputs to digital forms, multiplies them with complex weights, and then sums the weighted data from the 32 antenna elements to form the receive beams. In the full NFMRAD system design 30 or 32 simultaneous receive patterns are formed by weighting the data across the 32 receive channels 30 or 32 different ways, and individually summing each set to create the multiple beams. It is evident that either a large array of moderate speed multipliers (for parallel multiplication) or a modest number of ultra-high speed multipliers (for serial or sequential multiplication) are required here. Since each formed

received beam will go to a single discrete doppler filter, it seems obvious that the complex multiplications required for the doppler filter function (essentially phase rotations on a pulse-to-pulse time basis) can be combined with the beam forming complex weights (across the receive channels). Thus one complex multiplication by the product of the filter and beam forming coefficients can accomplish two purposes.

The adaptive null computer operates at a lower data rate than the regular search mode signal processor but uses the same digital data. It operates recursively to adaptively form nulls in the receive patterns where jammer energy is detected. It operates in conjunction with the coefficient computation and storage function, which in response to the adaptive null inputs, commanded azimuth pointing angle, and sample number (in the doppler filter formation sequence), computes and stores the complex multiplier coefficients. This computing function also generates the phase shift commands for the transmit beam; these go to the phase shifters ahead of the distributed power amplifiers. The analysis and functional description of the adaptive null computation are contained in Section 5.

The doppler filter processor is actually a relatively simple function in the full NFMRAD system. Each doppler filter has an output every 16 transmitted pulses (after an initial wait of 64 pulses at each beam position) but forms each filter from 64 pulses. Thus each filter must have four separate accumulators since there are four simultaneous filter accumulations at any given time. Each accumulator is preceded by an amplitude weighter.

The post processor converts the IQ filter outputs into magnitude data, performs post detection integration (PDI), and generates target detection "hits" with an adaptive threshold. It also contains track acquisition logic and a scan converter function for the display. The track processor processes the range bins containing the tracked target and forms only the applicable doppler filters. Thus the processing volume is much smaller than that of the regular search processing function. The track processor receives monopulse beam or overlapped beam signals so that an azimuth tracking discriminant can be formed for the angle tracking loop. Range tracking and frequency (velocity) tracking are also performed.

The master timing and mode control function interfaces the NFMRAD system with the operator controls, generates the basic system clocks and timing reference pulses, pulses the transmitter, generates the A/D sampling rates, generates the azimuth scan pattern, and generally synchronizes the various functional elements of the NFMRAD system together.

The PPI display, operator controls, power supplies, necessary interfaces, etc., complete the NFMRAD system.

Pulse Compression

The pulse compression function is shown outside the other functional elements because the initial study phase produced no clear guidance for its complete specification. Candidate pulse compression codes include Barker codes (0, 180 degree phase shifts), Frank codes (0, 90, 180, 270 degree phase shifts), other polyphase codes, and chirp (continuous phase shifts). The methods of pulse compression encoding on transmit that seem applicable to the NFMRAD system are FM ramp at the exciter (chirp), common phase shifting at the exciter, individual phase shift encoding at each RF module (perhaps using the beam steering phase shifters if the shifting rate capability is high enough), and surface acoustic wave (SAW) devices at either the exciter or RF modules. SAW devices have largely displaced dispersive delay lines for pulse compression purposes.

The applicable pulse compression decoding (on receive) methods to be considered are SAW components ahead of each A/D converter, digital decoding ahead of the doppler filters, and digital decoding after the doppler filters.

The final determination of the pulse compression mechanization approach is made during the actual system design. However, there is only a slight hardware cost impact of one mechanization relative to another. At this point, the best approach appears to be incorporation of SAW encoding and decoding devices on the RF modules. The arguments usually presented in favor of digital pulse compression decoding (greater dynamic range, smoothing of clutter spikes, etc.) are not as forceful since the A/D conversion is at a large number of bits, as dictated by jamming interference considerations.

HARDWARE CONSIDERATIONS

The hardware required to implement a NFMRAD system is discussed in this section; the areas critical with respect to cost, development effort, risk, etc., are stressed. In evaluating any proposed system not only must the performance (relative to mission requirements) be determined as accurately and realistically as possible through thorough analysis, but the cost, risk and schedule implications of the hardware represented by the new concept must be compared to those of alternative approaches.

From a hardware standpoint, the NFMRAD block diagram as shown in Figure 15 may be conveniently divided between the functions that are implemented (for the most part) with analog components and those that are composed essentially of digital components. The analog blocks are the antenna array, receiver array, transmitter, and PPI display. The remaining seven functional blocks fall into the digital category.

The 300 MHz frequency selected for the baseline NFMRAD is relatively low, and there are no extraordinary requirements in the parameters of average transmitter power, receiver noise figure, antenna beam scanning rates, etc. Therefore, no significant hardware difficulties should occur in the RF components due to any features or requirements unique to the NFMRAD concept. Similarly, the display should be more or less a standard CRT type, with no special problems.

Antenna, Receiver, Transmitter, and Exciter

The transmit/receive (T/R) module requirements are summarized in Table 1, and the functional configuration is shown in Figure 16.

TABLE 1. TRANSMIT/RECEIVE MODULE FUNCTIONAL REQUIREMENTS

Parameter	Requirement
Center Frequency	300 MHz
RF Bandwidth	10 MHz
Peak Power	1 kW (Nominal)
Average Power	40 W
Pulsewidth	60 μs
Receive Noise Figure	<4 dB
Transmit Phase Shifter	4 bits
Scan Limits	±60 degrees in azimuth

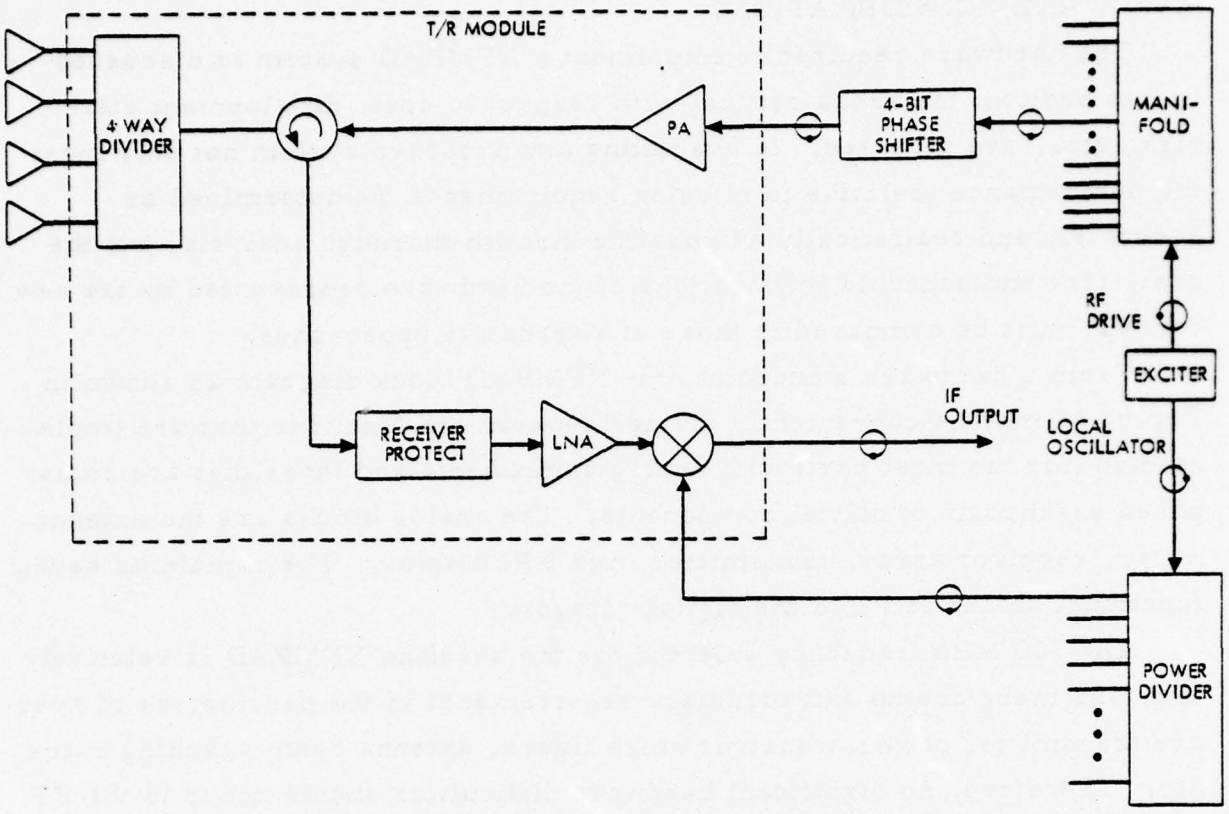


Figure 16. Transmit/Receive module functional configuration.

Referring to the block diagram in Figure 16, the exciter provides the 300 MHz transmitter drive to the array and the local oscillator for down conversion to IF of the echo return signals. A 32-port coaxial manifold configured from matched power dividers is postulated to provide transmitter drive power to each vertical row of Transmit/Receive elements; distribution via coax at this frequency is probably the smallest and least lossy approach. A 4-bit PIN diode phase shifter, selected for its relatively small size, provides the ±60 degree azimuth beam scan limits required of the radar. Because only one phase shifter, power amplifier, etc., is required for each group of four elements comprising a vertical row of elements, a four-way coaxial power divider is shown at the output of each module to manifold the vertical elements.

Within the T/R module, a solid-state transistor power amplifier (PA) operating from 28 VDC can be used to provide the required transmit peak power. Although the pulsed amplifier development effort in this frequency range has been modest, a considerable amount of CW development has been performed for communication, cable television (CATV), and mobile applications. Transistors with an excess of 100 watts cw power exist (e.g., CTC BM100-28, TRW J02015), and off-the-shelf amplifiers are available providing 500 watts of power (e.g., TRW CT-131-73), thus indicating that the solid-state power capability is basically achievable. For a uniformly illuminated array, the 1 kW peak power requirement obviously can be met with only a moderate amount of cw-to-peak power enhancement. To effect a taper for sidelobe reduction, however, the center elements would need to provide greater peak power to offset the reduced power in the edge elements. Since these peak powers undoubtedly would be achieved by paralleling devices or amplifiers, a basic building-block amplifier can be envisioned where the power distribution along the array is provided by appropriately combining amplifiers in parallel.

At the output of the PA, an isoduplexer (circulator) is shown followed by the module radiating element. To achieve a linear polarization, several types of radiators can be considered, including dipoles, loop radiators, blade antenna, cavity-backed slots, etc.; the former, when placed in front of a metal ground plane or mesh, would be a simple and compact approach.

At the receive port of the circulator, a diode-limiter will provide isolation against strong reflected transmit power. The low-noise amplifier (LNA) following the limiter can be designed with existing transistors for a noise figure of less than 2 dB. Assuming that the RF losses can be kept below a worst case 2 dB level, an overall module noise figure of less than 4 dB can be achieved easily.

Following the LNA, a mixer is provided to down-convert the received radar return to a convenient IF frequency.

Digital Signal Processing

Digital signal processing is one of the more recent disciplines applied to radar systems; it is still experiencing rapid growth both in regard to its range of application and to the technical accomplishment intrinsic to the digital devices themselves.

The first production airborne radar to employ full digital signal processing was the APG-63 for the F-15 fighter in the early 1970s. At that time Hughes had to agonizingly trade off performance against size and cost of the digital processor. Factors such as the number of range bins, the number of doppler filters, and the number of bits in a digital signal word, etc., had virtually a linear relationship on the number of components in the processor and thus on its production cost. The values of these parameters ended up as compromises between performance and cost. Since the time of the initial APG-63 development, significant strides have occurred in digital components, providing much more functional capability per device and thus per dollar. To illustrate, the original signal processor design used six memory modules containing a large number of 128 bit shift register ICs. Recently these modules have been replaced by two modules of 1024 bit random access memory (RAM) components. Also 10 timing and control modules similarly have been replaced with five modules that use newly developed components. The component development trend is continuing, with 4096 and 16,385 bit RAMs now available, and 65,536 bit devices predicted to appear in the near future. Therefore, where at one time the digital implementation costs of alternate functional approaches had to be considered seriously, this fact now is not as pressing. The cost represented by a given signal processing functional operation is expected to continue to decline with the introduction of improved components.

For the most part, the digital signal processing portion of the NFMRAD system could be implemented either by a hardwired pipeline processor, by a programmable signal processor (PSP), or by a microcomputer network of some type. Any of these options could be constructed from standard transistor-transistor logic (TTL), Schottky TTL, emitter-coupled logic (ECL), or complementary MOS (CMOS) components. The components could

be standard off-the-shelf units from the large semiconductor houses, custom large-scale integration (LSI) chips, or combinations of these. At this point, a hardwired pipeline processor, with perhaps local "microprocessor" architecture for track and null computation, constructed from standard Schottky TTL components seems to best match the NFMRAD requirements. A PSP is usually more appropriate for a system with many different processing modes, or where it is desired to have a common signal processor for several different systems. Generally custom LSI is used for very large production runs or during severe volume constraints. The particular form a signal processor takes, however, is often largely the result of the developer's previous experience, individual preference, or personal opinion. With exceptions to be discussed later, the NFMRAD computing and signal processing requirements are quite standard and may be scaled from signal processors which Hughes has produced. It is estimated that the adaptive null computer, coefficient computation and storage, master timing and mode control, doppler filter processor, track processor, and post processor (i.e., the NFMRAD digital portion less the beamformer) could be packaged in a unit costing $50 to $100K (assuming a production run of 50 units), occupying 1 to 2 cubic feet, weighing 40 to 60 pounds, and consuming 750 to 1500 watts. Substantial reductions in these figures should occur as the result of future digital hardware advances, but even so, it seems obvious that such a processor is not the pacing item in a NFMRAD system.

The beamformer, as it turns out, very definitely is the NFMRAD pacing item. The sampling or range bin rate in the search mode is 2.5 MHz. Thus digital data are being generated at a 2.5 MHz rate in each of the 32 receive channels. A data rate of 2.5 MHz (5 MHz for in-phase and quadrature components considered individually) until recently was about the upper conversion rate limit for analog-to-digital converters of approximately 10 bits. Converters with this capability were priced at $10K and higher. Recent advances in monolithic chips using new process technologies have allowed a significant breakthrough in A/D performance versus size, power, and cost. It is estimated that a 13-bit converter producing an IQ pair at a 2.5 MHz rate would cost $2000. Higher bit resolutions might be possible, but the intrinsic noise of the transistors on the chips will establish a practical limit

on the number of bits of the converter. The A/D converter cost, while sizeable, does not appear to be an overriding factor.

However, each data sample must be multiplied by 32 different complex coefficients to form the 32 separate receive patterns. A complex multiplication ordinarily consists of four real multiplications. Therefore, the required real multiplication rate is 4 x 32 x 2.5 MHz in each receive channel. The state of the art in digital multipliers is well represented by a 16-bit multiplier currently being developed by Hughes for the Ballistic Missile Defense Systems Command, Huntsville, Alabama. Its multiplication rate is 250 to 320 MHz, it dissipates approximately 50 watts, and it is packaged in a 2 x 2 inch large area hybrid package. A somewhat optimistic cost projection for the multiplier is $10K per unit. Thus for a complete NFMRAD system, requiring 32 such multipliers, the total cost is in the neighborhood of $320K and the total power consumption is 1600 watts.

To be thorough, an alternative implementation using a larger number of slower, less costly, multipliers should be investigated. The prime example of the state of the art of such devices is the MPY-16AJ unit recently offered by TRW. Since it can multiply at a 6.2 MHz rate, two units are required for a single complex multiplication per channel. With the 32 complex multiplications and 32 channels, a total of 2 x 32 x 32 = 2048 multipliers are required for the whole NFMRAD system.

The 1000-up lot price of the TRW LSI device is estimated at $150, resulting in an overall multiplier cost of about $307K, somewhat less than the cost of the 32 Hughes multipliers. But since 2048 rather than 32 components must be integrated into the system, it is suggested that the real support costs should more than make up the difference. Another consideration is that the TRW units, at 5 watts each, will require more than 10,000 watts total, compared with the 1600 watt requirement of the first multiplier approach.

A radar system accomplishing the NFMRAD search and track mission, but with a single low sidelobe receive channel rather than the complementary receive beam discrete digital filter arrangement, could satisfy its beam-forming complex multiplication requirements with about $10K in multiplier components. Thus it might be concluded that the one unique NFMRAD design

approach of multiple beams and complementary filters has a differential cost of over $300K.

To further identify the differential costs of systems employing various features, three related radar configurations are considered:

1. Conventional airborne search radar with a phased array antenna, but with standard single channel transmitter, receiver, and signal processor
2. Similar to (1) except multiple receivers and A/D converters are used to enable nulls to be placed adaptively in the receive antenna pattern
3. The complete NFMRAD system.

The relative cost differentials of various system components among the three systems are given in Table 2. The cost figures given in the table are included only for the purpose of showing the relative costs of the three system approaches and do not necessarily represent an accurate estimate of the absolute cost of individual components.

TABLE 2. SYSTEM COST COMPARISON[a]

Item	Standard System	System with Adaptive Null Capability	NFMRAD
Antenna Array	10	10	10
Receiver(s)	20	100	100
Transmitter(s)	40	100	100
Exciter	20	25	25
A/D Converter(s)	5	50	50
Beamformer	---	30	400
Adaptive Null Function	---	20	20
Doppler Filter Processor	20	20	10
Post Processor	30	30	30
Timing and Miscellaneous	20	25	25
Total	165	410	770

[a]Amounts are in thousands of dollars.

Beamforming Function

The functions to be performed by the beamforming circuitry include: conversion of the IF signals at each of the 32 receive channels to IQ video, sampling of this video at the range bin rate (2.5 MHz in search, 10 MHz in track, as per the preliminary NFMRAD parameters), holding the sampled values so that they can be converted to digital form by an analog-to-digital converter with the number of bits as dictated by the dynamic range requirements. Each digital sample must then be weighted by as many different complex weights as the number of receive beams being formed. Finally, the weighted samples must be summed together in the proper groups to form the beams.

An IF signal is converted to IQ video with an IQ detector, which consists of a pair of balanced mixers that are fed by the common IF signal and whose reference signals are 90 degrees out of phase. The frequency of the detector reference signals may either be fixed at the center IF frequency (in which case the doppler frequencies in the IQ output will be absolute), or the reference frequency may be made to vary as part of a clutter tracking loop that operates to keep mainlobe clutter at zero doppler or DC. In this latter case, the doppler frequencies of targets will be components of the targets' ground velocities along the radar line of sight. It is standard practice to include a mainlobe clutter tracking loop in a digital signal processor to maintain the strong clutter energy at DC so that any harmonics caused by IQ gain and/or phase imbalance will fall at DC also. If the sampling rate (or PRF) interval were spanned by N filters, and mainlobe clutter appears in filter n, then IQ imbalance would cause an "image" to emerge in filter N-n. In the case of the NFMRAD system, spectrum shifting to keep the mainlobe clutter at zero doppler may prove unnecessary since at the IQ detectors, mainlobe clutter is formed from the transmit beam only (the receive beams to be formed at a later point in the system), and IQ gain and phase balance may be dictated by the much stronger jamming signals expected. Therefore, a clutter tracking loop remains as an open question.

The sample-and-hold and analog-to-digital converter functions appear to be relatively standard. Only the difference between the 2.5 MHz sampling rate in search and the 10 MHz rate in track have to be discussed. One approach would be to require the A/D converter to be fully capable of the

worst case 10 MHz conversion rate. Since in track only two range gates are processed, it might be beneficial to have a dual set of sample-and-holds that are triggered 100 ns apart in time but hold the sampled values so that digital conversion may be accomplished at a slower rate. This scheme is possible only if pulse compression decoding is accomplished ahead of the sample-and-hold function by a SAW (or other) device. If digital pulse compression is used, then the full 10 MHz A/D conversion rate is required.

When signal data are carried in IQ form, the "phasor" representation of signals, often employed as a matter of mathematical convenience, is actually realized. A sample phasor (or vector) represented by its digital in-phase (I) and quadrature (Q) components is shown in Figure 17.

In terms of an equivalent polar coordinate system, $I = r \cos\theta$ and $Q = r \sin\theta$. The signal strength is represented by the length r of the vector and the signal frequency is indicated by the rotational rate of the vector, $\dot{\theta}$. Of course, the actual signal phasor of an operating system is the complex sum of many signals – thermal noise, clutter, actual targets, etc. – and the signal processor extracts the signal phasor of interest from the total signal. For signal phasors in IQ form, virtually all linear signal processing operations consist of

1. Phase shifting
2. Amplitude weighting
3. Vector summation.

The phase shift operation alters the angle of a phasor while maintaining the vector length. In mathematical terms

$$I' = I \cos\Psi - Q \sin\Psi$$

$$Q' = Q \cos\Psi + I \sin\Psi$$

where I, Q are the components of the vector before phase shifting, and I', Q' are the vector components of the vector after being shifted by an angle Ψ.

Amplitude weighting simply consists of multiplying both I and Q by a common factor, a. Vector summation is accomplished by adding 2 (or more) I components together and similarly summing the Q components together.

Phase shifting and amplitude weighting operations may be combined into a single complex multiplication. In complex arithmetic notation, a signal

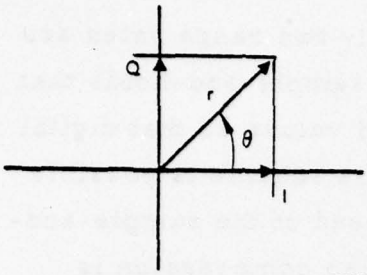


Figure 17. IQ representation of signal phasor.

phasor is given as $I + jQ$, and the complex multiplier is $a\cos\psi + ja\sin\psi$, where a and ψ are as previously defined. The complex product is $a(I\cos\psi - Q\sin\psi) + ja(Q\cos\psi + I\sin\psi)$. Four actual (real) multiplications and two additions are required to perform a complex multiplication.

An alternative method of complex multiplication may offer some hardware savings. Consider the general case in which $a + jb$ and $c + jd$ are to be multiplied together. The desired results are ac-bd for the real component and ad + bc for the imaginary component. If the terms a, b, c, and d are arranged in a simple product matrix as shown below

	c	d
a	ac	ad
b	bc	bd

the real component is the difference of the terms in one diagonal, and the imaginary component is the sum of the terms in the other diagonal.

The product $(a + b)(c + d) = ac + ad + bc + bd$ is seen to be the sum of all four terms of the matrix shown above. If this product is formed (through two additions and one multiplication), and the terms ac and bd are also individually formed (through two additional multiplications), then the real component ac-bd and the imaginary component ad + bc (equal to [ac+ad+bc+bd]-ac-bd) require only a further addition and a subtraction. The total arithmetic operations for this approach to complex multiplications, then, is three multiplies and five additions, as compared to the four multiplies and two additions used in the normal method. Depending on the particular hardware implementation, the trade of one multiplication for three additions may be worthwhile.

The complex coefficients used in the beam forming process may be precalculated from the aircraft velocity and other system parameters

discussed in Section 2 and stored in a memory in a basic NFMRAD design. The complex weights are used to steer the beam in azimuth through a linear phase shift profile across the elements, establish the nulls at the desired angles, and to establish the frequency of the doppler filter associated with a particular receive beam by the rate of phase shift from one pulse to the next. For adaptive null placement to counter jammers, a recursive process must be used; this subject is treated in detail in Section 5.

The summation of the weighted data to form the beams is straightforward and may be accomplished in parallel with adder trees, or sequentially by high speed multiplexers and accumulators.

Doppler Filter Function

In the full NFMRAD concept, each formed receive beam has a dedicated discrete doppler filter. The simplest filter consists of a complex weighter and an accumulator which sums the weighted data (see Section 3). Complex weighting of the data may be considered a combination of phase rotations, which establish the frequency of the filter, and real or amplitude weighting, which determines the frequency response curve of the filter. Since complex weighting is required for beam formation, the same complex multiplication can also serve the filter function; the complex coefficients are the precalculated products of the beam and filter weights. Since the heavy weighting necessary to achieve filters with steep slopes and low sidelobes would result in significant losses if butted arrays of data were used in the filters, it seems that overlapped filter formation is indicated. In this case, only the phase shifting component of the filter weights can be incorporated into the beamforming function, and each overlapped accumulator phase must be preceded by its own amplitude (real) weighter. A functional block diagram of the doppler filter function is shown in Figure 18.

The amplitude weighting profiles are identical but operate at different points or phases along the curve at any given time. The accumulators need to store approximately 4000 range bins of I and Q data. Each accumulator sums weighted data from 64 pulses. Because of overlap staggering, an output occurs from one accumulator every 16 pulses. Each accumulator is cleared or "dumped" after each output and a new accumulation begun. There, of course, are 30 or 32 individual filters such as that shown in Figure 18, one for each receive channel.

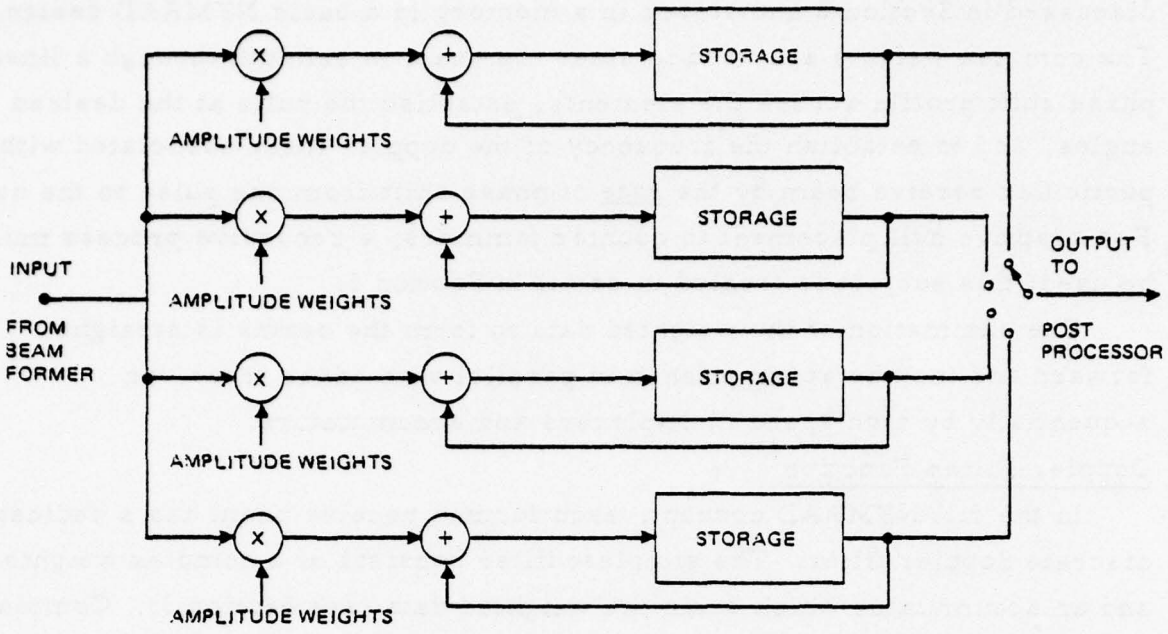


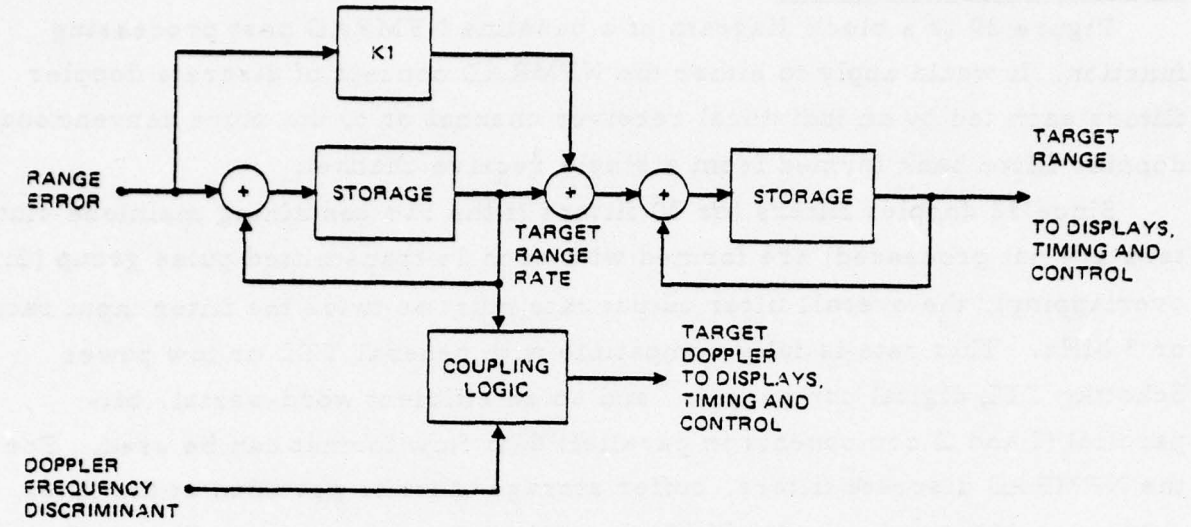
Figure 18. Doppler filter functional block diagram.

In a "single receive beam" NFMRAD design, the outputs from the antenna elements would be combined with only a single set of weights to form but one receive channel. In this case, the doppler filter function would be a bank of 32 doppler filters using a fast Fourier transform or other algorithm.

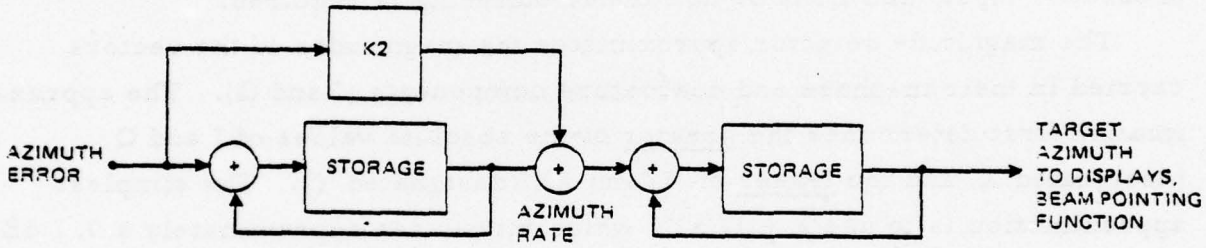
Track Processor

It is assumed that a designated target will be tracked in range, doppler frequency, and azimuth. A range error is developed by determining the difference between the signals in each of two split range gates and normalizing by dividing by the sum of the gate signals ("range discriminant"). A Class II servo is used; thus the range error represents target acceleration. The error is sent to an augmented integrator, whose output is proportional to target range rate. A second integrator converts range rate to target range, and this information is used by the timing and control function to position the track range gates in time. Figure 19 shows this portion of the tracking loop.

This figure also shows an open-loop frequency measurement (e.g., the difference between two adjacent doppler filters) being used to aid the range rate output from the range tracker. An alternative would be to form a closed



a. Range tracking loop



b. Azimuth tracking loop

Figure 19. Target track functional diagram.

loop system in which the doppler discriminant is used to position the spectrum (via a VCO) to center the target between two filters.

The azimuth tracking loop is shown in Figure 19b to be similar to the range tracking loop. The output of the double integrator is sent to the beam pointing function to complete the loop.

Both the data rate and functional operations are quite modest for the track processor, and either a microprocessor or dedicated hardwired circuit could be used. Some of the approaches of modern control theory (e.g., Kalman filtering) may be used instead of the classical track loops shown.

Post Processing Function

Figure 20 is a block diagram of a baseline NFMRAD post processing function. It would apply to either the NFMRAD concept of discrete doppler filters each fed by an individual receiver channel or to the more conventional doppler filter bank formed from a single receive channel.

Since 32 doppler filters (or 30 filters if the two containing mainlobe clutters are not processed) are formed with each 16 transmitted pulse group (2:1 overlapping), the overall filter output rate must be twice the filter input rate, or 5 MHz. This rate is fully compatible with general TTL or low power Schottky TTL digital components, and so an efficient word-serial, bit-parallel (I and Q components in parallel) data flow format can be used. For the NFMRAD discrete filters, buffer storage must be provided at the filter outputs to convert the "pulsed" filter output data to an even continuous flow at 5 MHz. For a single channel FFT filter bank, data storage is at the filter processor input, and little or no further buffering is required.

The magnitude detector approximates the magnitudes of the vectors carried in their in-phase and quadrature components (I and Q). The approximation first determines the greater of the absolute values of I and Q (designated X) and the lesser of $|I|$ and $|Q|$ (designated Y). The simplest approximation is to use $X + 1/2\ Y$, which introduces approximately a 0.1 dB loss in sensitivity. Somewhat more complicated algorithms provide greater accuracy. These include: (1) the greater of X and $(7/8X + 1/2Y)$ and (2) the greater of $(7/8X + 7/32Y)$ and $(3/4X + 1/2Y)$. If the processor were constructed from standard digital ICs, then the added complexity of the more accurate magnitude detector algorithms most likely cannot be justified. If a custom LSI chip is developed, then greater accuracy probably would cost no more and might as well be incorporated. The basic principle of the magnitude detector approximations is to phase rotate a signal vector until it is close to 0 degrees, then take the real component of the rotated vector. Generally a slight scale factor change is involved. For example, it can be shown that the operation $3/4X + 1/2Y$ is equivalent to $0.9\ (X \cos 33.7^{\circ} + Y \sin 33.7^{\circ})$ which is 0.9 times the real component of a vector $X + jY$ rotated through -33.7 degrees.

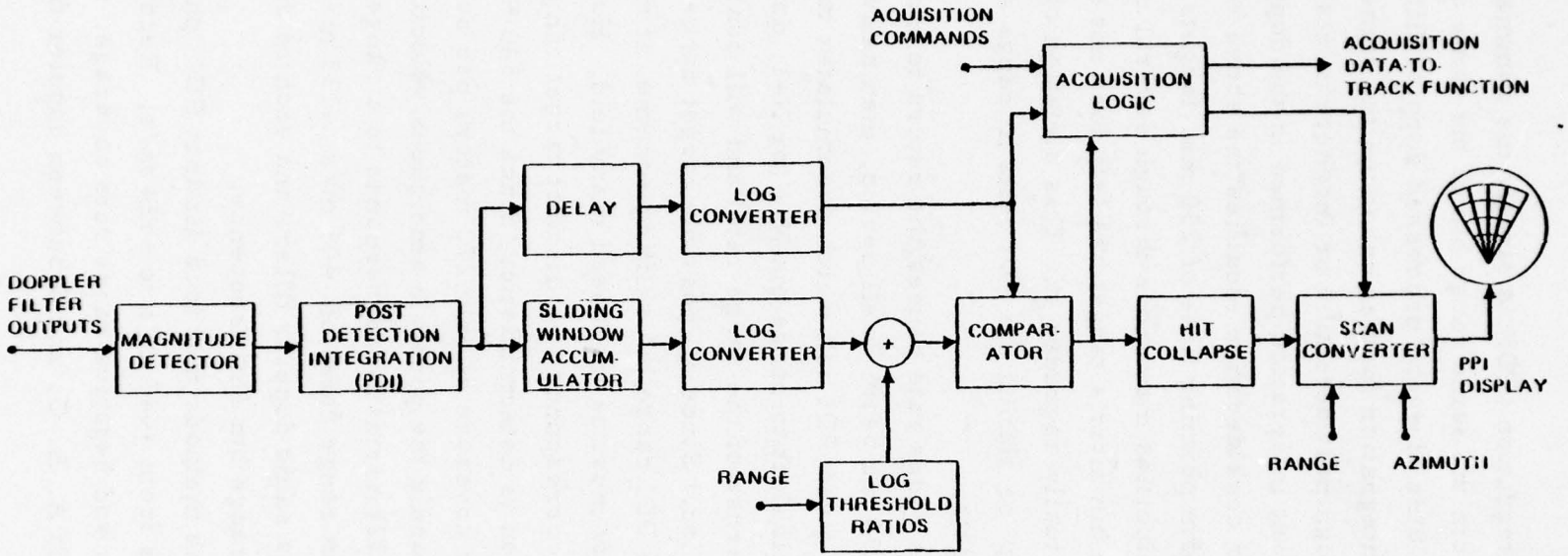


Figure 20. NFMRAD post processing function.

Post detection integration (PDI) is simply the summation of the magnitudes of data from the same range bin of the same doppler filter, and all appropriate range bins of every processed doppler filter are individually accumulated. This integration further enhances the signal-to-noise ratio of target returns, although post detection or incoherent integration is not as efficient as the coherent integration performed in the doppler filtering process. One further consideration modifies the above somewhat. During the relatively long beam pointing time of 750 ms, targets with the higher closing or opening velocities may move through several range bins. Continued PDI of a range bin after a target has left does not enhance the signal-to noise ratio, but actually degrades it! This situation can be remedied by periodically "slipping" or shifing the PDI cells in range according to the range rate of the targets.

Thus if a target's range rate causes the return to move through two range bins during a 750 ms beam dwell period, then halfway through the integration period, a given PDI cell which accumulates the magnitude data from range bin N, will shift to range bin N-1 (or N+1, depending on the positive or negative sense of the range rate) and will continue until the end of the integration period. Since all possible target range rates must be accommodated by the PDI range bin shifting scheme, it might seem that the PDI circuit complexity must be increased many fold. However, a given doppler filter output corresponds to a distinct target range rate, and so the range bin shift function is deterministic. Since the 540 Hz PRF has an unambiguous velocity coverage of only 270 meters per second, multiple PDI accumulators must handle the possible ambiguous velocities. For example, doppler filter 16 (of 32) normally corresponds to a range rate of 135 meters per second, but target range rates of -405 m/s, -135 m/s, and +405 m/s will also fold into this same doppler filter, and each of these range rates requires a different range bin shift sequence.

Table 3 shows the methods that four distinct PDI "phases" use to handle all target range rates from -447 m/s to +624 m/s. Because of the non-symmetrical positive and negative range rate coverage, there is a "break" in the sequence in PDI A, B, C, and D between doppler filters 10 and 11.

TABLE 3. PDI RANGE RATES AND RANGE BIN SHIFT PERIODS

Filter Number	PDI A		PDI B		PDI C		PDI D	
	$\dot{R}$, M/S	Shift	$\dot{R}$, M/S	Shift	$\dot{R}$, M/S	Shift	$\dot{R}$, M/S	Shift
0	-270	-7.5	0	-	270	7.5	540	3.8
1	-262	-7.7	8	-	278	7.3	548	3.7
2	-253	-8.0	17	-	287	7.1	557	3.6
3	-244	-8.3	25	-	295	6.9	565	3.6
4	-236	-8.6	33	-	303	6.7	573	3.5
5	-227	-8.9	42	-	312	6.5	582	3.5
6	-219	-9.2	50	-	320	6.3	590	3.4
7	-210	-9.6	59	-	329	6.2	599	3.4
8	-202	-10.0	67	-	337	6.0	607	3.3
9	-194	-10.4	75	-	345	5.9	615	3.3
10	-185	-10.9	84	-	354	5.7	624	3.2
11	-447	-4.5	-177	-11.4	92	22	362	5.6
12	-438	-4.6	-168	-12	101	20	371	5.5
13	-430	-4.7	-160	-13	109	19	379	5.3
14	-421	-4.8	-151	-13	118	17	388	5.2
15	-413	-4.9	-143	-14	126	16	396	5.1
16	-405	-5.0	-135	-15	135	15	405	5.0
17	-396	-5.1	-126	-16	143	14	413	4.9
18	-388	-5.2	-118	-17	151	13	421	4.8
19	-379	-5.3	-109	-19	160	13	430	4.7
20	-371	-5.5	-101	-20	168	12	438	4.6
21	-362	-5.6	-92	-22	177	11.4	447	4.5
22	-354	-5.7	-84	-	185	10.9	455	4.4
23	-345	-5.9	-75	-	194	10.4	464	4.4
24	-337	-6.0	-67	-	202	10.0	472	4.3
25	-329	-6.2	-59	-	210	9.6	480	4.2
26	-320	-6.3	-50	-	219	9.2	489	4.1
27	-312	-6.5	-42	-	227	8.9	497	4.1
28	-303	-6.7	-33	-	236	8.6	506	4.0
29	-295	-6.9	-25	-	244	8.3	514	3.9
30	-286	-7.1	-16	-	253	8.0	523	3.9
31	-278	-7.3	-8	-	261	7.7	531	3.8

Since each PDI accumulator receives an input every 16 pulses (or every 29.63 ms), this unit of time is used as the basic interval in determining the shift sequences. For 60 meter range bins, the number of basic intervals between range bin shifts is 60 x 540 ÷ 16 = 2025 divided by the range rate in meters per second. The shift periods are listed in Table 3 in units of the

29.63 ms PDI update intervals. These intervals are given to the nearest tenth; for example, a shift period of 5.2 would be implemented as a shift after 5 (5.2 rounded), 10 (10.4 rounded), 16 (15.6 rounded), and 21 (20.8 rounded) PDI inputs. There are 25 PDI input intervals in a beam dwell time, but the first PDI input does not occur until the fourth interval because 64 pulses are required to form a doppler filter.

Since there are 4000 active range bins, 30 doppler filters processed, and four PDI phases, there are 480,000 distinct PDI cells that undergo separate accumulation. This might be considered to represent a substantial hardware requirement, but 16K RAM (random access memory) chips should be quite common in the NFMRAD time period, and even if 16 bits are carried in the PDI, the storage requirement for the PDI function would be accomplished with 480 ICs, or only a few circuit boards of components.

The sliding window, log converters, log threshold ratios, and comparator comprise the constant false alarm rate (CFAR) hit-miss threshold function.

For thermal noise, the magnitude detector output will have a Rayleigh probability density distribution. The 22:1 PDI (19.9:1 effective) converts this distribution to approximately a non-zero mean, Gaussian form (a Rayleigh distribution convolved with itself about 20 times). To achieve a false alarm probability of approximately 5×10^{-9}, a threshold level must be established at about 6.4σ (standard deviations) higher than the mean. (If the distribution were fully Gaussian, then only 5.7σ would be required. A Rayleigh distribution would need a threshold 7.5σ above the mean.) For a Rayleigh distribution, the ratio of the standard deviation to the mean, σ/m, is $\sqrt{2/\pi}$ or 0.523. The effective 19.9:1 PDI reduces this ratio by $\sqrt{19.9}$, or to 0.117. Thus a threshold set 6.4σ above the mean is $6.4 \times 0.117 = 0.75$ means above the mean; i.e., the threshold-to-mean ratio is 1.75. Therefore, if a threshold value which is 1.75 times the noise mean level of the PDI output is established, then a false alarm probability of 5×10^{-9} should result regardless of various gain changes and other system vicissitudes.

The mean of a distribution must, of course, be estimated by one measurement method or another. The method proposed for the NFMRAD signal processor is to average 16 range bins to estimate the mean value. A detail of the sliding window implementation is shown in Figure 21. As a datum enters the 16 long shift register, it gets accumulated into the contents of the storage register where it remains until it is subtracted as it leaves the shift register. Thus the accumulation register maintains a running sum of the 16 range bins currently in the shift register. Subsequent division by 16 is a simple bit shift. To enable a range bin to be tested against a threshold derived from the mean level of its immediate neighbors, the signal is taken from the center tap of the shift register. Range bins from the same PDI phase of the same doppler filter are run through the sliding window accumulator, of course.

Two considerations modify the 1.75 threshold ratio. One is that the mean is, in fact, an estimate and is "noisy". Since 16 range bins are averaged to estimate the mean, the σ/m ratio of the mean estimate is only one-fourth that of the signal data. The noisiness does become amplified by the threshold multiplication ratio (i.e., 1.75) and effectively is added to the signal at the comparator. If the threshold ratio based on a perfect mean

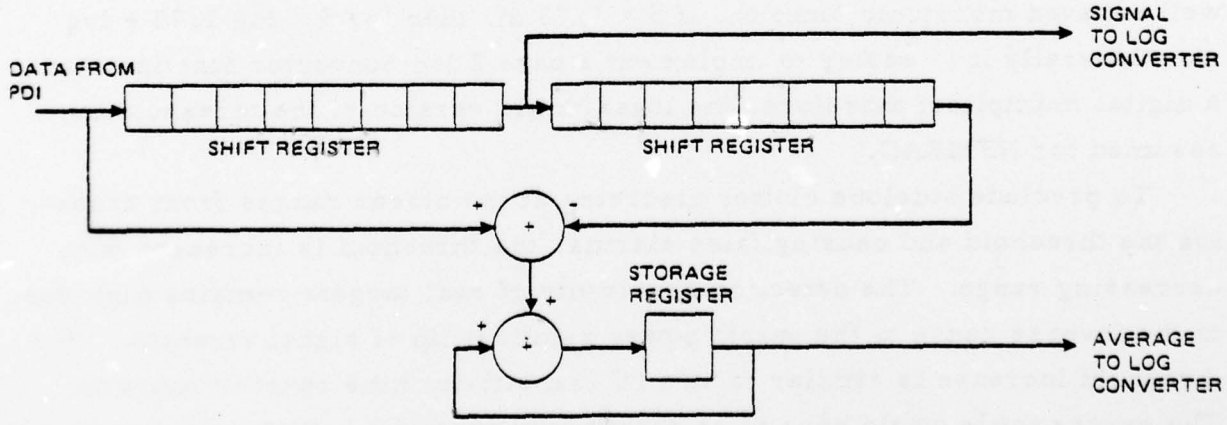


Figure 21. Sliding window accumulator detail.

level estimate is designated 1 + U, then the ratio C based on an average of N range bins is given by

$$C = \frac{1 + U\sqrt{1 + (1-U^2)/N}}{1 - U^2/N}$$

It can be seen that, if $N = \infty$, $C = 1 + U$. For $U = 0.75$ and $N = 16$, C from the above formula is 1.82.

The other threshold modifying consideration is that the signal itself is included in the mean estimate. For a signal right at the threshold level

$$S = R \times (15N+S)/16$$

where

S = signal level to cross threshold

R = corrected threshold ratio (to be determined)

N = noise mean level

Solving for R yields

$$R = \frac{16S}{15N+S} = \frac{16}{15N/S+1}$$

Since from the previous discussion $N/S = 1/1.82$, $R = 16/(15/1.82+1) = 1.73$.

In a straightforward mechanization of a threshold, a target hit would be generated if $S > 1.73\,\hat{m}$, where S is the signal cell being tested and $\hat{m}$ is the mean level estimate from the sliding window accumulator. Since the log is a well behaved monotonic function, if $S > 1.73\,\hat{m}$, then $\log S > \log 1.73 + \log \hat{m}$. Generally it is easier to implement a base 2 log converter function than a digital multiplier; therefore, the logarithmic version of the threshold is assumed for NFMRAD.

To preclude sidelobe clutter discretes at the closer ranges from crossing the threshold and causing false alarms, the threshold is increased with decreasing range. The detection sensitivity of real targets remains high due to the inverse range to the fourth power relationship of signal strength. The threshold increase is similar to an STC (sensitivity time control) function. The exact profile would have to be determined from the actual parameters of a particular application, including clutter levels.

After hits are established from the 4000-odd range bins of one PDI phase of a given doppler filter, similar data from another PDI phase are run through, etc., until the complete array from an antenna dwell time is covered. A hit collapse function is used to store hits in the proper range bin designation as they come through and thus collapse or logically "OR" all the hits for the same range from the various PDI phases of the doppler filters. (This would be modified if velocity information were displayed during search.)

The scan converter converts the hits from the threshold to the signal forms suitable for the display medium. It is assumed that the polar coordinate range azimuth system must be converted to x y coordinates, as required by the display CRT, and that the contents of the scan converter memory are repeatedly and rapidly read out to the CRT to provide a flicker-free display. The scan converter probably will include a controllable target aging function in which a target hit is displayed brightly when first generated, and then this hit is gradually dimmed with the passage of time. Thus helpful target "trails" are generated on the display.

It is assumed that a tracking mode will be entered into by positioning a cursor about a desired target and initializing an acquisition sequence by pushing a track button, etc. Such commands are sent through acquisition logic in the post processor so that the processor can "see" which target is desired to be tracked. The acquisition logic examines the hit-miss data at the commanded range, further compares all PDI phases and doppler filters that might have hits within the range window, and determines the strongest signal. Thus the target's range rate can be used to initialize the tracking loops.

Master Timing and Mode Control

In a typical radar system development program, the timing and control function is the last to be designed because the master timing and mode control function supplies the various clocks, timing signals, and other control synchronizing signals to the other functional areas. These signals cannot be specified until the design of the receiving circuitry has been established. In

broad terms, the signals generated by the master timing and control function include

1. Transmit pulse trigger
2. A/D range bin sampling strobe
3. Beam move command
4. Doppler filter formation timing strobe
5. PDI synchronizing strobe
6. Display synchronizing strobe
7. Interface data synchronizing signals
8. Master clock signals to entire system.

5.0 ELECTRONIC COUNTER-COUNTERMEASURES

The parallel receiving structure of the NFMRAD lends itself readily to incorporation of ECCM by the adaptive antenna nulling method. A typical scenario may be several jammers with unknown locations and powers interfering with the NFMRAD, and the objective of the ECCM is maximization of the signal-to-interference ratio (SIR) while still maintaining acceptable MTI performance. This section contains a description of a computer simulation of a proposed algorithm that computes a new weighting function and applies it to the receiving array during each PRI. The continual changing of the receiver antenna pattern compensates rapidly for changes in the jammer environment. The proposed implementation works as follows. After the jth pulse is transmitted, the received signal from each element of the array is sampled by the A/D converters connected to the I/Q detectors. The samples can be represented by a complex column vector, $\underline{y}_j$, written as

$$\underline{y}_j = \begin{bmatrix} y_1 \\ y_2 \\ \vdots \\ y_k \\ \vdots \\ y_{32} \end{bmatrix} \tag{13}$$

where

$$y_k = I_k + jQ_k \tag{14}$$

and I_k, Q_k are the sampled outputs of the kth I/Q detector.

If jammer nulling were not incorporated, then the receiver output for the pth beam would be obtained by weighting the received samples using a weight vector, $\underline{w}_j$, written as

$$\underline{w}_j = \begin{bmatrix} w_1^p \\ w_2^p \\ \vdots \\ w_k^p \\ \vdots \\ w_{32}^p \end{bmatrix} \tag{15}$$

where $\left\{w_k^p\right\}$ are complex scalars that weight the sampled outputs of the elements to maximize the signal-to-clutter ratio for the pth beam and a particular doppler filter output according to the basic NFMRAD concept. The receiver output, z, is given by the weighted sum of contributions from each element of the array or

$$z = \underline{w}_j^t \underline{y}_j \tag{16}$$

where $\underline{w}_j^t$ denotes the matrix transpose of $\underline{w}_j$.

For implementation of the adaptive algorithm for jammer nulling, samples should be obtained that have a large jammer-to-signal ratio (JSR) so that degradation of mainlobe gain is minimized. For a CW jammer, JSR is maximized by sampling either immediately before or after a transmitted pulse (as seen by the clutter profile curves) or during the time when radar return is suppressed by the first elevation sidelobe of the antenna. For pulsed jamming, the choice of sampling time is limited since the jammer must be sensed and sampled during the short time intervals when jamming is present. This matter is not critical since JSR will always be large if the

jammer is to be effective. Sidelobe blanking can also be used for pulsed jammers and will work in conjunction with the technique discussed here.

In the presence of jamming, $\underline{w}_j$ is not used but instead, the SIR is maximized by using a new weighting vector, $\underline{v}_j$, that is computed after the jth transmit pulse according to the equation

$$\underline{v}_j = c \wedge_j^{-1} \underline{w}_j \tag{17}$$

$\wedge_j^{-1}$ is the inverse of the covariance matrix of the interference, $\wedge_j$, and c is a complex scalar. $\wedge_j$ is defined in terms of the column vector of the interference $\underline{y}_j$ by the relation

$$\wedge_j = \underline{y}_j \underline{y}_j^* \tag{18}$$

where $\underline{y}_j^*$ is the complex conjugate transpose vector of $\underline{y}_j$; Equation (18) can be written out in expanded form as

$$\wedge_j = \begin{bmatrix} y_1 \\ y_2 \\ \vdots \\ y_k \\ \vdots \\ y_{32} \end{bmatrix} \begin{matrix} (y_1^* & y_2^* & \cdots & y_k^* & \cdots & y_{32}^*) \end{matrix}$$

$$= \begin{bmatrix} y_1y_1^* & y_1y_2^* & \cdots & y_1y_k^* & \cdots & y_1y_{32}^* \\ y_2y_1^* & y_2y_2^* & \cdots & y_2y_k^* & \cdots & y_2y_{32}^* \\ \vdots & \vdots & & \vdots & & \\ y_ky_1^* & \cdots & & y_ky_k^* & & y_ky_{32}^* \\ y_{32}y_1^* & y_{32}y_2^* & & y_{32}y_k^* & & y_{32}y_{32}^* \end{bmatrix} \tag{19}$$

where y_k^* is the complex conjugate of y_k. From Equation (19) it is seen that the element in the pth row and qth column of Λ_j, $y_p y_q^*$, is equal to the complex conjugate of the element in the qth row and pth column, $y_q y_p^*$. This property can be written concisely as

$$\Lambda_j^{*} = \Lambda_j \tag{20}$$

where Λ^* is the complex conjugate transpose of Λ; matrices with this property are called Hermitian.

The inverse of a Hermitian matrix can be easily shown to be also Hermitian or

$$(\Lambda_j^{-1})^{*} = \Lambda_j^{-1} \tag{21}$$

so that the computation of Λ_j^{-1} is greatly simplified since $N \cdot (N+1)/2 = 528$ rather than $N^2 = 1024$ complex numbers must be computed and stored. The instantaneous value of Equation (18) is not suitable for use in the algorithm since it fluctuates too rapidly because of the rapidly varying nature of the interference. For this reason an estimate of the covariance matrix is utilized that weights the previous matrix and the present data according to the equation

$$\Lambda_j = \alpha \Lambda_{j-1} + (1 - \alpha)\, \underline{y}_j \underline{y}_j^{*} \tag{22}$$

where Λ_{j-1} is the estimate of the covariance matrix after the j-1th sample. α is a real scalar between 0 and 1 that provides a relative weighting between present and past data and, therefore, controls the time constant of the algorithm. The algorithm used to compute Λ_j^{-1} efficiently is based on the matrix identity

$$(P + \underline{y}\,\underline{y}^{*})^{-1} = P^{-1} - P^{-1}\,\underline{y}(\underline{y}^{*} P^{-1}\,\underline{y} + 1)^{-1}\,\underline{y}^{*} P^{-1} \tag{23}$$

where P is an aribtrary matrix and $\underline{y}$ is an arbitrary complex column vector. The factor $(\underline{y}^{*} P^{-1}\,\underline{y} + 1)$ is a scalar which is readily inverted, so that

Equation (23) involves only matrix multiplications and no matrix inversions. By utilization of (23), Λ_j^{-1} can be written as

$$\Lambda_j^{-1} = \frac{1}{\alpha}\Lambda_{j-1} - \frac{(1-\alpha)}{\alpha^2}\left[\frac{1-\alpha}{\alpha}\underline{y}_j^{*}\,\Lambda_{j-1}^{-1}\,\underline{y}_j + 1\right]^{-1}\left(\Lambda_{j-1}^{-1}\,\underline{y}_j\right)\left(\Lambda_{j-1}^{-1}\,\underline{y}_j\right)^{*} \tag{24}$$

Equation (24) can be computed rapidly since it requires no matrix inversions and only six matrix multiplications and several additions. As stated previously further reduction in time results because 528 rather than 1024 complex numbers need to be computed because Λ_j^{-1} is Hermitian.

In the preceding paragraphs an algorithm was described that should greatly enhance the performance of NFMRAD in a hostile jamming environment. Before the value of the algorithm can be judged however, the potential anti-jam performance that may be achieved, the degradation that may be imposed on the basic NFMRAD functions, and the complexity of implementation of this algorithm must be evaluated. The performance parameters of interest are effects on the antenna pattern such as main beam gain loss, degradation of doppler filter nulls, jammer nulling depths, and general sidelobe behavior. The parameters of interest in the implementation are layout, timing, number of multiplications and additions required and number of storage registers needed. The functional implementation of the algorithm, evaluation of its performance, and conclusions and recommendations for further study are given in the remainder of this section.

FUNCTIONAL IMPLEMENTATION

This section is a description of a proposed functional implementation of the ECCM algorithm, and its storage, computation, and timing requirements are presented. The chosen implementation is designed to reduce the overall computation time used by the algorithm by minimizing the number of arithmetic operations. The sequence of computations performed in the algorithm are illustrated in Figure 22. After the ECCM is turned on the inverse covariance matrix is set equal to the identity matrix, I, (1's along diagonal and 0's elsewhere),

$$\Lambda_1^{-1} = I. \tag{25}$$

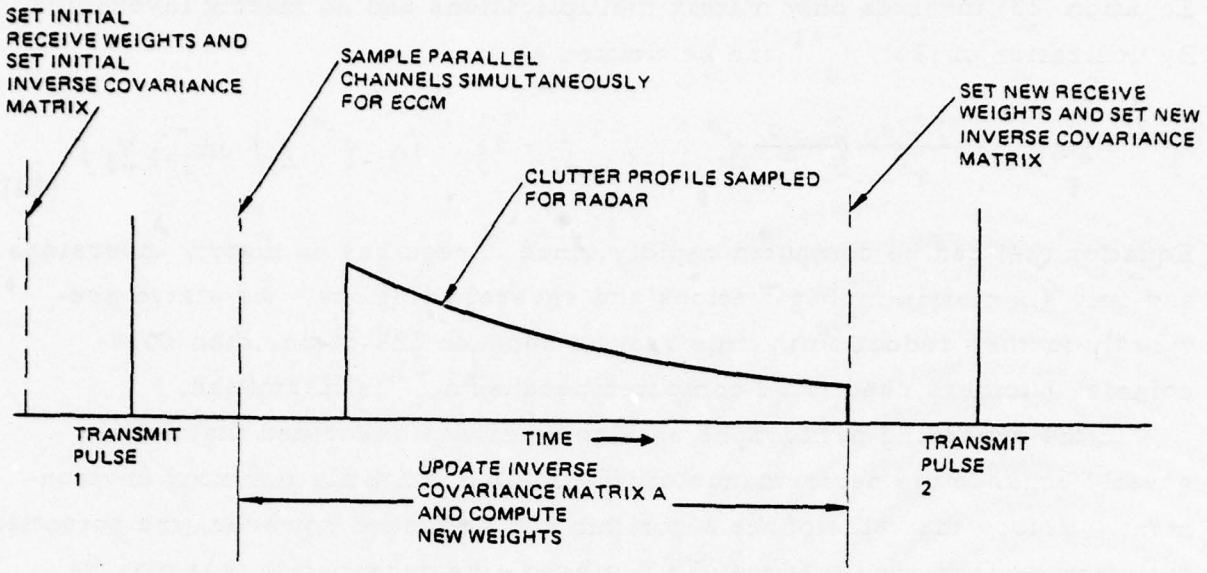


Figure 22. Timing diagram of NFMRAD incorporating ECCM algorithm.

The NFMRAD is then scanned to the first receive beam position. The non-ECCM weight vector, $\underline{w}_1$, corresponding to that beam position and a given doppler filter output are available from storage as the initial non-ECCM weight vector.

A pulse is transmitted, and the received signals are sampled simultaneously by the A/D converters before the radar pulse returns as shown in Figure 22. The computations required for one iteration of the algorithm that are shown in detail in the flowgraph in Figure 23 are then performed; a new inverse covariance matrix and a new weight vector related by Equation (17) result. This sequence of events is repeated after each transmit pulse, and, as will be described, the weight vector converges rapidly to a vector that maximizes the SIR by minimizing the jamming signals. The inverse covariance matrix also converges to a matrix that is a function of the jamming environment alone and not the receive beam position or doppler filter output. At the end of the first dwell time, the NFMRAD is scanned to the next receive beam position, and the same sequence of events is repeated. The convergence will now be more rapid than previously because the starting inverse covariance will be taken as the last computed inverse covariance matrix for the first beam position which has already converged; it is

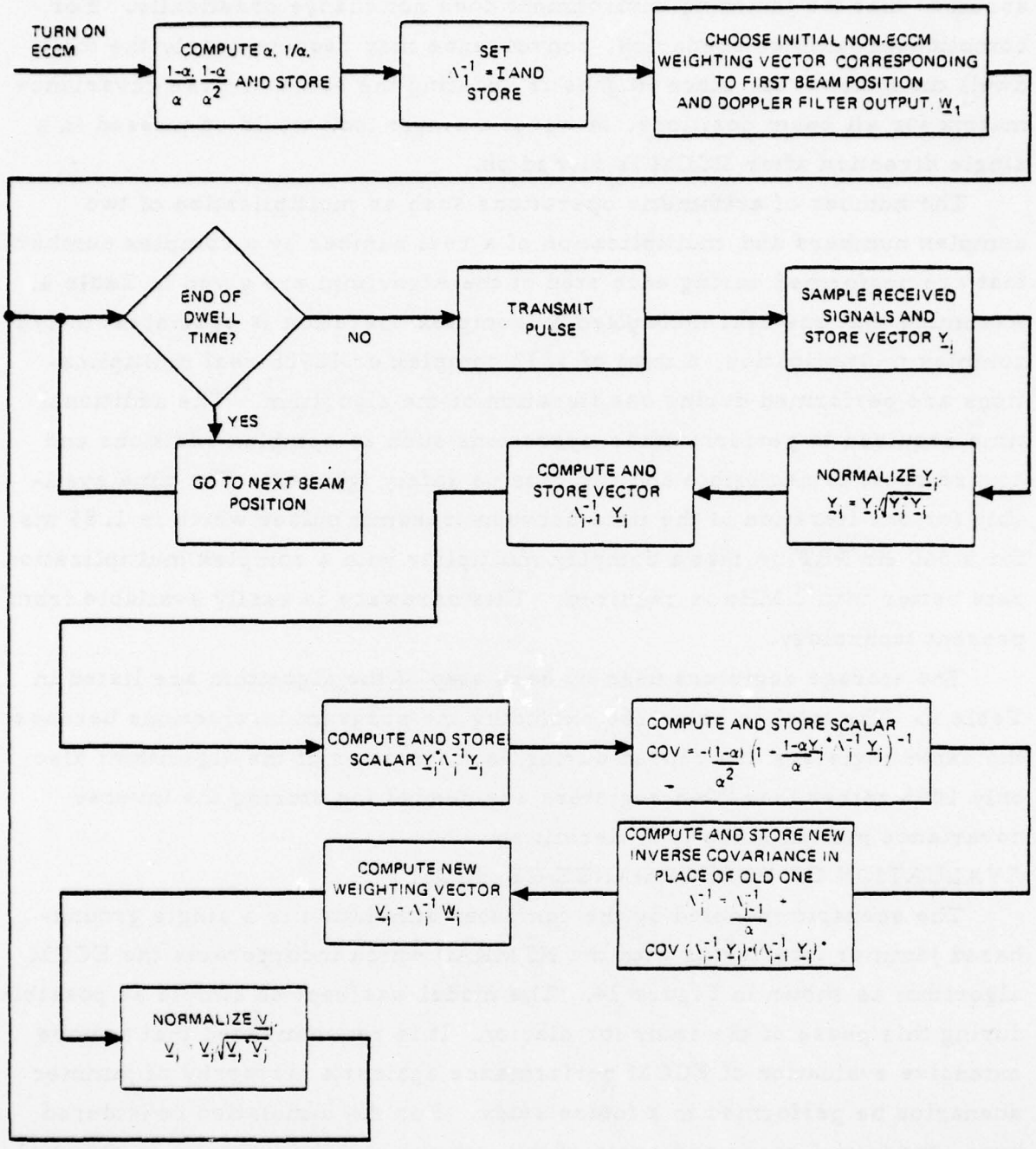


Figure 23. Implementation of ECCM adaptive algorithm.

BEST AVAILABLE COPY

assumed that the jamming environment does not change drastically. For complicated jammer scenarios, convergence may require nearly the total dwell time; however, since Hughes is updating the same inverse covariance matrix for all beam positions, at worst a single look would be missed in a single direction after ECCM is turned on.

The number of arithmetic operations such as multiplication of two complex numbers and multiplication of a real number by a complex number that are performed during each step of the Algorithm are given in Table 4. Assuming that one real multiplied by complex operation is equivalent to 1/2 complex multiplication, a total of 3232 complex or 12928 real multiplications are performed during one iteration of the algorithm. The additional time required to perform other operations such as complex additions and square roots is negligible and can thus be safely ignored. The time available for one iteration is the time between transmit pulses which is 1.85 ms for a 540 Hz PRF so that a complex multiplier with a complex multiplication rate better than 2 MHz is required. This hardware is easily available from present technology.

The storage registers used by each step of the algorithm are listed in Table 4. The total is only 1260 excluding the program instructions because the same registers are reused during each iteration of the algorithm; also only 1056 rather than 2048 registers are needed for storing the inverse covariance matrix since it is Hermitian.

EVALUATION OF PERFORMANCE OF ECCM

The scenario modeled by the computer simulation is a single ground-based jammer interfering with the NFMRAD which incorporates the ECCM algorithm as shown in Figure 24. The model was kept as simple as possible during this phase of the study for clarity. It is recommended that a more extensive evaluation of ECCM performance against a hierarchy of jammer scenarios be performed in a future study. For the simulation considered here, the initial range and angle of the jammer and the jammer-to-thermal noise ratio were specified as input parameters; the simulation includes the change of jammer angle with time that results from the relative motion of the aircraft with respect to the jammer. The receive beam position was chosen as $\theta=0$ degrees or broadside to the flight vector. The weight vector for

TABLE 4. NUMBER OF OPERATIONS AND NUMBER OF STORAGE REGISTERS USED BY ECCM ALGORITHM

Sequence of Computations	Type of Operation				Number of Distinct Storage Registers Used
	CXC	C+C	RXC	RXR R÷R	
1. Compute and store α, $1/\alpha$, $(1-\alpha)/\alpha$, $(1-\alpha)/\alpha^2$				4	4
2. Normalize $\underline{y}_j$, $\underline{y}_j = \underline{y}_j \Big/ \sqrt{\underline{y}^*_j \underline{y}_j}$	32		32		64+1
3. $\Lambda_{j-1}^{-1} \underline{y}_j$	1024	1024			64
4. $\underline{y}_j^* \Lambda_{j-1}^{-1} \underline{y}_j$	32	32			1
5. $\mathrm{COV} = \frac{-(1-\alpha)}{\alpha^2} (1 + \frac{1-\alpha}{\alpha} \underline{y}_j^* \Lambda_{j-1}^{-1} \underline{y}_j)^{-1}$				3	1
6. $(\Lambda_{j-1}^{-1} \underline{y}_j)(\Lambda_{j-1}^{-1} \underline{y}_j)^*$	528				
7. $\mathrm{COV}\,(\Lambda_{j-1}^{-1} \underline{y}_j)(\Lambda_{j-1}^{-1} \underline{y}_j)^*$			528		2
8. $\Lambda_{j-1}^{-1} / \alpha$			528		2
9. $\Lambda_{j-1}^{-1} = \frac{\Lambda_{j-1}^{-1}}{\alpha}$ + COV. $(\Lambda_{j-1}^{-1} \underline{y}_j)(\Lambda_{j-1}^{-1} \underline{y}_j)^*$		528			1056
10. $\underline{v}_j = \Lambda_j^{-1} \underline{W}_j$	1024	1024			64
11. Normalize $\underline{v}_j$, $\underline{v}_j = \underline{v}_j \Big/ \sqrt{\underline{v}_j^* \underline{v}_j}$	32		32		1
Totals	2672	2608	1120	7	1260

C = Complex Number R = Real Number

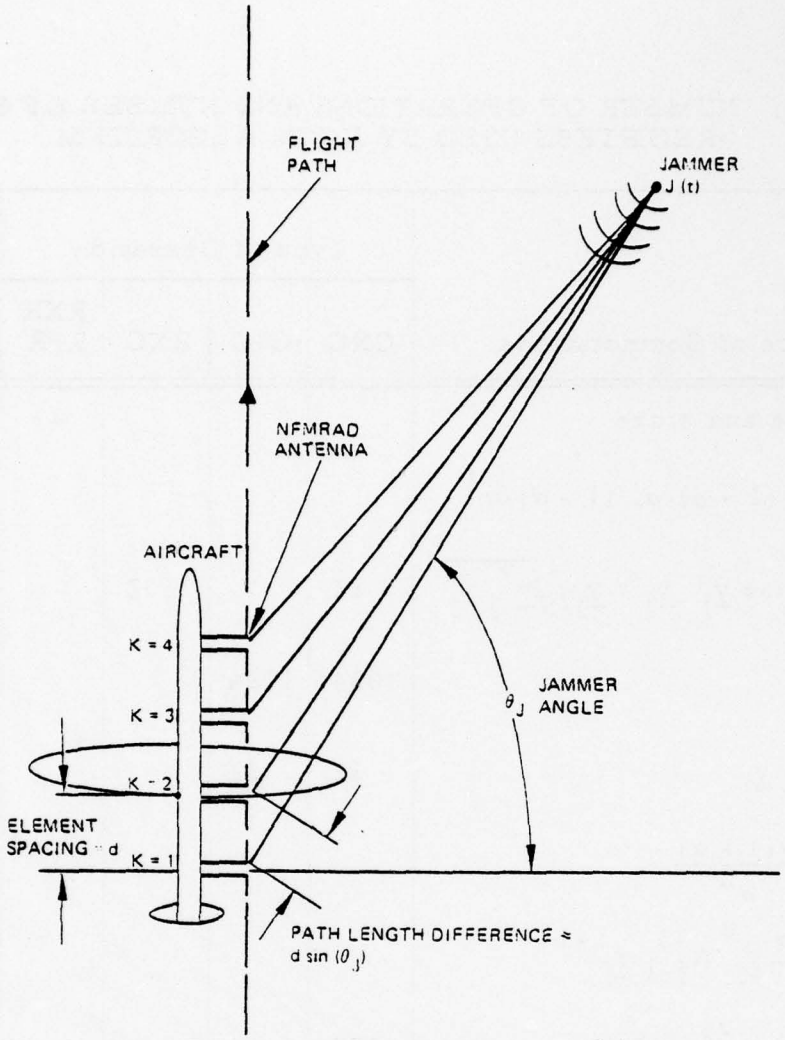


Figure 24. Geometry of NFMRAD and interfering jammer.

the non-ECCM case was constructed by placing nulls over sidelobe clutter angular regions corresponding to a typical doppler filter, and a computer program developed on another Hughes task was used for this purpose. Although these weights will not produce optimum target-to-clutter ratios, the departure from the optimum will be negligible. The wavelength was chosen to be 1 meter and the platform velocity 270 m/s which result in a range of sidelobe clutter doppler frequencies from -540 to 540 Hz. The PRF chosen to be 540 Hz for a maximum unambiguous range coverage of 150 n. mi resulted in a 2:1 velocity ambiguity and both positive and negative sidelobe clutter angular regions. The doppler filter chosen for the simulation covers

AD-A046 242 HUGHES AIRCRAFT CO CULVER CITY CALIF F/G 17/9
THE NULL FILTER MOBILE RADAR FEASIBILITY STUDY.(U)
JUL 77 R A BIRGENHEIER, C H LARSON F19628-76-C-0175
UNCLASSIFIED HAC-P77-161 RADC-TR-77-233 NL

2 OF 2
AD
A046242



END
DATE
FILMED
12-77
DDC

from 270.0 to 286.95 Hz which corresponds to two angular clutter regions, -30 to -28 degrees and 30 to 32.1 degrees.

The interference is the sum of jammer signal and thermal noise, and its jth sample is given by the complex vector, $\underline{y}_j$, where

$$\underline{y}_j = \underline{J}_j + \underline{n}_j \tag{26}$$

$\underline{n}_j$ is a complex thermal noise vector given by

$$\underline{n}_j = \begin{bmatrix} n_1 \\ n_2 \\ \vdots \\ n_k \\ \vdots \\ n_{32} \end{bmatrix} \tag{27}$$

where n_k is a complex number equal to the sampled thermal noise at the kth element. It is assumed that the $\{n_k\}$ are samples from stationary random processes with independent identical Gaussian probability distributions. $\underline{J}_j$ is a complex jammer vector written as

$$\underline{J}_j = \begin{bmatrix} J_1 \\ J_2 \\ \vdots \\ J_k \\ \vdots \\ J_{32} \end{bmatrix} \tag{28}$$

where J_k is a complex number equal to the sampled jammer signal at the kth element. Jammer signals received by different elements will have different time delays due to different path lengths as shown in Figure 24. Each J_k,

therefore, is sampled from the same jammer signal, J(t), but with a different relative time delay. J_k is thus given by

$$J_k = J(t_j - \tau_k) \tag{29}$$

where t_j is the sampling time and τ_k is the relative time delay of the kth element which is written as

$$\tau_k = (32 - k)\, d \sin(\theta_J)/c \tag{30}$$

where θ_J is the angle of the jammer from broadside and d is the interelement spacing as shown in Figure 24 and c is the speed of light.

The jammer signal is assumed to be narrow band so that it can be expressed as the product of a slowly varying envelope and a carrier or

$$J(t) = \underbrace{J_0(t)}_{\text{envelope}} \underbrace{\exp(j2\pi f_0 t)}_{\text{carrier}} \tag{31}$$

where f_0 is the carrier frequency. Equation (29) can then be written as

$$\begin{aligned} J_k &= J_0(t_j - \tau_k) \exp(j2\pi f_0 (t_j - (32 - k)\tfrac{d}{c} \sin\theta_J)) \\ &= J_0(t_j - \tau_k) \exp(j2\pi f_0 (t_j - 32\tfrac{d}{c} \sin\theta_J)) \\ &\quad \exp(jkk_0 U_0) \end{aligned} \tag{32}$$

where k_0 is the wavenumber and U_0 is given by

$$U_0 = d \sin(\theta_J) \tag{33}$$

so that

$$k_0 U_0 = 2\pi d \sin\theta_J/\lambda \tag{34}$$

where λ is the wavelength. Substitution of Equation (32) into (28) yields

$$J_j = \exp(j\psi_0) \begin{bmatrix} J_0(t_j - \tau_1)\exp(jk_0 U_0) \\ J_0(t_j - \tau_2)\exp(j2k_0 U_0) \\ \vdots \\ J_0(t_j - \tau_k)\exp(jkk_0 U_0) \\ \vdots \\ J_0(t - \tau_{32})\exp(j\,32\,k_0\,U_0) \end{bmatrix} \tag{35}$$

where

$$\psi_0 = 2\pi f_0 (t_j - 32\frac{d}{c}\sin\theta_J) \tag{36}$$

Since $J_0(t)$ is slowly varying, the relative delays can be neglected, and thus it may be assumed that $\tau_k = \tau_1$ in (23). The J_0 terms can then be factored out yielding

$$J_j = \exp(j\psi_0) J_0(t_j - \tau_1) \begin{bmatrix} \exp(jk_0 U_0) \\ \exp(j2k_0 U_0) \\ \vdots \\ \exp(jkk_0 U_0) \\ \vdots \\ \exp(j\,32\,k_0 U_0) \end{bmatrix} \tag{37}$$

Each term in the column vector of (23), $\exp(jkk_0 U_0)$, is the well-known complex phase factor of a linear antenna array. $J_0(t_j - \tau_1)$ is assumed to be sampled from a stationary random process with real and imaginary parts that are Gaussian and essentially uncorrelated over a sampling interval. The random numbers used to simulate samples of the jammer and the thermal noise are computed using random number generators, which are available in the DEC 10 computer library which was used for the simulation.

Several parameters were computed during the simulation to evaluate the system performance.

One parameter of interest is the antenna gain versus angle obtained at the jth iteration of the algorithm, $G_j(\theta)$, which is defined as

$$G_j(\theta) = \left| \underline{v}_j^t \underline{\xi}(\theta) \right|^2 \tag{38}$$

where

$$\xi(\theta) = \begin{bmatrix} \exp(jk_0U) \\ \exp(j2k_0U) \\ \vdots \\ \exp(jkk_0U) \\ \vdots \\ \exp(j32k_0U) \end{bmatrix} \tag{39}$$

and

$$U = d \sin\theta \tag{40}$$

Plots of $G_j(\theta)$ for increasing j will show the gradual pattern improvement resulting from repeated use of the ECCM algorithm. A related parameter is the integrated power over the angular regions corresponding to the doppler filter frequency band which is defined by

$$I_j(\theta_1, \theta_2) = \int_{\theta_1}^{\theta_2} G_j \, d\theta \tag{41}$$

where θ_1 and θ_2 are the lower and upper limits of an appropriate angular region. The change of I_j with increasing j will quantitatively estimate the NFMRAD degradation resulting from repeated use of the algorithm. Another important parameter is the jammer-to-noise ratio at the jth iteration, which is given as

$$(JNR)_j = (JNR)_0 \, G_j(\theta_j)/G_0(\theta_j) \tag{42}$$

$(JNR)_j$ estimates how rapidly the jammer is nulled by repeated use of the algorithm.

The simulation was run for cases whose parameters are consistent with those used in the rest of the study. These parameters for the case whose numerical results will be discussed here are given in Table 5. The jammer was nulled deeply and rapidly as shown in Figure 25 which is a plot of jammer-to-noise ratio versus time for 24 iterations of the ECCM algorithm. JNR dropped rapidly from 75 to 45 dB during the first 5 iterations and then decreased at a slower rate to 0 dB during the next 19 iterations. This behavior is expected because the initial inverse covariance matrix, Λ_1^{-1}, was equal to the identity matrix which deviates considerably from Λ_{24}^{-1}. As described in Section 5 more rapid convergence will be achieved for successive receive beam positions and doppler filter outputs assuming that the jammer environment does not change drastically since we will be updating the same inverse covariance matrix that has already converged. Assuming that ten iterations of the algorithm are sufficient for convergence during the second and succeeding beam positions and a typical dwell time of 0.75 s, only 2.5 percent of the dwell time will be needed for the algorithm to converge.

TABLE 5. PARAMETERS CHOSEN FOR SIMULATION

Parameter	Value Assumed
Jammer-to-Thermal Noise Ratio	75.0 dB
Jammer Range at t = 0	20 n. mi.
Jammer Angle at t = 0	20 degrees
PRF	540 Hz
Airplane Speed (KC-135)	270 m/s
α (Weight Parameter)	0.9
Receive Beam Direction	0 degrees
Doppler Filter Frequency Band	270 to 286.955 Hz
Element Spacing	0.5 wavelength
Carrier Frequency	300 MHz

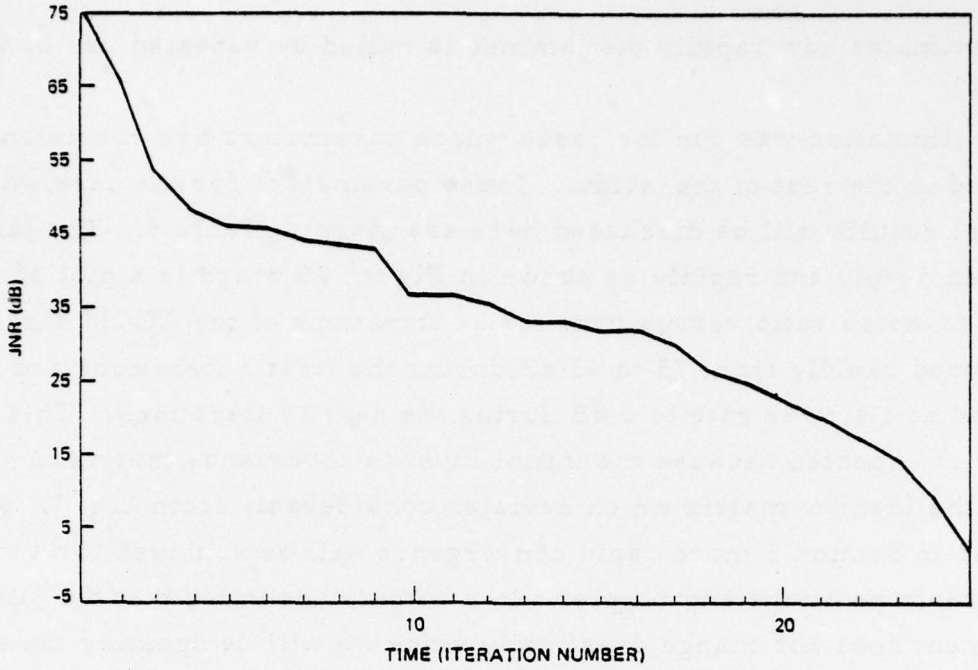


Figure 25. Jammer-to-noise ratio versus time.

The mainlobe gain loss after 24 iterations is only 0.016 dB and the general sidelobe structure is good as shown by plots of antenna gain versus angle before and after 24 iterations of the algorithm in Figure 26. Unfortunately, the NFMRAD performance is degraded as evidenced by filling in of the two null regions. The integrated powers for these two regions were computed according to Equation (41) and are listed in Table 6. In the process of nulling a jammer, degradation of low sidelobes in the vicinity of the jammer will generally occur. The degradation generally diminishes as the separation of the jammer and sidelobe region increases. The effect of jammer position is illustrated by the greater null filling of the positive angular region as compared to the negative angular region as shown in Table 6.

For extremely large jammer-to-thermal noise ratios numerical problems occur in implementation of the algorithm proposed herein. These problems result from the fact that for high power jammers, the matrix $\underline{Y}_j \underline{Y}_j^*$, which is singular, forces Λ_j to be ill-conditioned. Because of the non-linear effects of A/D conversion and saturation, however, it is not anticipated that ill-conditioning will really be a problem; nevertheless,

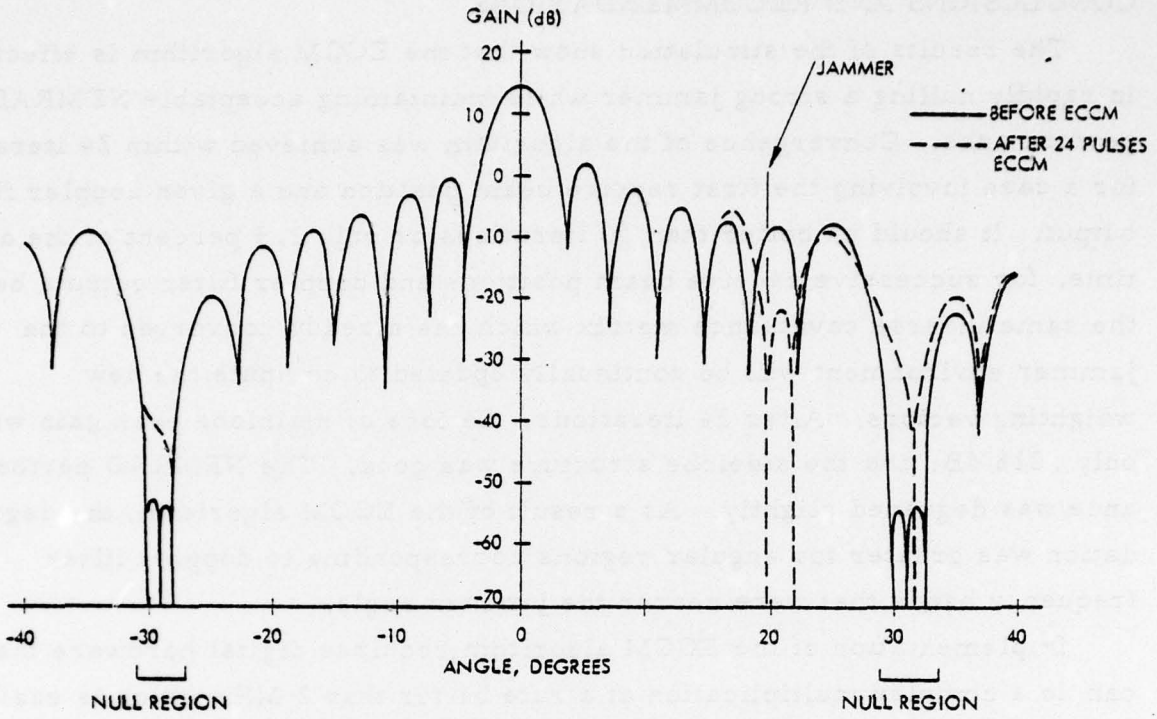


Figure 26. NFMRAD antenna pattern versus angle.

TABLE 6. INTEGRATED POWER OVER ANGULAR REGIONS CORRESPONDING TO DOPPLER FILTER FREQUENCY BAND

Angular Region	Before ECCM j = 1	After 24 Iterations ECCM j = 24	Total Change
I_j(-31 degrees, -27 degrees) dB	-51.200	-47.277	+ 3.923
I_j(29 degrees, 33 degrees) dB	-51.573	-40.085	+11.488

potential computational problems should be investigated further in the follow-on study.

CONCLUSIONS AND RECOMMENDATIONS

The results of the simulation show that the ECCM algorithm is effective in rapidly nulling a strong jammer while maintaining acceptable NFMRAD performance. Convergence of the algorithm was achieved within 24 iterations for a case involving the first receive beam position and a given doppler filter output. It should be better than 10 iterations or only 2.5 percent of the dwell time, for successive receive beam positions and doppler filter outputs because the same inverse covariance matrix which has already converged to the jammer environment will be continually updated to compute the new weighting vectors. After 24 iterations, the loss of mainlobe peak gain was only .016 dB, and the sidelobe structure was good. The NFMRAD performance was degraded slightly. As a result of the ECCM algorithm, the degradation was greater for angular regions corresponding to doppler filter frequency bands that were nearer the jammer angle.

Implementation of the ECCM algorithm requires digital hardware that can do a complex multiplication at a rate better than 2 MHz which is easily achievable with present technology. The storage required is only 1260 registers excluding the program instructions for the algorithm.

It is recommended that the simulation will be extended to characterize more realistic NFMRAD situations. Multiple jammers with pulsed modulation should be included as a possible jammer model. The effect on convergence of the proximity of the jammer angle to the angular regions corresponding to the frequency band of the doppler filter should be more thoroughly investigated. Different receive beam positions should be considered to evaluate their effect on the convergence rate and NFMRAD performance. The numerical problems experienced with large jammer to thermal noise ratios could also be investigated. The effect of computational errors due to truncation and roundoff should be studied by controlling the word sizes used in the simulations. The effect of saturation on the algorithm was not included during the present phase but should be included in the follow on study model.

6.0 AN ALTERNATIVE NFMRAD APPROACH

From the results in the previous sections, it was concluded that because of requirements for large dynamic range, the 2.5 MHz A/D sampling rate and the large amount of real-time computation required for doppler filtering and nulling of sidelobe clutter, the cost of the complex multipliers required for NFMRAD is very high. Moreover, it was found that for detection of targets with one square meter or greater radar cross-section against the mean level clutter level used for this study, adequate clutter suppression could be achieved simply by utilizing an antenna with -30 dB, peak, one way sidelobes. Therefore, unless it is necessary to detect targets with very low radar cross-sections, e.g. missiles for which σ = 0.1 square meters or the clutter levels are substantially higher than those used in this study, then it may be more cost effective to design a low sidelobe antenna that will provide adequate sidelobe suppression without the null filters.

In this section a system approach is briefly described that employs low antenna sidelobes for sidelobe clutter suppression and the NFMRAD concept for detection of [illegible] in mainlobe clutter. ECCM is provided by adaptive multipliers for each element of the array. This approach will substantially reduce the cost of NFMRAD by reducing the high-precision complex multiplication rate and will provide the additional capability of slow moving target indication. The description of the approach presented here will be brief; however, the feasibility of adding slowly moving target indication to NFMRAD will be studied during the next phase of this program.

GENERAL DESCRIPTION

A block diagram of an alternative NFMRAD approach is presented in Figure 27. The transmit-receive part of the system is identical to that considered previously; however, the digital processor is simplified considerably by performing adaptive weighting on all channels for jammer suppression and then combining the 32 channels into three channels for detection and tracking of slow moving targets. The NFMRAD concept could be implemented for detection of targets within mainlobe clutter by utilizing only two channels; however, if it becomes necessary to track a target while nulling clutter,

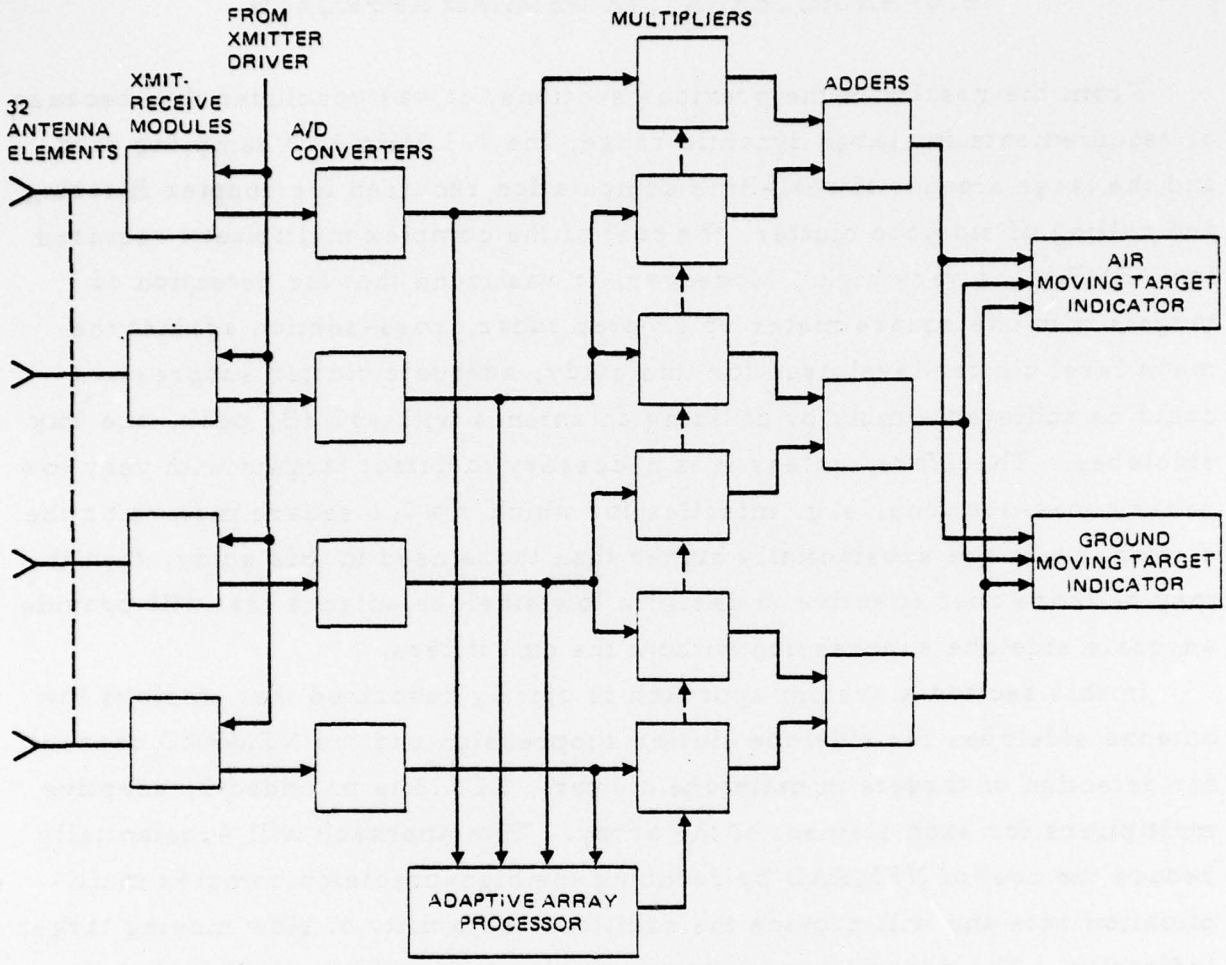


Figure 27. Three-channel MTI radar with adaptive jammer nulling.

then at least three channels are required. The three channel approach presented here reduces the number of complex multiplications per channel from 32 to 1.7 per A/D output which is a reduction by a factor of 19. The 1.7 multiplications per channel is obtained by assuming that 50 percent of the channels require two multipliers because of overlapping of subarrays and that five multiplications per A/D output are required for doppler filtering.

ADAPTIVE SUBARRAYS

The antenna is divided into three subarrays to provide the three channels required for detection and location estimation of movers whose doppler frequencies are within mainlobe clutter. Factors that influence the configuration of subarrays are:

1. The sum of the three channels must have low sidelobes to allow detection of movers in sidelobe clutter
2. The sum of the three channels should have high directivity to maximize MTI performance
3. The subarray patterns should be identical to minimize processor complexity
4. The directivity and separation of the phase centers of the subarrays should be increased to maximize performance of detection and estimation.

Factors 2 through 4 would lead to the utilization of uniformly weighted, contiguous (non-overlapping) subarrays; however, the requirement for low sidelobes necessitates an amplitude taper on the array. One method for achievement of low sidelobes is utilization of a symmetrical taper on each of the subarrays and overlapping of subarrays as shown in Figure 28. This approach has the advantage of high gain, low sidelobes, identical subarray patterns and better ECCM performance as will be discussed. The disadvantages are the requirement for 50 percent more complex multipliers and a separation of subarrays of only one-half the total array length. A tradeoff among advantages and disadvantages is required before a definitive approach can be recommended, but it appears that the advantages of overlapping subarrays override the disadvantages.

If the subarrays are controlled adaptively so that each subarray pattern has nulls in the direction of jammers, then any linear combination of the subarray outputs will also have nulls in the direction of jammers. By overlapping subarrays as shown in Figure 28, each subarray has half the number of controlled elements of the full array which should provide adequate control against complicated jammer threats. Since the subarrays have a larger beamwidth than the full array, more antenna gain is lost when nulling in the

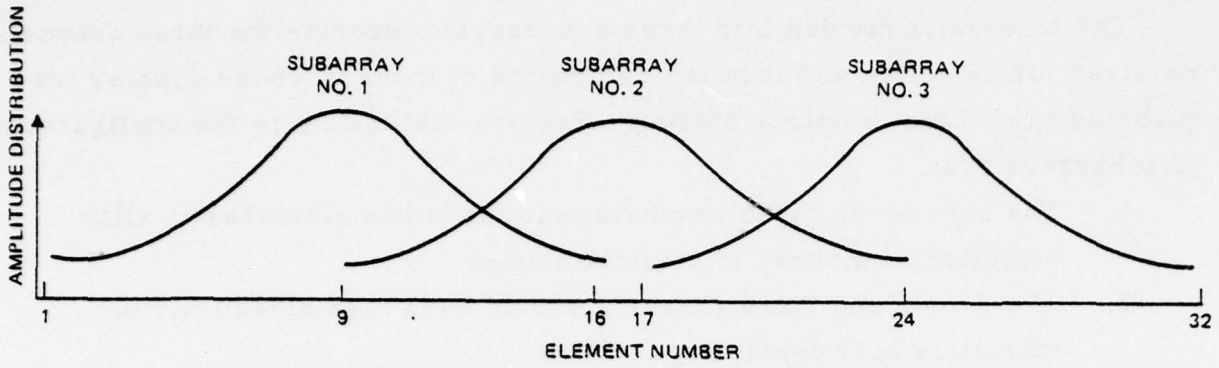


Figure 28. Amplitude weighting of overlapped subarrays.

mainlobe by producing a null in each of the subarray patterns as opposed to only producing a null in the total array pattern. The increased number of controlled elements and the decreased beamwidth obtained by overlapping subarrays is a distinct advantage for jammer nulling. The amount of computation required for adaptive control of the three subarrays is less than for control of the full array so that the computational load for adaptive nulling should not be a problem.

GROUND MOVING TARGET INDICATION (GMTI)

The block diagram of Figure 27 shows the three subarray outputs feeding the AMTI and GMTI processors. The AMTI utilizes the sum of the subarray outputs with an amplitude weighting for further reduction of antenna sidelobes. Doppler filtering in which the entire frequency interval between PRF lines is spanned by 32 filters or so, as described in section 4.0, is performed by the AMTI processor. The filters that span mainlobe clutter are not used by the AMTI processor, but the mainlobe clutter spectra is processed for GMTI.

The doppler frequencies of slowly moving targets are contained in the frequency band of mainlobe clutter; consequently, slow movers cannot be reliably detected by conventional MTI. The NFMRAD concept was originally conceived for improvement of detection of targets in sidelobe clutter; however, this method can be extended to detection of slow movers as well.

The maximum spread of mainlobe clutter and, consequently, the maximum range of target velocities occurs for the beam pointed at broadside. For a platform velocity of 270 m/s and a PRF of 540 Hz, the doppler spread of mainlobe clutter is approximately 540B cos θ, where B is the azimuth beamwidth and θ is the azimuth beam pointing direction relative to broadside. Since the null-to-null beamwidth of a uniformly weighted array of 32 elements with $\lambda/2$ spacing is $1/(8 \cos \theta)$, the maximum doppler spread of mainlobe clutter is approximately 60 Hz. Since the doppler frequency of a moving target is 540 sin θ Hz for the parameters considered here, any mover with a relative radial velocity of less than 15 meters/s would produce an output from the GMTI filters.

The NFMRAD requires a separate doppler filter bank for each of the receiver channels. If the NFMRAD concept is utilized only for detection of targets in mainlobe clutter, then only two channels are required. If in addition to target detection, accurate estimation of target location is necessary, then a third channel is required. Three identical doppler filter banks each fed by one of the subarray outputs is depicted by Figure 29. For any doppler filter of one filter bank there are identical filters for the other two banks so that by combining filter outputs the subarrays can be combined for each of the doppler filters to maximize T/C for target detection and estimation of target location.

In the NFMRAD described in the preceding sections, a single doppler filter passes clutter return over a range of approximately one-half a beamwidth so that nulls one-half beamwidth wide were required. If such a wide null were placed within the mainlobe, then mainlobe gain would be essentially destroyed. Consequently, extension of the NFMRAD concept to detection of slow movers within mainlobe clutter necessitates an improvement of doppler resolution so that narrowband nulls can be employed. The best MTI performance can be achieved if the clutter can be removed by placing only a single zero in the antenna pattern for each doppler filter. Based upon this criterion, the width of the doppler filters can be estimated by consideration of the width of three channels that are weighted to maximize T/C for a discrete target and clutter. This optimum weighting which

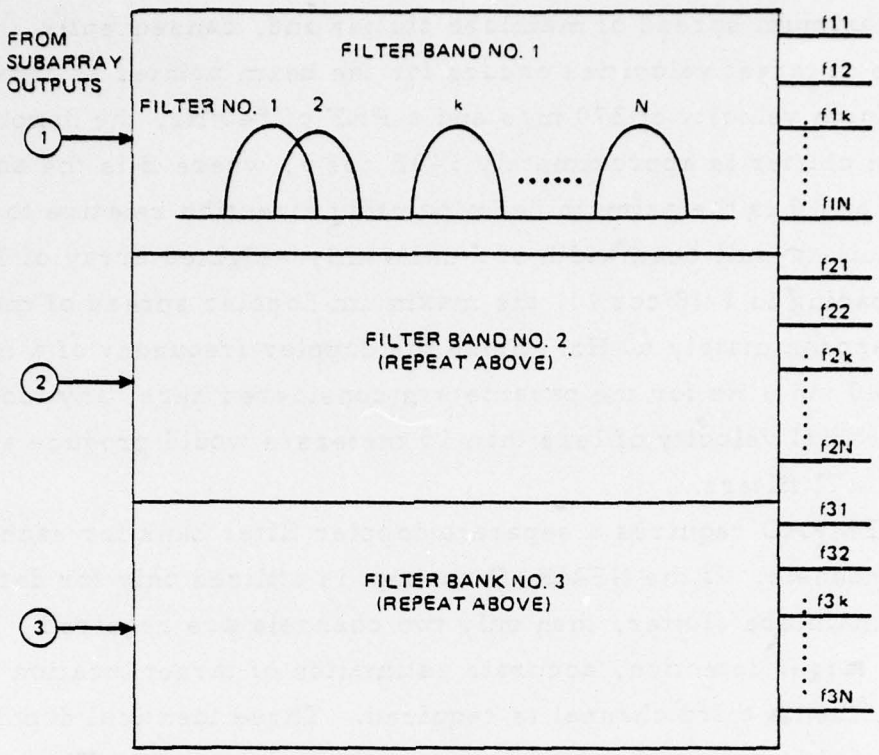


Figure 29. GMTI doppler processor.

is derived in appendix B is given by Equation (B-5). Utilizing this weighting for the case of infinite clutter-to-thermal noise ratio, the gain in the direction of a target was computed as a function of separation of the target and clutter; a curve is presented in Figure 30. From Figure 30, it can be seen that if it is desired to suppress clutter by at least 50 dB at the ends of the doppler filter band then the doppler filter bandwidth should be equivalent to 1/256th of an antenna beamwidth. Since the doppler filters must span two antenna beamwidths, 512 doppler filters are required. If 1024 pulses are utilized to form a filter output and the PRF is 540 Hz, then a dwell time of approximately two seconds would be required for the GMTI mode.

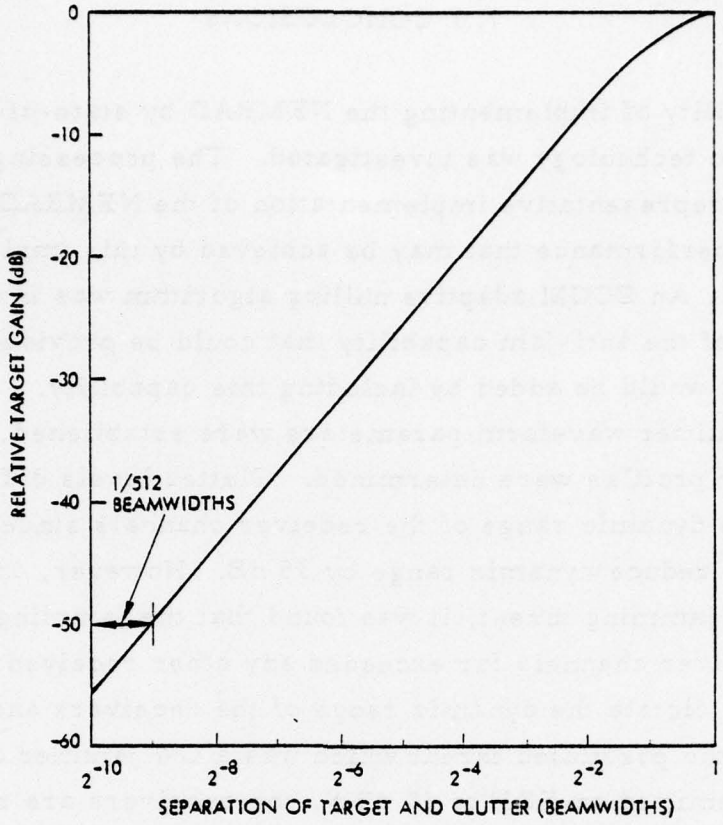


Figure 30. Three-channel null-pattern gain.

SUMMARY

This section gave an introduction of an approach that combines the 32 channels of NFMRAD into three channels that can be utilized for detecting and tracking of targets that reside in mainlobe clutter. During the next phase of this study, slow moving target indication (SMTI) will be studied in sufficient depth to allow the determination of the feasibility of incorporating an SMTI capability into the NFMRAD processor design.

7.0 CONCLUSIONS

The feasibility of implementing the NFMRAD by state-of-the-art LSI microelectronic technology was investigated. The processing hardware required for a representative implementation of the NFMRAD was determined and the performance that may be achieved by this implementation was addressed. An ECCM adaptive nulling algorithm was investigated in determination of the anti-jam capability that could be provided and the complexity that would be added by including this capability.

The transmitter waveform parameters were established, and the receiver power profiles were determined. Clutter levels did not impact severely on the dynamic range of the receiver channels since STC could be employed to reduce dynamic range by 35 dB. However, in consideration of a postulated jamming threat, it was found that the jamming signals in the individual receiver channels far exceeded any other received signals and probably would dictate the dynamic range of the receivers and A/D converters. For the postulated threat which was a CW jammer at a range of 20 n. mi. that emitted an ERP of 50 dBW, the receivers are required to have a 90 dB dynamic range and the A/D converters are required to have 14 bits.

The hardware requirements for a representative design of NFMRAD were determined and it was found that although the receivers and A/D converters represented a significant hardware investment, the digital multipliers required for the complementary beam-forming and doppler filtering far exceeded the cost of any other major segment of NFMRAD. It was found, for example, that the addition of the complex multipliers required to perform the full NFMRAD function represented an incremental cost of approximately 300 thousand dollars which may be twice the cost of an entire, conventional, pulse-doppler radar.

Signal-to-clutter ratios at a range-bin/doppler filter output were calculated for the clutter model and radar parameters considered for this study. From the SCR calculations, it was found that -50 dB two-way peak antenna sidelobes could provide adequate clutter suppression for detecting

1.0 square meter targets against the mean level clutter background. For severe cases in which the clutter background consists of a high density of large discretes, and it is desired to detect, for example, 0.1 square meter targets, -80 dB two way peak sidelobes may be required. Thermal receiver noise presents no problem in achieving excellent detection performance for the radar parameters chosen as was verified by a calculation of the probability of detection for a false alarm rate of one per hour.

The implementation of an ECCM technique was studied in some detail and the algorithm was tried through computer simulations. The algorithm generally worked well; however, for very high JNR's, problems were experienced with ill-conditioned matrices that will have to be resolved during the follow-on study.

Since the implementation of the full NFMRAD approach is expensive because of the very large amount of digital multiplication required per unit time, a simpler approach was suggested that still employs 32 parallel channels for ECCM but utilizes only two or three for MTI. This approach relies on non-adaptive, low antenna sidelobes for providing adequate sidelobe clutter suppression and the NFMRAD concept for detection of slow movers that reside in mainlobe clutter.

The general conclusions of this study are that the NFMRAD concept is technically feasible, although expensive. Several issues arose, however, that require further investigation before a design can be offered that represents a practicable solution to the MTI problem, both in terms of cost and performance. One very important area of investigation that has not been addressed in the current study is the limitation imposed by errors. The effects of the airframe presence and flexures on NFMRAD patterns must be examined. The magnitude and effects of system type errors such as velocity measurements and RF and PRF instabilities must be examined. It may turn out that, because of the error contributions, the open-loop NFMRAD approach considered here would not be feasible, in which case a clutter-based calibration technique or closed-loop, null filtering approach may be necessary.

In addition to the evaluation of the magnitude and effects of errors, further development and evaluation of adaptive jammer nulling is required and methods for reducing the cost of NFMRAD must be considered. These may involve alternative processor approaches and/or a departure from the full NFMRAD approach.

APPENDIX A. EFFECTIVE POST DETECTION INTEGRATION OF OVERLAPPED DATA

Consider the signal processing function shown in Figure A-1.

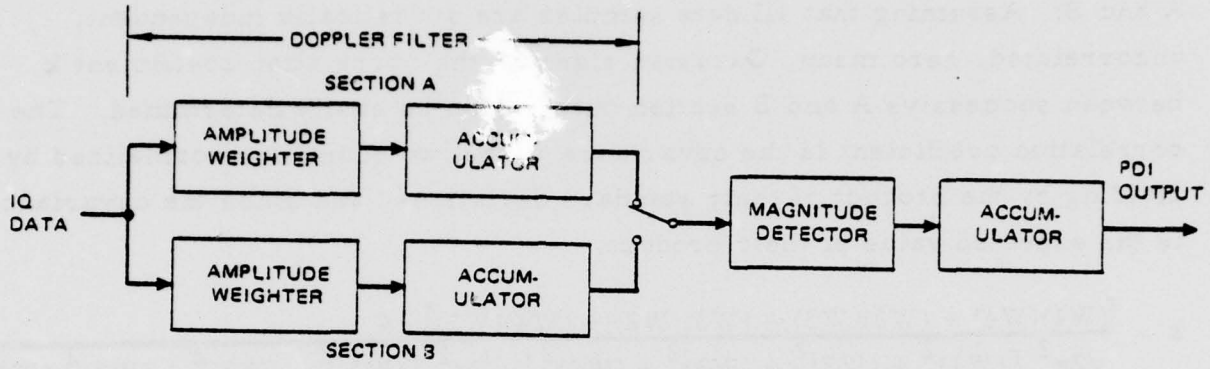


Figure A-1. Signal processing function.

Input IQ data is amplitude weighted and accumulated in a doppler filter circuit (for simplicity, a DC or zero doppler filter is shown). However, the two halves (A and B) of the filter are "out of phase" and yield outputs at alternate times. Figure A-2 shows how the doppler filter sections operate on common data in an overlapped fashion.

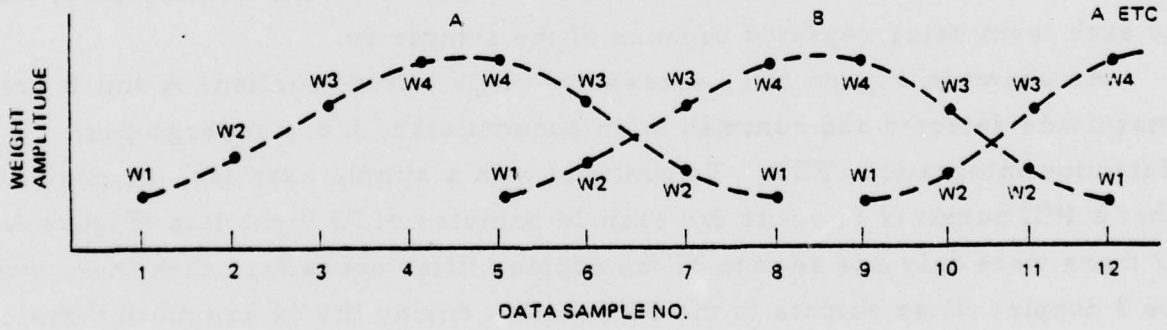


Figure A-2. Filter overlap operation.

Again for simplicity, for each doppler filter formation, eight data points are weighted with the symmetrical weights W1 through W4, and summed in an accumulator. Thus section A weights and sums samples 1 through 8 as shown. But section B similarly weights and sums samples number 5 through 12. It is seen that samples 5, 6, 7 and 8 are common to both the A and B filter formations, and so there will be some degree of correlation between A and B. Assuming that all data samples are statistically independent, uncorrelated, zero mean, Gaussian signals, the correlation coefficient k between successive A and B section outputs can be easily determined. The correlation coefficient is the covariance of the two quantities normalized by dividing by the product of their standard deviations, and since the covariance is the expected value of their product,

$$k = \frac{\left[(W1)(W4) + (W2)(W3) + (W3)(W2) + (W4)(W1)\right] \sigma^2}{\sqrt{2\sigma^2\left[(W1)^2 + (W2)^2 + (W3)^2 + (W4)^2\right]}\sqrt{2\sigma^2\left[(W1)^2 + (W2)^2 + (W3)^2 (W4)^2\right]}}$$

$$= \frac{(W1)(W4) + (W2)(W3)}{(W1)^2 + (W2)^2 + (W3)^2 + (W4)^2}$$

where σ^2 is the variance of the pre-weighted Gaussian signal (and gets cancelled out).

In general, the correlation coefficient of two overlapped weighted arrays is the sum of the products of the overlapped weights (in pairs) divided by the sum of the squares of the weights. For symmetrical weights, only half the terms need to be calculated for both the numerator and denominator, due to each term being repeated because of the symmetry.

As shown in Figure A-1, successive outputs from sections A and B are magnitude detected and summed in an accumulator, i. e., undergo post detection integration (PDI). To continue with a simple example, suppose that a PDI output is to occur for each 24 samples of IQ input data (Figure A-1). If there were only one section of the doppler filter operating, then there would be 3 doppler filter outputs to the PDI section during the 24 sample interval, since 8 samples comprise each doppler filter formation. But with a 2 section

50 percent overlap arrangement, there would be 5 doppler filter outputs during a 24 sample period. The 5 outputs from sections A and B are:

Input Sample No.	Section Output
8	A
12	B
16	A
20	B
24	A

In general, a 50 percent overlap increases a PDI ratio of N to 2N-1. If there were 4 filter sections operating on a 75 percent overlap basis, then the PDI ratio becomes 4N-3.

However, the effective PDI ratio will be less than the numerical ratio indicated above, due to the correlation introduced by overlapping. The probability density of the magnitude detector output will have a Rayleigh distribution, and there will be some correlation between successive outputs which is a function of the correlation of the Gaussian IQ signal entering the magnitude detector. The derivation of the functional relationship between the correlation coefficients of the magnitude detector input and output is somewhat involved, and is presented in the following paragraphs.

Consider two magnitude detector outputs, each the detected output of Gaussian noise having unity power (total). Each output has a Rayleigh probability density, and will have a power of 2. (The input power to the magnitude detector may be though of as unity for the I channel and unity for the Q channel, making a power output of 2 for the magnitude detector.) The power in each output may be considered as having a DC power component and an AC power component. It can be shown (Dwight, 850.1 ff)[A-1] that, for a unit power Gaussian input, the DC power of a detector output is $\pi/2$.* The AC power is the total power minus the DC power, or $(4-\pi)/2$.

A-1. H. B. Dwight, Tables of Integrals and Other Mathematical Data, The Macmillan Co., N. Y.

* The probability density of the Rayleigh output is given by: $p(x) = xe^{-x^2/2}$ and the value or mean is given by $\overline{x} = \int_0^\infty x^2 e^{-x^2/2}\, dx$; substituting $y = \frac{x^2}{2}$, $\overline{x} = \sqrt{2}\int_0^\infty y^{1/2} e^{-y}\, dy = \sqrt{2}\,\Gamma(3/2) = \sqrt{\pi/2}$.

If the two outputs are multiplied together, and the product averaged over a long period of time, the result would be the average of $(m_1+\sigma_1)(m_2+\sigma_2)$, where m is the mean or DC component, and σ is the AC or fluctuating component. The product is $m_1 m_2 + \sigma_1 m_2 + \sigma_2 m_1 + \sigma_1 \sigma_2$. The average value of the product is equivalent to the sum of the average values of each of the terms in the product. The product $m_1 m_2$ is simply the DC power, numerically equal in this case to $\pi/2$. The average values of $\sigma_1 m_2$ and $\sigma_2 m_1$ must both be zero, since by definition an AC fluctuation must average out to zero. The remaining term is $\sigma_1 \sigma_2$. If the AC components were completely uncorrelated, then the average of their products should be zero, because when one is positive, the other may be either positive or negative, and the product over the long run should average out to zero. However if σ_1 and σ_2 are completely correlated, they are in fact identical and in this case the average of the product $\sigma_1 \sigma_2$ is σ^2, which by definition is the AC power. If the AC powers are separated into two components, one of which is completely uncorrelated, and the other which is completely correlated or common between the two detector outputs, then the average $\sigma_1 \sigma_2$ product will have a zero contribution from the uncorrelated components, and will have a contribution equal to the power in the correlated components. If we designate the portion of the AC power which is correlated by ρ, then the average value of $\sigma_1 \sigma_2$ will be $\rho(4-\pi)/2$, since the value of the AC power has already been shown to be $(4-\pi)/2$ for a detector output with a unit power Gaussian input. In considering both the DC and AC components, the average value of the product of the two detectors is

$$\overline{E_1 E_2} = \frac{\pi}{2} + \rho(4-\pi)/2 \qquad \text{(A-1)}$$

Equation 9.23 of Middleton[A-2] gives

$$\overline{E_1 E_2} = \Psi\left[2E(k_o) - (1-k_o^2)\,K(k_o)\right]$$

A-2. D. Middleton, An Introduction to Statistical Communication Theory, McGraw-Hill, NY, 1960.

where Ψ is the Gaussian noise power entering the detector and k_o is the pre-detection correlation coefficient, which has been called k in this appendix. E is the complete elliptic integral of the second kind, and K is the complete elliptic integral of the first kind. The noise power Ψ has been normalized to unity, and may be ignored.

From Dwight, [A-3]

$$E(k) = \frac{\pi}{2}\left(1 - \frac{1}{2^2}k^2 - \frac{1^2 \cdot 3}{2^2 \cdot 4^2}k^4 - \frac{1^2 \cdot 3^2 \cdot 5}{1^2 \cdot 4^2 \cdot 6^2}k^6 - \ldots.\right)$$

And from Dwight, [A-4]

$$K(k) = \frac{\pi}{2}\left(1 + \frac{1^2}{2^2}k^2 + \frac{1^2 \cdot 3^2}{2^2 \cdot 4^2}k^4 + \frac{1^2 \cdot 3^2 \cdot 5^2}{2^2 \cdot 4^2 \cdot 6^2}k^6 + \ldots.\right)$$

Combining these series with Equation 9.23 of Middleton[A5] results in

$$\begin{aligned}
\overline{E_1 E_2} &= \pi\left(1 - \frac{1}{2^2}k^2 - \frac{1^2 \cdot 3}{2^2 \cdot 4^2}k^4 - \frac{1^2 \cdot 3^2 \cdot 5}{2^2 \cdot 4^2 \cdot 6^2}k^6 - \ldots.\right) \\
&\quad - \frac{\pi}{2}\left(1 + \frac{1^2}{2^2}k^2 + \frac{1^2 \cdot 3^2}{2^2 \cdot 4^2}k^4 + \frac{1^2 \cdot 3^2 \cdot 5^2}{2^2 \cdot 4^2 \cdot 6^2}k^6 + \ldots.\right) \\
&\quad + \frac{\pi}{2}\left(0 + k^2 + \frac{1^2}{2^2}k^4 + \frac{1^2 \cdot 3^2}{2^2 \cdot 4^2}k^6 + \ldots.\right) \\
&= \frac{\pi}{2} + \frac{\pi}{2}\left[\left(1 - \frac{1^2}{2^2} - \frac{2}{2^2}\right)k^2 + \left(\frac{1^2}{2^2} - \frac{1^2 \cdot 3^2}{2^2 \cdot 4^2} - \frac{2 \cdot 1^2 \cdot 3}{2^2 \cdot 4^2}\right)k^4 \ldots.\right] \\
&= \frac{\pi}{2} + \frac{\pi}{2}\sum_{n=1}^{\infty}(a_n - b_n - c_n)k^{2n} \qquad \text{(A-2)}
\end{aligned}$$

where

$$a_1 = 1,\ b_1 = 1/4, \text{ and } c_1 = 1/2$$

A-3. Dwight, op. cit., 774.1.

A-4. Ibid., 773.1.

A-5. Middleton, op. cit.

and where the following recursive relationships apply.

$$a_{n+1} = a_n \frac{(2n-3)^2}{(2n-2)^2}$$

$$b_{n+1} = b_n \frac{(2n-1)^2}{(2n)^2}$$

$$c_{n+1} = c_n \frac{(2n-1)(2n-3)}{(2n)^2}$$

Because Equations (A-1) and (A-2) each solve for $\overline{E_1 E_2}$, they must be equal to each other. Setting them equal to each other and solving for ρ yields

$$\rho = \frac{\pi}{4 - \pi} \sum_{n=1}^{\infty} (a_n - b_n - c_n) k^{2n}$$

Solving the above equation yields

$$\rho = 0.914948\, k^2 + 0.057184\, k^4 + 0.014296\, k^6 + 0.005584\, k^8 + \ldots.$$

Incidentally, it is shown by Middleton[A-6] that for a square law detector $\rho = k^2$.

Given that the correlation coefficient ρ of the AC component of successive magnitude detector outputs is determined (the DC components, of course, are always fully correlated), the effective post detection integration (PDI) may be calculated from the numerical PDI ratio and the correlation coefficient. This calculation is discussed below.

Assume that for simplicity the AC component of a magnitude detector output has been normalized to unity. Two successive magnitude outputs may each be considered to have an AC power component ρ which is completely correlated or in common between the two outputs, and an uncorrelated component $1-\rho$. If there are N successive magnitude detector outputs and all correlation exists only between adjoining outputs, then the addition of these N outputs may be represented as in Figure A-3.

A-6. Middleton, op. cit.

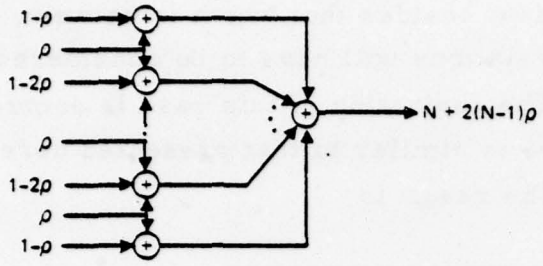


Figure A-3. Representation of addition of N outputs with adjacent correlations.

As shown, the correlated powers ρ are identically fed to adjacent outputs. Thus each output (except for the end points) has 2 ρ of correlated powers, leaving 1-2 ρ of uncorrelated power. The identical ρ signals, when added, double in amplitude, or become 4ρ in power. There are N-1 such 4ρ power contributors. As shown in Figure A-3, there are two "1-ρ" and N-2 "1-2ρ" uncorrelated power contributors, for a total of (N-1) 4ρ + 2 (1-ρ) = (N-2) (1-2ρ) = N + 2(N-1)ρ.

The Rayleigh distributed signal out of a detector (with a Gaussian noise input) will exhibit an AC to DC power ratio of $(4-\pi)/\pi$ or about 0.276. For no correlation, an M:1 PDI ratio will increase the AC power by a factor of M and the DC power by a factor of M^2; it thus changes the AC to DC power ratio by a factor of 1/M. This reduction of AC power relative to DC power is of course the purpose of having PDI, and so is a measure of the effectiveness of PDI. This can be turned around to say that M, the effective PDI ratio, is determined by how much the ratio of DC power to AC power has increased. In the example of N:1 PDI with a correlation coefficient ρ, the DC power has increased by a factor of N^2 (the DC power increase is always N^2, regardless of the value of ρ), and the AC power increase was shown to be N + 2(N-1)ρ. Thus, the ratio of the DC power increase to the AC power increase is

$$\frac{N^2}{N + 2(N-1)\rho} = \frac{N}{1 + 2\,\frac{N-1}{N}\,\rho} = M$$

where M is the apparent PDI ratio, i.e., the PDI ratio of an uncorrelated signal which would yield the equivalent reduction in the AC/DC power ratio.

If there are correlations among the data besides that which is between adjacent values, then all the various correlations will have to be considered in determining the effective PDI ratio. The derivation of this case is somewhat more complicated, but the procedure is similar to that presented here for the simplest correlation situation. The result is

$$M = \frac{N}{1 + 2\frac{N-1}{N}\rho_1 + 2\frac{N-2}{N}\rho_2 + 2\frac{N-3}{N}\rho_3 + \ldots}$$

$$= \frac{N}{1 + \frac{2}{N}\left[(N-1)\rho_1 + (N-2)\rho_2 + (N-3)\rho_3 + \ldots\right]}$$

where

M = effective PDI ratio

N = numerical PDI ratio after overlap

ρ_1 = correlation coefficient between adjacent PDI inputs (or detector outputs)

ρ_2 = correlation coefficient between PDI inputs having one intervening input

ρ_3 = correlation coefficient between PDI inputs having two intervening inputs

Etc.

It should be noted that the effective PDI ratios analyzed here have been based upon Gaussian noise only, and are applicable to establishing threshold ratios which achieve a given false alarm probability, etc. The signal-plus-noise case virtually defies analysis (see Middleton[A-7]) and would be required to determine probability of detection curves, etc. However, the trend of the signal-plus-noise case can be found from intuitive argument. The correlated component of the detector input noise apparently undergoes something like the "small signal suppression" phenomenon, in that it is reduced by the detection process.

The amount of relative reduction is greater for correlated components which are a smaller portion of the total power. Therefore, when the introduction of a signal makes the correlated noise component proportionally smaller, the detector output correlation becomes even more suppressed, and the effective PDI becomes closer to the straight numerical ratio. This

A-7. Middleton, op. cit., p. 416.

causes the AC fluctuations about the mean of the PDI output to shrink as the mean of the distribution becomes larger (due to a stronger signal). The net effect on the probability of detection curve is as that shown by the dotted line in Figure A-4. The point of the 50 percent probability of detection is essentially unchanged.

The computer program which follows (Table A-1) was used to calculate the effective PDI of the 64 point filter described in Section 3. The program was also used to generate the amplitude weights and determine the actual frequency response. As shown by the program execution printout (Table A-2) which follows the program listing, the applicable correlation coefficients ρ_1 and ρ_2 are 0.053772 and 0.000804, respectively. There also is a ρ_3, but it may be ignored, because it is so small.

Incidentally, the amplitude weighting loss of about 4.5 dB is calculated relative to 64:1 coherent integration, which is equivalent to 1.5 dB relative to 32:1 coherent integration.

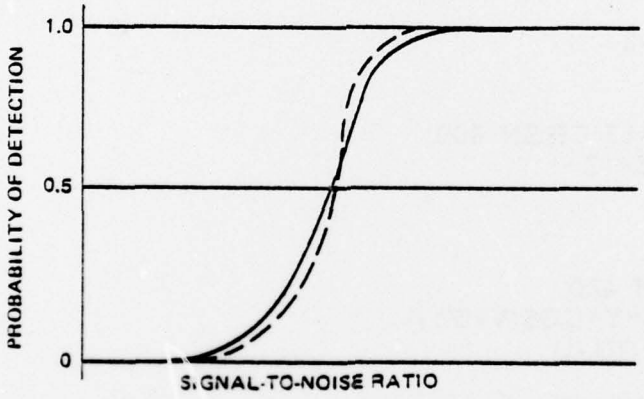


Figure A-4. Effect of correlation on probability of detection (with PDI processing)

TABLE A-1. PROGRAM LISTING

```
FILTER

1:####.# ####.# ####.# ####.# ####.# ####.# ####.# ####.# ####.# ####.#
100 DIM W(128)
110 READ N,F1
120 H=73
130 K=3.14159265/(N/2)
140 PRINT H:"DB.",N;"POINT CHEBYSHEV-COSINE FILTER"
150 PRINT
160 PRINT " NO.       CHEBYSHEV     COSINE      PRODUCT"
170 PRINT "___        __________    ______      ___________"
180 H1=EXP(H*LOG(10)/20)
190 A=EXP(2*(LOG(H1+SQR(H1^2-1))/(N-1)))
200 A=(A-1)^2/(A+1)^2
210 S1=S2=0
220 FOR I=N/2 TO 1 STEP -1
230 V=K*((N+1)-(2*I))
240 P=I-2
250 Q=N-I
260 X=Q*A
270 IF I>1 THEN 300
280 Y=1
290 GO TO 420
300 Y=0
310 Z=1
320 FOR S=0 TO I-2
330 Y=Y+X
340 Q=Q-1
350 IF ABS(X)<1E-15 THEN 400
360 X=X*P*Q*A/(Z*(Z+1))
370 P=P-1
380 Z=Z+1
390 NEXT S
400 IF I<N/2 THEN 420
410 M1=1/((2-2/N)*Y*COS(V*F1))
420 Y=Y*M1*(N-1)/(N-I)
430 Y1=COS(V*F1)
440 W(I)=W(N-I+1)=Y*Y1
450 PRINT USING 460,I,Y,Y1,W(I)
460 :####         ##.######         ##.######         ##.######
470 S1=S1+W(I)*2
480 S2=S2+(W(I))^2*2
490 NEXT I
```

(Continued)

(Table A-1, concluded)

```
500 PRINT
510 PRINT "AMP. WT. LOSS=";10/LOG(10)*LOG(S1^2/(N*S2));"DB."
520 PRINT
530 R1=R2=0
540 D=N/4
550 FOR I=1 TO 3/4*N
560 R1=R1+W(I)*W(I+D)
570 NEXT I
580 D=N/2
590 FOR I=1 TO N/2
600 R2=R2+W(I)*W(I+D)
610 NEXT I
620 X=(R1/S2)^2
630 A1=.914948*X+.057184*X^2+.014296*X^3+.005584*X^4
640 X=(R2/S2)^2
650 A2=.914948*X+.057184*X^2+.014296*X^3+.005584*X^4
660 PRINT "CORRELATION COEFFICIENTS:"
670 PRINT
680 PRINT "1/4","1/2"
690 PRINT "---","---"
700 PRINT USING "##.###### ##.######",A1,A2
710 PRINT
720 PRINT "PDI","EFF. PDI"
730 PRINT "---","--------"
740 PRINT
750 I=22
760 PRINT I,I/(1+2/I*(A1*(I-1)+A2*(I-2)))
770 PRINT
780 PRINT
790 PRINT "FREQUENCY RESPONSE IN STEPS OF 0.1 FILTER SPACINGS"
800 PRINT
810 FOR I=0 TO N/4-1
820 FOR J=0 TO .91 STEP .1
830 F=I+J
840 X=0
850 FOR 0=1 TO N/2
860 X=X+W(0)*2*COS(((N+1)-(2*0))*K*F)
870 NEXT 0
880 G(INT(10*J+.01))=20/LOG(10)*LOG(ABS(X/S1))
890 NEXT J
900 PRINT USING 1,G(0),G(1),G(2),G(3),G(4),G(5),G(6),G(7),G(8),G(9)
910 NEXT I
920 DATA 64
930 DATA .45
940 END
```

TABLE A-2. PROGRAM PRINTOUT

FILTER

73 DB. 64 POINT CHEBYSHEV-COSINE FILTER

NO.	CHEBYSHEV	COSINE	PRODUCT
32	1.000977	0.999024	1.000000
31	0.993344	0.991230	0.984632
30	0.978234	0.975702	0.954465
29	0.955954	0.952562	0.910605
28	0.926951	0.921990	0.854640
27	0.891804	0.884225	0.788555
26	0.851198	0.839561	0.714632
25	0.805913	0.788346	0.635339
24	0.756795	0.730982	0.553204
23	0.704735	0.667914	0.470702
22	0.650643	0.599635	0.390148
21	0.595424	0.526678	0.313597
20	0.539956	0.449611	0.242771
19	0.485069	0.369037	0.179008
18	0.431522	0.285584	0.123236
17	0.379993	0.199902	0.075962
16	0.331063	0.112661	0.037298
15	0.285210	0.024541	0.006999
14	0.242801	-0.063770	-0.015484
13	0.204096	-0.151584	-0.030938
12	0.169246	-0.238216	-0.040317
11	0.138302	-0.322988	-0.044670
10	0.111221	-0.405241	-0.045071
9	0.087879	-0.484332	-0.042562
8	0.068082	-0.559645	-0.038102
7	0.051583	-0.630591	-0.032528
6	0.038091	-0.696617	-0.026535
5	0.027287	-0.757209	-0.020662
4	0.018838	-0.811892	-0.015294
3	0.012409	-0.860242	-0.010675
2	0.007674	-0.901880	-0.006921
1	0.005923	-0.936481	-0.005547

AMP. WT. LOSS=-4.47858 DB.

CORRELATION COEFFICIENTS:

1/4	1/2
0.053772	0.000804

PDI	EFF. PDI
22	19.9254

FREQUENCY RESPONSE IN STEPS OF 0.1 FILTER SPACINGS

0.0	-0.0	-0.2	-0.4	-0.8	-1.3	-2.1	-3.1	-4.3	-6.0
-8.0	-10.4	-13.3	-16.8	-21.0	-26.1	-32.3	-40.1	-50.6	-67.5
-98.1	-76.0	-72.5	-82.1	-75.3	-69.9	-71.3	-84.0	-74.7	-69.6
-70.2	-77.5	-79.3	-70.6	-69.3	-72.6	-95.0	-73.8	-69.5	-70.0
-75.8	-84.3	-71.8	-69.3	-71.0	-79.5	-78.8	-70.9	-69.4	-72.0
-84.0	-76.4	-70.4	-69.6	-72.9	-90.1	-75.1	-70.1	-69.8	-73.7
-102.8	-74.2	-69.9	-70.0	-74.4	-99.5	-73.7	-69.8	-70.1	-75.0
-92.5	-73.3	-69.8	-70.3	-75.4	-89.5	-73.1	-69.8	-70.4	-75.8
-87.9	-72.9	-69.7	-70.5	-76.0	-87.0	-72.8	-69.7	-70.5	-76.2
-86.5	-72.7	-69.7	-70.6	-76.3	-86.3	-72.7	-69.7	-70.6	-76.3
-86.3	-72.7	-69.8	-70.6	-76.3	-86.5	-72.8	-69.8	-70.6	-76.2
-86.9	-72.8	-69.8	-70.5	-76.1	-87.4	-72.9	-69.8	-70.5	-75.9
-88.1	-73.0	-69.8	-70.5	-75.8	-89.0	-73.1	-69.9	-70.4	-75.6
-90.2	-73.3	-69.9	-70.4	-75.4	-91.6	-73.4	-69.9	-70.3	-75.2
-93.4	-73.6	-69.9	-70.3	-74.9	-95.8	-73.8	-70.0	-70.2	-74.7
-99.2	-73.9	-70.0	-70.2	-74.5	-105.2	-74.1	-70.1	-70.1	-74.3

APPENDIX B. THREE-CHANNEL PROCESSOR FOR MAXIMIZATION OF TARGET-TO-INTERFERENCE RATIO

DETECTION

In this appendix, the three-channel weighting function for maximization of the target-to-clutter plus noise ratio T/(C+N) at a doppler filter output is derived. Since mainlobe clutter is considered here, nulling of clutter results in loss of target gain; consequently, the optimum depth of a null depends on clutter-to-thermal noise ratio.

Consider a three-channel system in which each channel has a subarray pattern given as $G_0(\theta)$ as shown in Figure B-1. Now, consider that a particular doppler filter will pass clutter arriving from angle θ_1 and a target echo with the same doppler frequency but from a different angle θ_0. The objective is maximization of T/(C+N) by weighting and summing the three channel outputs.

Since the doppler filter is narrowband, a narrowband representation can be used for the radar return and thermal noise. Therefore, the outputs from the three receiver channels can be written as the column vector

$$\underline{y} = G_0(\theta_0)\ T(t)\,\underline{\zeta}_0 + G_0(\theta_1)\ C(t)\,\underline{\zeta}_1 + \underline{n}(t) \qquad \text{(B-1)}$$

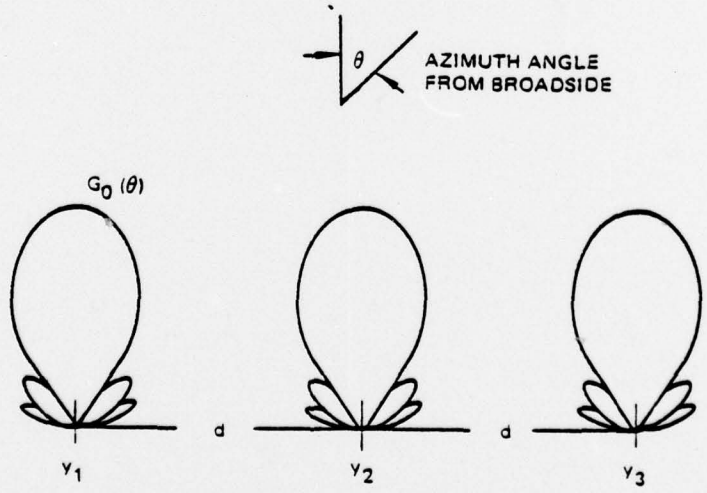


Figure B-1. Three channel array.

where:

$$\underline{y} = \begin{pmatrix} y_1 \\ y_2 \\ y_3 \end{pmatrix}, \quad \underline{n} = \begin{pmatrix} n_1 \\ n_2 \\ n_3 \end{pmatrix}$$

$$\underline{\zeta}_k = \frac{1}{\sqrt{3}} \begin{pmatrix} \exp(-j\frac{2\pi}{\lambda} d \sin\theta_k) \\ 1 \\ \exp(j\frac{2\pi}{\lambda} d \sin\theta_k) \end{pmatrix}$$

n_k is the thermal noise at the kth channel; T(t) and C(t) are the complex envelopes of the target and clutter, respectively. The target-to-clutter plus noise ratio at the doppler filter output is maximized by applying the weighting

$$\underline{w} = C_o R^{-1} \underline{\zeta}_o \tag{B-2}$$

to produce the output, $z = \underline{w}^*\underline{y}$. In these expressions, w* is the complex-conjugate transpose of $\underline{w}$, C_o is an arbitrary constant, and R is the covariance matrix of the clutter plus thermal noise. R can be written as

$$R = \sigma_c^2 \left|G_o(\theta_1)\right|^2 \underline{\zeta}_1 \underline{\zeta}_1^* + \sigma_n^2 I \tag{B-3}$$

where $\sigma_c^2 = E\{C(t)\, C^*(t)\}$, σ_n^2 is the variance of the noise at an individual channel, and I is an identity matrix. Since the concern here is with mainlobe clutter for which $G_o(\theta_1)^2$ is essentially constant, this term is allowed simply to be unity and σ_c^2 to equal the clutter power that passes through the particular doppler filter of interest. From a matrix inversion lemma (Noble[B-1]), R^{-1} can be written as:

$$R^{-1} = \sigma_n^{-2} \left[I - \frac{\sigma_c^2}{\sigma_c^2 + \sigma_n^2} \underline{\zeta}_1 \underline{\zeta}_1^* \right] \tag{B-4}$$

[B-1] B. Noble, Applied Linear Algebra, Prentice-Hall, NJ, 1969, p. 147.

Therefore, the weighting that will maximize the T/(C+N) is

$$\underline{w}_{opt.} = \underline{\zeta}_0 - \frac{\sigma_c^2}{\sigma_c^2 + \sigma_n^2} \underline{\zeta}_1 \, \underline{\zeta}_1^* \, \underline{\zeta}_0$$

or if

$$S_0(\theta_0 - \theta_1) \equiv \underline{\zeta}_1^* \, \underline{\zeta}_0$$

which is simply the normalized array factor of the three channels, then the optimum weighting is

$$\underline{w}_{opt} = \underline{\zeta}_0 - \frac{\sigma_c^2}{\sigma_c^2 + \sigma_n^2} S_0(\theta_0 - \theta_1) \, \underline{\zeta}_1 \qquad \text{(B-5)}$$

A T/C improvement factor can be defined as the improvement in the ratio of gain in the target direction to gain in the clutter direction. This ratio is given as

$$F = \left(\frac{\underline{w}^*_{opt.} \, \underline{\zeta}_0}{\underline{w}^*_{opt.} \, \underline{\zeta}_1} \right) \frac{\underline{\zeta}^*_0 \, \underline{\zeta}_1}{\underline{\zeta}^*_0 \, \underline{\zeta}_0} = 1 + \frac{\sigma_c^2}{\sigma_n^2} \left[1 - S_0^2 (\theta_0 - \theta_1) \right] \qquad \text{(B-6)}$$

From Equation (B-6), it is seen that F increases as the array factor $S_0^2(\theta_0 - \theta_1)$ decreases from its maximum value when $\theta_0 = \theta_1$; therefore, it is desirable to minimize the beamwidth of $S_0(\theta_0 - \theta_1)$. The beamwidth of $S_0(\theta_0 - \theta_1)$ is minimized by maximizing d; however, other factors influence the selection of the subarray separation as discussed in section 6.

METRIC SYSTEM

BASE UNITS:

Quantity	Unit	SI Symbol	Formula
length	metre	m	...
mass	kilogram	kg	...
time	second	s	...
electric current	ampere	A	...
thermodynamic temperature	kelvin	K	...
amount of substance	mole	mol	...
luminous intensity	candela	cd	...

SUPPLEMENTARY UNITS:

plane angle	radian	rad	...
solid angle	steradian	sr	...

DERIVED UNITS:

Acceleration	metre per second squared	...	m/s
activity (of a radioactive source)	disintegration per second	...	(disintegration)/s
angular acceleration	radian per second squared	...	rad/s
angular velocity	radian per second	...	rad/s
area	square metre	...	m
density	kilogram per cubic metre	...	kg/m
electric capacitance	farad	F	A·s/V
electrical conductance	siemens	S	A/V
electric field strength	volt per metre	...	V/m
electric inductance	henry	H	V·s/A
electric potential difference	volt	V	W/A
electric resistance	ohm		V/A
electromotive force	volt	V	W/A
energy	joule	J	N·m
entropy	joule per kelvin	...	J/K
force	newton	N	kg·m/s
frequency	hertz	Hz	(cycle)/s
illuminance	lux	lx	lm/m
luminance	candela per square metre	...	cd/m
luminous flux	lumen	lm	cd·sr
magnetic field strength	ampere per metre	...	A/m
magnetic flux	weber	Wb	V·s
magnetic flux density	tesla	T	Wb/m
magnetomotive force	ampere	A	...
power	watt	W	J/s
pressure	pascal	Pa	N/m
quantity of electricity	coulomb	C	A·s
quantity of heat	joule	J	N·m
radiant intensity	watt per steradian	...	W/sr
specific heat	joule per kilogram-kelvin	...	J/kg·K
stress	pascal	Pa	N/m
thermal conductivity	watt per metre-kelvin	...	W/m·K
velocity	metre per second	...	m/s
viscosity, dynamic	pascal-second	...	Pa·s
viscosity, kinematic	square metre per second	...	m/s
voltage	volt	V	W/A
volume	cubic metre	...	m
wavenumber	reciprocal metre	...	(wave)/m
work	joule	J	N·m

SI PREFIXES:

Multiplication Factors	Prefix	SI Symbol
1 000 000 000 000 = 10^{12}	tera	T
1 000 000 000 = 10^{9}	giga	G
1 000 000 = 10^{6}	mega	M
1 000 = 10^{3}	kilo	k
100 = 10^{2}	hecto*	h
10 = 10^{1}	deka*	da
0.1 = 10^{-1}	deci*	d
0.01 = 10^{-2}	conti*	c
0.001 = 10^{-3}	milli	m
0.000 001 = 10^{-6}	micro	μ
0.000 000 001 = 10^{-9}	nano	n
0.000 000 000 001 = 10^{-12}	pico	p
0.000 000 000 000 001 = 10^{-15}	femto	f
0.000 000 000 000 000 001 = 10^{-18}	atto	a

* To be avoided where possible.

MISSION
of
Rome Air Development Center

RADC plans and conducts research, exploratory and advanced development programs in command, control, and communications (C^3) activities, and in the C^3 areas of information sciences and intelligence. The principal technical mission areas are communications, electromagnetic guidance and control, surveillance of ground and aerospace objects, intelligence data collection and handling, information system technology, ionospheric propagation, solid state sciences, microwave physics and electronic reliability, maintainability and compatibility.

Printed by
United States Air Force
Hanscom AFB, Mass. 01731